SVHEAT SVENVIRO

1D/2D/3D FINITE ELEMENT
FREEZE/THAW MODELING

Theory Manual

Written by:
The Bentley Systems Team

Last Updated: Tuesday, June 23, 2020

Bentley Systems Incorporated

COPYRIGHT NOTICE

Copyright © 2020, Bentley Systems, Incorporated. All Rights Reserved.
Including software, file formats, and audiovisual displays; may only be used pursuant to applicable software license agreement; contains confidential and proprietary information of Bentley Systems, Incorporated and/or third parties which is protected by copyright and trade secret law and may not be provided or otherwise made available without proper authorization.

TRADEMARK NOTICE

Bentley, "B" Bentley logo, SoilVision.com, SoilVision logo, and SOILVISION, SVSLOPE, SVOFFICE, SVOFFICE 5/GE, SVOFFICE 5/GT, SVOFFICE 5/WR, SVSOILS, SVFLUX, SVSOLID, SVCHEM, SVAIR, SVHEAT, SVSEISMIC and SVDESIGNER are either registered or unregistered trademarks or service marks of Bentley Systems, Incorporated. All other marks are the property of their respective owners.

1 INTRODUCTION 5

2 HEAT TRANSFER THEORY 6

2.1 HEAT FLOW GOVERNING EQUATION 6
2.1.1 Transient-State Heat Flow without Considering Thermal Convection 8
2.1.2 Steady-State Heat Flow without Considering Thermal Convection 8
2.1.3 Transient-State Heat Flow Including Thermal Convection 9
2.1.4 Steady-State Heat Flow Including Thermal Convection 10

3 COUPLED EQUATIONS OF MOISTURE FLOW, AIR FLOW AND HEAT FLOW 11

3.1 BASIC COUPLED EQUATIONS GOVERNING MOISTURE FLOW, AIR FLOW, AND HEAT FLOW 11
3.1.1 Basic Equations for the Flow of Moisture, Including Water and Vapor 11
3.1.1.1 Water flow 11
3.1.1.2 Vapor flow 12
3.1.2 Basic Equations for Heat Flow 14
3.1.3 Basic Equations for Air Flow 16
3.1.4 Determination of Ice and Hydraulic Conductivity Reduction 18
3.2 COUPLED MODEL OF MOISTURE AND HEAT FLOW 19
3.2.1 Transient-State Coupled Model for Moisture and Heat Flow 19
3.2.2 Steady-State Coupled Model of Moisture and Heat Flow 22
3.3 COUPLED MODEL FOR HEAT AND AIR FLOW 24
3.3.1 Transient-State Coupled Model of Heat Flow and Air Flow 24
3.3.2 Steady-State Coupled Model of Heat Flow and Air Flow 26
3.3.3 Heat Flow and Air Flow due to Natural Convection 27
3.4 FULLY COUPLED MODEL OF MOISTURE, AIR, AND HEAT FLOW 28

4 MATERIAL THERMAL PROPERTIES 34

4.1 THERMAL CONDUCTIVITY CURVE 34
4.1.1 Johansen Approach (1973) 34
4.1.2 Improved Johansen – Lu et al., (2007) 38
4.1.3 De Vries Approach (1963) 40
4.1.4 Côté and Konrad (2005) 41
4.1.5 Comparison of Thermal Conductivity Calculated with Johansen, Lu et al., and De Vries Approach 43
4.1.6 Measured by Experimental Data 45
4.1.7 Estimated by Empirical Expression 49
4.1.8 Thermal Conductivity of Snow 49
4.2 VOLUMETRIC HEAT CAPACITY 50
4.2.1 Constant Formulation 50
4.2.2 Jame-Newman Formulation 51
4.2.3 Curve Comparison 52
4.3 SOIL FREEZING CHARACTERISTIC CURVE (SFCC) 52
4.3.1 Estimated SFCC with SWCC 53
4.3.2 Estimated SFCC by Empirical Expression 53
4.3.3 Exponential Expression of SFCC 55
4.3.4 Determine SFCC with Multi-lines 56
4.3.5 Determine SFCC by Experimental Data 57
4.4 HYDRAULIC CONDUCTIVITY REDUCTION 58
4.4.1 Impedance Factor (Jame, 1977) 58
4.4.2 Estimated by SWCC 58

5 BOUNDARY CONDITIONS 59

5.1 RULES TO SPECIFY BOUNDARY CONDITIONS 59
5.2 CLIMATE BOUNDARY CONDITIONS 60
5.2.1 Equal to Air Temperature 60
5.2.2 N-Factor 60
5.2.3 Boundary with Snow Cover 60
5.2.4 Energy Balance 62

5.2.5 Thermosyphon *64*
5.2.6 Convection/Radiation *65*
5.3 INSULATION BOUNDARY CONDITION 65
5.3.1 Inner Insulation boundary *66*
5.3.2 Outer Insulation boundary *66*
5.4 CAUCHY BOUNDARY CONDITION 66
5.5 FLUX SECTIONS 67

6 WELLS AND TUNNELS 68

6.1 INTRODUCTION 68
6.2 EQUATIONS 68
6.3 GEOMETRY 69
6.4 SETTING THE INFLUENCE DISTANCE 70
6.5 BOUNDARY CONDITIONS 70
6.5.1 Rate *70*
6.5.2 Temperature *70*
6.5.3 Thermosyphon *70*
6.6 PARAMETERS 71
6.7 REMARKS 71

7 NUMERICAL IMPLEMENTATION 73

7.1 EQUATION ANALYZER 73
7.2 MESH GENERATION 73
7.3 MESH REFINEMENT 74
7.4 INTERPOLATION ORDER 74
7.5 TIME STEPPING 74
7.5.1 Time Integration *74*
7.5.2 Timestep Control *75*

8 REFERENCES 77

1 INTRODUCTION

Conductive heat flow problems in geotechnical and geo-environmental engineering involve the solution of a partial differential equation referred to as a PDE. The PDE must be solved for all "finite elements" which when combined form a "continuum" (or the geometry of the problem). The theory of heat flow expressed in mathematical form embraces the physical behavior of the material (e.g., soil) and the conservative laws of physics (i.e., conservation of energy). The physical behavior or many materials, (particularly unsaturated soils), is non-linear and as a consequence, the PDE becomes non-linear in character. It is well-known that the solution of non-linear PDEs can present a challenge to the numerical modeler.

The purpose of the theory manual is to provide the user with details regarding the theoretical formulation of the PDE as well as the numerical method used in the solution. The intent of the theory manual is not to provide an exhaustive summary of all theories associated with heat flow. Rather, the intent is to clearly describe details of the theory used in the SVHEAT software.

The SoilVision finite element software packages utilize the FlexPDE generic finite element solver to solve the partial differential equation for heat flow. The FlexPDE solver algorithm has implemented cutting-edge numerical solution techniques that can accommodate linear and highly non-linear PDEs. The solution technique utilizes automatic mathematically designed mesh generation as well as automatic mesh refinement. The application of these advanced numerical techniques is particularly valuable in solving highly non-linear and complex problems. Most commonly it is the unsaturated soil portion of the soil continuum that brings in non-linear soil behavior. The advanced FlexPDE solver makes it possible to obtain converged and accurate solutions for many problems that were previously unsolvable.

The primary attributes of the SoilVision solution process are as follows:

- Fully automatic mesh generation.
- Fully automatic mesh refinement based on any model variable.
- Integrated climatic calculations.
- Fully implicit approach in the solver, which provides for a robust solution of difficult models with convergence issues.
- Energy-balance tracking.
- Axisymmetric and plan analysis formulations.
- 3, 6, or 9-noded triangles as elements for 2D analysis and 4, 10, or 20-noded tetrahedrons in 3D elements.
- Adaptive time-stepping with automatic generation and control of time steps.
- Newton-Raphson convergence iteration schemes.
- Use matrix preconditioning in conjugate-gradient solutions. The default preconditioner is the diagonal-block inverse matrix.

2 HEAT TRANSFER THEORY

SVHEAT is formulated to mathematically model the movement of heat in a material. SVHEAT is capable of modeling heat transfer by the conduction or convection processes. Modeling of convection may be accomplished when coupled with seepage (SVFLUX) and can accommodate saturated and unsaturated materials. The software is also formulated to simulate the freezing and thawing phase change between ice and water. The following manual describes the formulation used by SVHEAT to model heat transfer in materials.

2.1 HEAT FLOW GOVERNING EQUATION

The equation governing heat flow can be generally written as follows (Harlan 1973, Jame 1977, Flerchinger and Saxton 1989, Neman 1995):

$$\frac{\partial}{\partial x}\left(\lambda \frac{\partial T}{\partial x}\right) - C_w q_w \frac{\partial T}{\partial x} = C\frac{\partial T}{\partial t} - L_f \frac{\rho_i}{\rho_w}\frac{\partial \theta_i}{\partial t} \qquad [1]$$

where:

λ	= thermal conductivity, *J/(s-m-°C)*,
C	= volumetric heat capacity of soil, $J/(m^3\text{-}°C)$,
C_w	= volumetric heat capacity of water, $J/(m^3\text{-}°C)$,
q_w	= water flow flux (Darcian velocity), *m/s*,
L_f	= volumetric latent heat of fusion of water 3.34×10^8 J/m^3,
ρ_i	= ice density, kg/m^3,
ρ_w	= water density, kg/m^3,
θ_i	= volumetric ice content, m^3/m^3,
T	= temperature, *°C*,
t	= time, *s*, and
x	= coordinate, *m*.

On the left side of equation [1], the first term represents the heat flow driven by thermal conduction; the second term is the heat flow due to thermal convection. On the right side of equation [1], the term of $L_f \frac{\partial \theta_i}{\partial t}$ is the heat release or absorption caused by phase change of water freezing, and the term of $C\frac{\partial T}{\partial t}$ is the heat storage in the system.

There are two dependent variables of T and θ_i in equation [1]. The ice content is associated with the soil temperature and water content. At any time the total volumetric water content is expressed as follows.

$$\theta = \theta_u + \frac{\rho_i}{\rho_w}\theta_i \qquad [2]$$

where:

θ	= volumetric water content, m^3/m^3,
θ_u	= volumetric unfrozen water content at a given negative temperature , m^3/m^3,
θ_i	= volumetric ice content, m^3/m^3.
ρ_w	= water density, kg/m^3, and
ρ_i	= ice density, kg/m^3.

The unfrozen water content, θ_u, is uniquely determined by the given soil temperature, T, in terms of negative degrees Celsius. The relationship between unfrozen water content and the temperature is referred to as Soil Freezing Characteristic Curve (SFCC). Similar to the Soil Water Characteristic Curve (SWCC), SFCC is an important soil property related to soil freezing behavior.

Since the total volumetric water content is a constant value in thermal transfer only model, and using the chain-rule derivative $\frac{\rho_i}{\rho_w}\frac{\partial \theta_i}{\partial t} = \frac{\rho_i}{\rho_w}\frac{\partial \theta_i}{\partial T}\frac{\partial T}{\partial t} = -\frac{\partial \theta_u}{\partial T}\frac{\partial T}{\partial t}$, the equation [1] can be rewritten as follows:

$$\frac{\partial}{\partial x}\left(\lambda\frac{\partial T}{\partial x}\right)-C_w q_w\frac{\partial T}{\partial x}=\left(C+L_f m_2^i\right)\frac{\partial T}{\partial t} \qquad [\,3\,]$$

$$C_\rho = C + L_f m_2^i \qquad [\,4\,]$$

$$m_2^i=\frac{\partial\theta_u}{\partial T} \quad if\ T_{ef}<T\geq T_{ep}$$
$$m_2^i=0 \quad otherwise \qquad [\,5\,]$$

where:

T	= temperature, °*C*, and
t	= time, *s*.
λ	= Thermal conductivity, *J/(s-m-°C)*,
C_w	= volumetric heat capacity of water, $J/(m^3\text{-}°C)$,
C	= volumetric heat capacity of soil, $J/(m^3\text{-}°C)$,
q_w	= water flow flux (Darcian velocity), *m/s*,
L_f	= volumetric latent heat of fusion of water 3.34×10^8 J/m^3,
ρ_w	= water density, kg/m^3,
m_2^i	= the rate of change of unfrozen water content with temperature (i.e., the slope of soil freezing characteristic curve), $m^3/(m^3\text{-}°C)$,
T_{ef}	= Soil freezing point, or sometime it is referred as the temperature of fusion (liquidus), °*C*,
T_{ep}	= Soil temperature at the end of the freezing phase change, or sometime it is defined as the temperature of solidification (solidus), °*C*,
C_ρ	= apparent volumetric heat capacity for heat storage, $J/(m^3\text{-}°C)$.

The term of $\rho_l L_f m_2^i$ in equation [3] represents the energy release or absorption due to the phase change of soil freezing. Care must be taken in use of m_2^i. For unsaturated soil, if the soil water content at the temperature above the soil freezing point is less than the unfrozen soil water content at the given soil negative temperature, no phase change happens because the soil is too dry to freeze. For example, suppose soil sample1 and soil sample2 have the same soil properties of SFCC, but the initial volumetric water content for soil sample 1 is 0.45 m^3/m^3 and for soil sample 2 is 0.15 m^3/m^3. The phase change starts for soil sample 1 at the soil temperature below −0.05 °*C*, but the phase change does not happen to the soil sample 2 until the soil temperature drops down to −0.2 ℃, as shown in Figure 1.

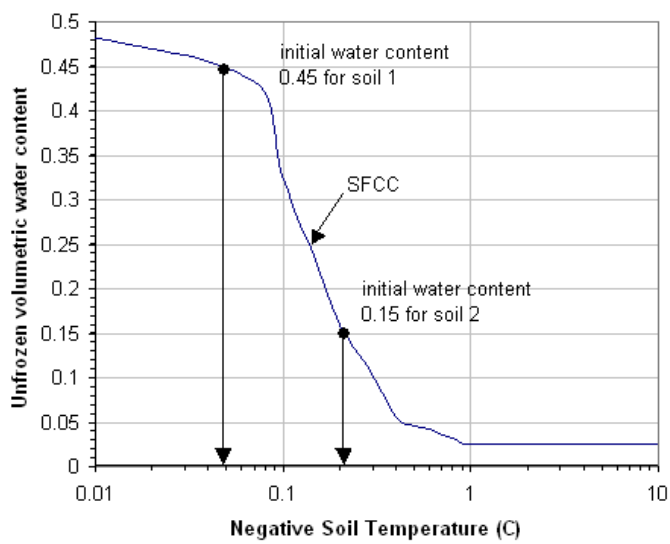

Figure 1 Illustrative phase changing at different initial water content

Thermal conductivity, heat capacity, and the soil freezing characteristic curve are the most important properties of a material. Please see the Material Properties section of this document for how to calculate, determine, or estimate these material thermal properties.

Equation [1] is the general formulation of heat transfer including the mechanism of thermal conduction, convection and phase change of water freezing. In geotechnical engineering such as soil cover, the thermal convection with water flow can be

neglected. For materials such as wood, iron and steel, plastics, etc., used in model domain, the phase change is not needed to be considered (i.e., $m_2^i = 0$). The following sections describe the different applications implemented in SVHEAT package.

2.1.1 Transient-State Heat Flow without Considering Thermal Convection

Heat flow due to the convection of moisture flow in a model domain is usually two or more orders of magnitude less than conductive heat flow in all but the coarsest of soils (Pentland, 2000). The conductive heat flow is generally the greatest significance of heat transfer in geotechnical engineering. Consequently, by the default, the thermal convection flow is not included when a model is created with SVHEAT. In this case the governing equation [3] can be rewritten as follows:

- **1D Horizontal**

$$\frac{\partial}{\partial x}\left(\lambda_x \frac{\partial T}{\partial x}\right) = \left(C + L_f m_2^i\right)\frac{\partial T}{\partial t} \qquad [\ 6\ ]$$

- **1D Vertical**

$$\frac{\partial}{\partial y}\left(\lambda_y \frac{\partial T}{\partial y}\right) = \left(C + L_f m_2^i\right)\frac{\partial T}{\partial t} \qquad [\ 7\ ]$$

- **2D or Plane**

$$\frac{\partial}{\partial x}\left(\lambda_x \frac{\partial T}{\partial x}\right) + \frac{\partial}{\partial y}\left(\lambda_y \frac{\partial T}{\partial y}\right) = \left(C + L_f m_2^i\right)\frac{\partial T}{\partial t} \qquad [\ 8\ ]$$

- **Axis-Symmetric**

$$\frac{\partial}{\partial r}\left(\lambda \frac{\partial T}{\partial r}\right) + \frac{\lambda_r}{r}\frac{\partial T}{\partial r} + \frac{\partial}{\partial z}\left(\lambda_z \frac{\partial T}{\partial z}\right) = \left(C + L_f m_2^i\right)\frac{\partial T}{\partial t} \qquad [\ 9\ ]$$

- **3D**

$$\frac{\partial}{\partial x}\left(\lambda_x \frac{\partial T}{\partial x}\right) + \frac{\partial}{\partial y}\left(\lambda_y \frac{\partial T}{\partial y}\right) + \frac{\partial}{\partial z}\left(\lambda_z \frac{\partial T}{\partial z}\right) = \left(C + L_f m_2^i\right)\frac{\partial T}{\partial t} \qquad [\ 10\ ]$$

where:

$\lambda_x, \lambda_y, \lambda_z, \lambda_r$,	= Thermal conductivity in x, y, z direction of Cartesian coordinate, or r-direction of cylindrical coordinate, *J/(s-m-°C)*,
C	= volumetric heat capacity of soil, *J/(m-°C)*,
L_f	= volumetric latent heat of fusion of water 3.34×10^8 J/m^3,
m_2^i	= the rate of change in unfrozen water content with temperature (i.e., the slope of soil freezing characteristic curve), $m^3/(m^3\text{-}°C)$,
T	= temperature, *°C*,
t	= time, *s*,
x, y, z	= Cartesian coordinate, *m*, and
r	= horizontal direction in cylindrical coordinate.

The thermal conductivity, heat capacity, and SFCC can be determined using the measured data, or calculated with different approaches. Please see Thermal Material Properties section for details.

2.1.2 Steady-State Heat Flow without Considering Thermal Convection

In steady state the temperature does not change with time. The heat flow equations are simplified as follows:

- **1D Horizontal**

$$\frac{\partial}{\partial x}\left(\lambda_x \frac{\partial T}{\partial x}\right) = 0 \qquad [\ 11\ ]$$

- **1D Vertical**

$$\frac{\partial}{\partial x}\left(\lambda_y \frac{\partial T}{\partial y}\right) = 0 \qquad [\ 12\ ]$$

- **2D or Plane**

$$\frac{\partial}{\partial x}\left(\lambda_x \frac{\partial T}{\partial x}\right) + \frac{\partial}{\partial y}\left(\lambda_y \frac{\partial T}{\partial y}\right) = 0 \qquad [\ 13\ ]$$

-

- **Axis-Symmetric**

$$\frac{\partial}{\partial r}\left(\lambda_r \frac{\partial T}{\partial r}\right)+\frac{\lambda_r}{r}\frac{\partial T}{\partial r}+\frac{\partial}{\partial z}\left(\lambda_z \frac{\partial T}{\partial z}\right)=0 \qquad [14]$$

- **3D**

$$\frac{\partial}{\partial x}\left(\lambda_x \frac{\partial T}{\partial x}\right)+\frac{\partial}{\partial y}\left(\lambda_y \frac{\partial T}{\partial y}\right)+\frac{\partial}{\partial z}\left(\lambda_z \frac{\partial T}{\partial z}\right)=0 \qquad [15]$$

where:

$\lambda_x, \lambda_y, \lambda_z, \lambda_r$,	= Thermal conductivity in x, y, z direction of Cartesian coordinate, or r-direction of cylindrical coordinate, *J/(s-m-°C)*,
T	= temperature, *°C*,
t	= time, *s*,
x, y, z	= Cartesian coordinate, *m*, and
r	= horizontal direction in cylindrical coordinate.

2.1.3 Transient-State Heat Flow Including Thermal Convection

To include the thermal convection of water flow and airflow, select the "Convection" option in SVHEAT.

- **1D Horizontal**

$$\frac{\partial}{\partial x}\left(\lambda_x \frac{\partial T}{\partial x}\right)-\left(C_w q_x^w + C_a q_x^a\right)\frac{\partial T}{\partial x}=\left(C+L_f m_2^i\right)\frac{\partial T}{\partial t} \qquad [16]$$

- **1D Vertical**

$$\frac{\partial}{\partial y}\left(\lambda_y \frac{\partial T}{\partial y}\right)-\left(C_w q_y^w + C_a q_y^a\right)\frac{\partial T}{\partial y}=\left(C+L_f m_2^i\right)\frac{\partial T}{\partial t} \qquad [17]$$

- **2D or Plane**

$$\frac{\partial}{\partial x}\left(\lambda_x \frac{\partial T}{\partial x}\right)+\frac{\partial}{\partial y}\left(\lambda_y \frac{\partial T}{\partial y}\right)-\left(C_w q_x^w + C_a q_x^a\right)\frac{\partial T}{\partial x}-\left(C_a q_y^w + C_a q_y^a\right)\frac{\partial T}{\partial y} =\left(C+L_f m_2^i\right)\frac{\partial T}{\partial t} \qquad [18]$$

- **Axis-Symmetric**

$$\frac{\partial}{\partial r}\left(\lambda_r \frac{\partial T}{\partial r}\right)+\frac{\lambda_r}{r}\frac{\partial T}{\partial r}+\frac{\partial}{\partial z}\left(\lambda_z \frac{\partial T}{\partial z}\right)-\left(C_w q_r^w + C_a q_r^a\right)\frac{\partial T}{\partial r} -\left(C_w q_z^w + C_a q_z^a\right)\frac{\partial T}{\partial z}=\left(C+L_f m_2^i\right)\frac{\partial T}{\partial t} \qquad [19]$$

- **3D**

$$\frac{\partial}{\partial x}\left(\lambda_x \frac{\partial T}{\partial x}\right)+\frac{\partial}{\partial y}\left(\lambda_y \frac{\partial T}{\partial y}\right)+\frac{\partial}{\partial z}\left(\lambda_z \frac{\partial T}{\partial z}\right) -\left(C_w q_x^w + C_a q_x^a\right)\frac{\partial T}{\partial x}-\left(C_w q_y^w + C_a q_y^a\right)\frac{\partial T}{\partial y}-\left(C_w q_z^w + C_a q_z^a\right)\frac{\partial T}{\partial z} =\left(C+L_f m_2^i\right)\frac{\partial T}{\partial t} \qquad [20]$$

where:

$\lambda_x, \lambda_y, \lambda_z, \lambda_r$,	= Thermal conductivity in x, y, z direction of Cartesian coordinates, or r-direction of cylindrical coordinates, *J/(s-m-°C)*,
C_w	= volumetric heat capacity of water, *J/(m³-°C)*,
C_a	= volumetric heat capacity of air, *J/(m³-°C),*
C	= volumetric heat capacity of soil, *J/(m³-°C)*,
q_x^w, q_y^w, q_z^w, q_r^w	= water flow velocity (Darcian velocity) in x, y, z-direction of Cartesian coordinates, or r-direction of cylindrical coordinates, *m/s*,
q_x^a, q_y^a, q_z^a, q_r^a	= air flow velocity (Darcian velocity) in x, y, z-direction of Cartesian coordinates, or r-direction of cylindrical coordinates, *m/s*,
L_f	= volumetric latent heat of fusion of water 3.34×10^8 *J/m³*,
m_2^i	= the rate of change of unfrozen water content with temperature, i.e., the

slope of soil freezing characteristic curve, $m^3/(m^3\text{-}°C)$,

T = temperature, $°C$,

t = time, s.

x, y, z = Cartesian coordinates, m, and

r = horizontal direction in cylindrical coordinates.

2.1.4 Steady-State Heat Flow Including Thermal Convection

For steady-state conditions the partial differential equation that describes heat flow is as follows:

- **1D Horizontal**

$$\frac{\partial}{\partial x}\left(\lambda_x \frac{\partial T}{\partial x}\right) - \left(C_w q_x^w + C_a q_x^a\right)\frac{\partial T}{\partial x} = 0 \qquad [21]$$

- **1D Vertical**

$$\frac{\partial}{\partial y}\left(\lambda_y \frac{\partial T}{\partial y}\right) - \left(C_w q_y^w + C_a q_y^a\right)\frac{\partial T}{\partial y} = 0 \qquad [22]$$

- **2D or Plane**

$$\frac{\partial}{\partial x}\left(\lambda_x \frac{\partial T}{\partial x}\right) + \frac{\partial}{\partial y}\left(\lambda_y \frac{\partial T}{\partial y}\right) - \left(C_w q_x^w + C_a q_x^a\right)\frac{\partial T}{\partial x} - \left(C_w q_y^w + C_a q_y^a\right)\frac{\partial T}{\partial y} = 0 \qquad [23]$$

- **Axis-Symmetric**

$$\begin{aligned}&\frac{\partial}{\partial r}\left(\lambda_r \frac{\partial T}{\partial r}\right) + \frac{\lambda_r}{r}\frac{\partial T}{\partial r} + \frac{\partial}{\partial z}\left(\lambda_z \frac{\partial T}{\partial z}\right)\\ &- \left(C_w q_r^w + C_a q_r^a\right)\frac{\partial T}{\partial r} - \left(C_w q_z^w + C_a q_z^a\right)\frac{\partial T}{\partial z} = 0\end{aligned} \qquad [24]$$

- **3D**

$$\begin{aligned}&\frac{\partial}{\partial x}\left(\lambda_x \frac{\partial T}{\partial x}\right) + \frac{\partial}{\partial y}\left(\lambda_y \frac{\partial T}{\partial y}\right) + \frac{\partial}{\partial z}\left(\lambda_z \frac{\partial T}{\partial z}\right)\\ &- \left(C_w q_x^w + C_a q_x^a\right)\frac{\partial T}{\partial x} - \left(C_w q_y^w + C_a q_y^a\right)\frac{\partial T}{\partial y} - \left(C_w q_z^w + C_a q_z^a\right)\frac{\partial T}{\partial z} = 0\end{aligned} \qquad [25]$$

where:

$\lambda_x, \lambda_y, \lambda_z, \lambda_r$, = Thermal conductivity in x, y, z direction of Cartesian coordinates, or r-direction of cylindrical coordinates, $J/(s\text{-}m\text{-}°C)$,

C_w = volumetric heat capacity of water, $J/(m^3\text{-}°C)$,

C_a = volumetric heat capacity of air, $J/(m^3\text{-}°C)$,

q_x^w, q_y^w, q_z^w, q_r^w = moisture flow flux (Darcian velocity), m/s,

q_x^a, q_y^a, q_z^a, q_r^a = air flow velocity (Darcian velocity) in x, y, z-direction of Cartesian coordinates, or r-direction of cylindrical coordinates, m/s, and

T = temperature, $°C$.

3 COUPLED EQUATIONS OF MOISTURE FLOW, AIR FLOW AND HEAT FLOW

This section discusses the coupled equation governing moisture flow, air flow and heat flow. Depending on different applications, three cases are considered:

- Heat flow coupled with moisture flow,
- Heat flow coupled with air flow,
- Heat flow coupled with moisture, and air flow.

3.1 BASIC COUPLED EQUATIONS GOVERNING MOISTURE FLOW, AIR FLOW, AND HEAT FLOW

3.1.1 Basic Equations for the Flow of Moisture, Including Water and Vapor

The following assumptions and considerations are made:

- The soil moisture flow obeys Darcy's law,
- Moisture evaporation is included only when a climate boundary condition applied,
- The convection between moisture and heat flow is considered,
- Hydraulic conductivity reduction in frozen soil regime is considered. The same approaches are used to calculate hydraulic conductivity as the function of soil suction as described in SVFLUX Theory Manual, but soils suction in the freezing and frozen regime is determined by Clapeyron equation.

The equation governing moisture flow, including liquid flow, vapor flow, and freezing is described as follows:

3.1.1.1 Water flow

Volumetric moisture content (including water, vapor, and ice) can be generally expressed as

$$\theta = \theta_l + \theta_v + \delta(T_{ef} - T)\frac{\rho_i \theta_i}{\rho_w} \qquad [26]$$

where:

θ	= total volumetric water content, m^3/m^3,
θ_l	= liquid water content, m^3/m^3,
θ_v	= water vapor content, m^3/m^3,
θ_i	= ice content, m^3/m^3,
ρ_i	= ice density, kg/m^3,
ρ_w	= water density, kg/m^3,
$\delta(x)$	= a unit function having the value of $\delta(x)$ = 1 if x > 0, $\delta(x)$ = 0 else.
T_{ef}	= temperature at soil freezing point, °*C*, and
T	= soil temperature, °*C*.

Water flow due to the hydraulic head gradient and the temperature gradient can be generally obtained by the modified Darcy law:

$$q_L = -\left(\frac{k_w}{\gamma_w}\frac{\partial u_w}{\partial z} + k_w + k_{LT}\frac{\partial T}{\partial z}\right) \qquad [27]$$

$$k_{LT} = \frac{k_w}{\gamma_w}\frac{\partial \Psi(T)}{\partial T} = m_2^{\varphi}\frac{k_w}{\gamma_w} \qquad [28]$$

$$m_2^{\varphi} = \frac{\partial \Psi(T)}{\partial T} \qquad [29]$$

where:

k_w	= hydraulic conductivity due to water head, *m/s*,
k_{LT}	= hydraulic conductivity introduced by temperature gradient, $m^2/s\text{-}^oC$,
γ_w	= unit weight of water, kN/m^3,
$\psi(T)$	= a relation of matric suction to the temperature,
m_2^{φ}	= slope of the relation of matric suction to the soil temperature, kPa/°C, and
T	= Temperature, ^oC.

For the unfrozen soil, the following relationship between matric suction and temperature is used (Milly, 1984; Heitman, et al., 2008):

$$\Psi = \Psi(T_0)\exp\left[-\alpha\left(T - T_0\right)\right] \quad [30]$$

$$m_2^{\varphi} = -\alpha\Psi(T_0)\exp\left[-\alpha\left(T - T_0\right)\right] \quad [31]$$

where:

$\psi(T_0)$	= matric suction at a reference temperature, *kPa*, which is determined by soil water characteristic curve (SWCC),
α	=2.09X10^{-3}, 1/^oC,

Noborio et al., (1996b) used the following expression for k_{LT}, as given

$$m_2^{\varphi} = u_w G_{wT}\frac{1}{\gamma_0}\frac{\partial\gamma}{\partial T} = -u_w G_{wT}(1.98\times10^{-3} + 6.62\times10^{-6}T) \quad [32]$$

$$\gamma = 75.6 - 0.1425T - 2.38\times10^{-4}T^2 \quad [33]$$

where:

G_{wT}	= gain factor, a dimensionless factor,
γ_0	= 71.89, g/s^2, and
γ	= surface tension of soil water, g/s^2.

For the frozen soil, the Clapeyron equation may be used to obtain the matric suction as the function of temperature (Daanen et al., 2007):

$$\Psi = \frac{\gamma_w L_f T}{\rho_w g T_o} = m_2^{\varphi} T \quad [34]$$

$$m_2^{\varphi} = \frac{\gamma_w L_f}{273.15 g \rho_w} \quad [35]$$

NOTE:

1. The unit of variable *T* in [34] is °*C* and T_o is 273.15 *K*
2. It is not very clear for the mechanics of liquid water flow caused by a temperature gradient. SVHEAT may not fully support this feature in the current version.

3.1.1.2 Vapor flow

Vapor flow due to the vapor concentration in the pore air is given according to Fick's law (Fredlund and Gitirana 2005, Saito et al., 2006, and Heitman et al., 2008):

$$q_v = -D_v\beta\frac{\partial\theta_v}{\partial z} = -\frac{D_v\beta\theta_a}{\rho_w}\left(\frac{\partial\rho_v}{\partial\Psi}\frac{\partial\Psi}{\partial z} + \frac{\partial\rho_v}{\partial T}\frac{\partial T}{\partial z}\right) \quad [36]$$

$$D_v = 2.29\times10^{-5}\left(1 + \frac{T}{273.15}\right)^{1.75} \quad [37]$$

$$\beta = \left(\theta_a\right)^{2/3} = (n - \theta_L)^{2/3} \quad [38]$$

$$\theta_v = \frac{\theta_a \rho_v}{\rho_w} \quad [\ 39\ ]$$

$$\rho_v = \rho_{sv0} h_r \quad [\ 40\ ]$$

$$h_r = e^{\frac{-g\omega_v \Psi}{\gamma_w R(27315+T)}} \quad [\ 41\ ]$$

$$\psi = (u_a - u_w) + \pi \quad [\ 42\ ]$$

where:

q_v	= vapor flow rate in soil pore air, *m/s*,
D_v	= molecular diffusivity of vapor in soil pore air, m^2/s,
β	= soil tortuosity of a dimensionless factor,
θ_a	= volumetric air content, m^3/m^3,
θ_v	= volumetric vapor content, m^3/m^3,
ρ_w	= water density, kg/m^3,
ρ_v	= vapor density, kg/m^3,
ρ_{sv0}	= saturation vapor density that is dependent on temperature, kg/m^3,
h_r	= relative humidity,
γ_w	= unit weight of water, kN/m^3,
Ψ	= total suction, *kPa*,
u_a	= pore air pressure, *kPa*,
u_w	= pore water pressure, *kPa*,
π	= osmotic suction, *kPa*,
ω_v	= molecular weight of vapor, 0.018016 *kg/mol*,
R	= universal gas constant 8.3144 *J/mol-K*, and
T	= soil temperature, ^oC.

Using the equation [40], [41], and expanding the equation [36] gives

$$q_v = -D_v \beta \frac{\partial \theta_v}{\partial z} = -\frac{D_v \beta \theta_a}{\rho_w}\left[\rho_{sv0}\frac{\partial h_r}{\partial \Psi}\frac{\partial \Psi}{\partial z} + \left(h_r \frac{\partial \rho_{sv0}}{\partial T} + \rho_{sv0}\frac{\partial h_r}{\partial T}\right)\frac{\partial T}{\partial z}\right] \quad [\ 43\ ]$$

If water vapor is considered as an ideal gas (Fredlund and Gitirana 2005), the saturated vapor density is given by

$$\rho_{sv0} = \frac{C_u \omega_v u_{sv0}}{R(273.15+T)} \quad [\ 44\ ]$$

$$\begin{aligned} u_{sv0} &= 0.6183580754 + 0.041142732\,T + 0.0017217473\,T^2 \\ &+ 0.0000174108\,T^3 + 0.0000003985\,T^4 + 0.0000000022\,T^5 \end{aligned} \quad [\ 45\ ]$$

where:

u_{vs0}	= saturated vapor pressure, *kPa*,
C_u	= unit conversion coefficient, C_u = 1000 for metric unit, and C_u = 1 for imperial unit.

Saito et al., (2006) and Heitman et al., (2008) use the different expressions to describe the saturation vapor density, but Figure 2 shows that equation [44] has a good agreement with the experimental data from the online compared with other approaches. The experimental data is from the website: http://hyperphysics.phy-astr.gsu.edu/hbase/kinetic/relhum.html#c3.

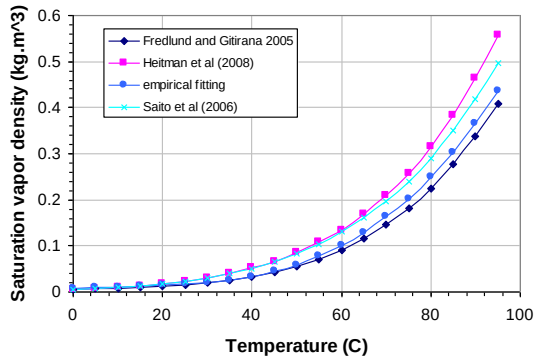

Figure 2 Comparison of different approaches to calculate the saturation vapor density.

Insertion of the equation [44] into the equation [43] results in the vapor flow rate:

$$q_v = -\left(\frac{k_{vh}}{\gamma_w} \frac{\partial u_w}{\partial z} + k_{vT} \frac{\partial T}{\partial z} - \frac{k_{vh}}{\gamma_w} \frac{\partial u_a}{\partial z} \right) \qquad [\ 46\ ]$$

$$k_{vh} = \frac{\beta \theta_a g D_v \omega_v \rho_{sv0} h_r}{\rho_w R(273.15 + T)} \qquad [\ 47\ ]$$

$$k_{vT} = \frac{k_{vh}}{\gamma_w} \left[\frac{\rho_w}{\rho_{svo}} \left(\frac{\partial u_{sv0}}{\partial T} - \frac{u_{sv0}}{(273.15 + T)} \right) + \frac{u_a - u_w}{(273.15 + T)} \right] \qquad [\ 48\ ]$$

The total moisture (water and vapor) flow rate becomes

$$q_w = q_L + q_v = -\left[\frac{k_w + k_{vh}}{\gamma_w} \frac{\partial u_w}{\partial z} + k_w + (k_{LT} + k_{vT}) \frac{\partial T}{\partial z} - \frac{k_{vh}}{\gamma_w} \frac{\partial u_a}{\partial z} \right] \qquad [\ 49\ ]$$

Based on the mass conservation, the equation governing moisture flow can be written as the format like

$$\frac{\partial}{\partial z} \left[k_{11} \frac{\partial u_w}{\partial z} + k_{12} \frac{\partial T}{\partial z} + k_{13} \frac{\partial u_a}{\partial z} + k_w \right] = \frac{\partial \theta_u}{\partial t} + \frac{\rho_i}{\rho_w} \frac{\partial \theta_i}{\partial t} \qquad [\ 50\ ]$$

$$k_{11} = \frac{k_w + k_{vh}}{\gamma_w}, \quad k_{12} = k_{LT} + k_{vT}, \quad k_{13} = -\frac{k_{vh}}{\gamma_w} \qquad [\ 51\ ]$$

where:

k_w	= hydraulic conductivity, *m/s*,
k_{vh}	= water vapor conductivity by diffusion within the air phase, *m/s*,
k_{vT}	= water vapor conductivity due to temperature gradient, $m^2/s\text{-}^oC$,
k_{LT}	= water conductivity introduced by temperature gradient, $m^2/s\text{-}^oC$,
T	= temperature, ^oC,
u_w	= pore water pressure, *kPa,*
u_a	= pore air pressure, *kPa*,
γ_w	= unit weight of water, kN/m^3,
ρ_w	= water density, kg/m^3,
θ_u	= unfrozen volumetric water content, including liquid and vapor, m^3/m^3,
θ_i	= volumetric ice content, m^3/m^3,
ρ_i	= ice density, $kg/\ m^3$,
z	= elevation, *m*, and
t	= time, *s*.

3.1.2 Basic Equations for Heat Flow

The energy conservation of heat flow that contains the thermal conduction, convection, water vapor and freezing phase change can be generally expressed as

$$\frac{\partial}{\partial z}\left[\lambda\frac{\partial T}{\partial Z}-L_v q_v-\left(C_w q_L+C_v q_v+C_a q_a\right)T\right]=C\frac{\partial T}{\partial t}+L_v\frac{\partial\theta_v}{\partial t}-L_f\frac{\rho_i}{\rho_w}\frac{\partial\theta_i}{\partial t} \qquad [\ 52\ ]$$

$$C=C_s\theta_s+C_w\theta_L+C_v\theta_v+C_i\theta_i+C_a\theta_a \qquad [\ 53\ ]$$

where:

λ	= thermal conductivity, *J/(s-m-°C)* or *w/m-°C*,
T	= temperature, *°C*,
L_v	= volumetric latent heat of water vaporization, 2.5×10^9 *J/ m³*, if $T > T_{ef}$, otherwise, $L_v = 0$ otherwise.
L_f	= volumetric latent heat of fusion of water 3.34×10^8 *J/m³*, if $T > T_{ef}$ or $T < T_{ep}$, then $L_f = 0$,
T_{ef}	= temperature at soil freezing point, or liquidus temperature, *°C*,
T_{ep}	= temperature at the end of ice phase, or solidus temperature, *°C*,
q_L	= water flow velocity (Darcian velocity) (i.e., equation [27]), *m/s*,
q_v	= water vapor flow velocity (Darcian velocity) (i.e., equation [46]), *m/s*,
q_a	= air flow velocity (Darcian velocity) (i.e., equation [66]), *m/s*,
C	= Heat capacity of a material,
C_s	= volumetric heat capacity of solid phase of the soil, *J/m³-°C*,
C_w	= volumetric heat capacity of liquid phase of the soil, *J/m³-°C*,
C_v	= volumetric heat capacity of vapour phase of the soil, *J/m³-°C*,
C_i	= volumetric heat capacity of ice phase of the soil, *J/m³-°C*,
C_a	= volumetric heat capacity of dry air phase of the soil, *J/m³-°C*,
θ_s	= volumetric solid component content of the soil, *m³/m³*,
θ_L	= volumetric water content of the soil, *m³/m³*,
θ_v	= volumetric water vapor content of the soil, (i.e., equation [53]) *m³/m³*,
θ_i	= volumetric ice content of the soil, *m³/m³*, and
θ_a	= volumetric dry air content of the soil, *m³/m³*.

On the left side of the equation [52], the first term is the sensible heat by conduction, the second term is the latent heat of vapor, and the third term is the sensible heat by convection due to the water flow, vapor flow and dry air flow. The right side of the equation represents the heat storage with the soil heat capacity, vapor, and heat fusion in ice phase change.

Inserting vapor flow rate of equation [46] into the term of $L_v q_v$ in the equation [53], and get the following equation:

$$\begin{aligned}&\frac{\partial}{\partial z}\left[\left(\lambda+L_v k_{vT}\right)\frac{\partial T}{\partial z}+\frac{L_v k_{vh}}{\gamma_w}\frac{\partial u_w}{\partial z}-\frac{L_v k_{vh}}{\gamma_w}\frac{\partial u_a}{\partial z}\right]-\left(C_w q_L+C_v q_v+C_a q_a\right)\frac{\partial T}{\partial z}\\&=C\frac{\partial T}{\partial t}+L_v\frac{\partial\theta_v}{\partial t}-L_f\frac{\rho_i}{\rho_w}\frac{\partial\theta_i}{\partial t}\end{aligned} \qquad [\ 54\ ]$$

Equation [50] and equation [54] are coupled through the ice content θ_i and vapour. After the term of $\frac{\rho_i}{\rho_w}\frac{\partial\theta_i}{\partial t}$ in the equation [50] is inserted into the equation [54], the following equation is used for the heat flow governing equation coupled with moisture and air flow:

$$\begin{aligned}&\frac{\partial}{\partial z}\left(k_{21}\frac{\partial u_w}{\partial z}+k_{22}\frac{\partial T}{\partial z}+k_{23}\frac{\partial u_a}{\partial z}+L_f k_w\right)-\left(C_w q_L+C_v q_v+C_a q_a\right)\frac{\partial T}{\partial z}\\&=\left(C+L_f m_2^i+L_v m_2^v\right)\frac{\partial T}{\partial t}-L_v m_2^{vh}\frac{\partial(u_a-u_w)}{\partial t}\end{aligned} \qquad [\ 55\ ]$$

$$k_{21}=\frac{L_f k_w+L_v k_{vh}}{\gamma_w} \qquad [\ 56\ ]$$

$$k_{22} = \lambda + L_v k_{vT} + L_f k_{LT} \quad [\ 57\ ]$$

$$k_{23} = -\frac{L_v k_{vh}}{\gamma_w} \quad [\ 58\ ]$$

$$m_2^i = \frac{\partial \theta_u}{\partial T} \quad [\ 59\ ]$$

$$m_2^v = \frac{(n-\theta_w) g \omega_v h_r}{\gamma_w R(273.15+T)} \left[\frac{\partial u_{vsat}}{\partial T} - \frac{u_{vsat}}{273.15+T} + \frac{\rho_{vsat}}{\rho_w} \frac{u_a - u_w}{(273.15+T)} \right] \quad [\ 60\ ]$$

$$m_2^{vh} = \frac{\rho_{vsat} h_r}{\rho_w} \left[m_2^w + \frac{g \omega_v (n-\theta_w)}{\gamma_w R(273.15+T)} \right] \quad [\ 61\ ]$$

where:

u_w	= pore water pressure, *kPa*,
u_a	= pore air pressure, *kPa*,
k_w	= hydraulic conductivity, *m/s*,
k_{vh}	= water vapour conductivity due to the vapour pressure gradient (i.e., equation [47]), m/s,
k_{vT}	= water vapour conductivity due to the temperature gradient, as defined in equation [48]), *m/s*,
k_{LT}	= hydraulic conductivity introduced by the temperature gradient, as defined in equation [28], *m/s*,
m_2^i	= slope of soil freezing characteristic curve, and
θ_u	= volumetric unfrozen water content, m^3/m^3.

It should be noted that in the derivation of the above equation [55], the term of $L_f k_{vh}$ or $L_f k_{vT}$ are excluded, because the evaporation phase change and freezing phase change couldn't happen at the same time. It is assumed that the water evaporation only occurs at the temperature above soil freezing, and the occurrence of soil freezing phase change is constrained to the temperature interval between the liquidus temperature, T_{ef}, to solidus temperature, T_{ep}. In other words, the term of $L_f k_{vh}$ or $L_f k_{vT}$ is always 0. For the purpose of ease in the implementation, the latent heat of evaporation, L_v, and latent heat of fusion, L_f, is expressed as:

$$L_v = L_v(T)\delta(T - T_{ef}) \quad [\ 62\ ]$$

$$L_f = L_f(T) \frac{|m_2^i|}{|m_2^i| + \varepsilon} U(T - T_{ep}, T - T_{ef}) \quad [\ 63\ ]$$

where:

$L_v(T)$	= volumetric latent heat of water vaporization at the given temperature, J/m^3,
$L_f(T)$	= volumetric latent heat of fusion of water at the given temperature, J/m^3,
$\delta(x)$	= a unit function with value of $\delta(x) = 1$ *if* $x > 0$, *else* 0,
$U(x_1, x_2)$	= a unit function with value of $U(x_1, x_2) = 1$ if $x_1 > 0$ and $x_2 < 0$, else 0
ε	= an arbitrary small number, $\varepsilon = 10^{-6}$, and
m_2^i	= the slope of soil freezing curve.

The equation [62] and equation [63] are used to ensure $L_v = 0$ if $T < T_{ef}$, and $L_f = 0$ if $m_2^i = 0$ *or* $T > T_{ef}$ *and* $T < T_{ep}$.

3.1.3 Basic Equations for Air Flow

The following considerations and assumptions are made for the derivation of air flow with the two phases (water and gas):

- The air is a compressible gas,
- The bulk flow of the pore dry air is mainly driven by air pressure gradient,
- The flow of the partially dissolved air in water is governed by the water head gradient (Fredlund and Gitirana 2005; Thomas and He, 1997), and

- The diffusive effect of pore dry air can be neglected (Thomas and He, 1997).

The mass conservation of air flow can be modified on the basis of SVAIR theory manual:

$$\frac{\partial\left[\rho_a(n-(1-H_c)\theta_w\right]}{\partial t}+\frac{\partial\left[\rho_a\left(q_a+H_c q_w\right)\right]}{\partial y}=0 \qquad [\ 64\ ]$$

where:

ρ_a	= air density, *kg/m³*,
n	= porosity, dimensionless,
H_c	= Henry's volumetric coefficient of air solubility in the water, m^3/m^3,
θ_w	= volumetric water content, m^3/m^3,
q_a	= bulk air-flow, *m/s*,
q_w	= water flow, *m/s*,
y	= elevation, *m*, and
t	= time, *s*.

If the air is considered as an ideal gas, its density is

$$\rho_a = C_u \frac{\omega_a(u_a+u_{atm})}{R(273.15+T)} \qquad [\ 65\ ]$$

where:

ρ_a	= air density, kg/m^3,
u_a	= pore air pressure, *kPa*,
u_{atm}	= atmospheric pressure, *kPa*,
ω_a	= average molecular weight, 0.0288 *kg/mol*,
R	= universal gas constant 8.3144 *J/mol-K*,
T	= pore air temperature, ^oC, and
C_u	= unit conversion coefficient, for Metric units, $C_u = 1000$, and for Imperial units, $C_u = 1$.

The air flow velocity with the bulk motion obeys the Darcy law:

$$q_a = -\left[k_a + \frac{k_a}{\gamma_a}\frac{\partial u_a}{\partial y}\right] \qquad [\ 66\ ]$$

$$\gamma_a = g\rho_a / C_u$$

where:

q_a	= air flow velocity, *m/s*,
k_a	= air conductivity, *m/s*, which is the function of the degree of water saturation, and
γ_a	= unit weight of air, *kN*.

After the substitution of the equation [66] into the equation [64], the air flow governing equation is written with the format as follows:

$$\frac{\partial}{\partial z}\left[k_{31}\frac{\partial u_w}{\partial z}+k_{32}\frac{\partial T}{\partial z}+k_{33}\frac{\partial u_a}{\partial z}+\gamma_a(k_a+H_c k_w)\right]= \frac{g\omega_a}{R(273.15+T)}\left[\begin{array}{l}\left(n-(1-H_c)\theta_w\right)\frac{\partial u_a}{\partial t}+(u_a+u_{atm})\frac{\partial}{\partial t}\left(n-(1-H_c)\theta_w\right)\\ -\frac{\left(n-(1-H_c)\theta_w\right)(u_a+u_{atm})}{273.15+T}\frac{\partial T}{\partial t}\end{array}\right] \qquad [\ 67\ ]$$

Let $\theta_a = n-(1-H_c)\theta_w$, the above equation can be rewritten as

$$\frac{\partial}{\partial z}\left[k_{31}\frac{\partial u_w}{\partial z}+k_{32}\frac{\partial T}{\partial z}+k_{33}\frac{\partial u_a}{\partial z}+\gamma_a(k_a+H_c k_w)\right]= \frac{g\omega_a}{R(273.15+T)}\left[(\theta_a)\frac{\partial u_a}{\partial t}+(u_a+u_{atm})\frac{\partial}{\partial t}(\theta_a)-\frac{(\theta_a)(u_a+u_{atm})}{273.15+T}\frac{\partial T}{\partial t}\right] \quad [68]$$

$$k_{31}=\frac{\gamma_a H_c k_w}{\gamma_w},\ k_{32}=0,\ k_{33}=k_a \quad [69]$$

The Henry's coefficient of air solubility in the air is dependent of the temperature, and it is approximated with the following expression based on the data fitting as shown in Figure 3.

$$H_c=10^{-5}\left(4-9\times10^{-2}T+1\times10^{-3}T^2\right) \quad [70]$$

where:

H_C = Henry's coefficient of air solubility in the water, m^3/m^3, and

T = Temperature, ^oC.

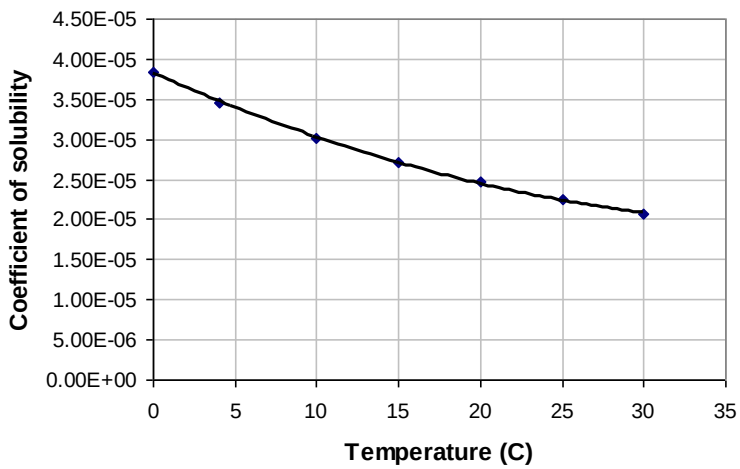

Figure 3 The relation of Henry's coefficient of air solubility in the water vs. temperature (Fredlund and Rahardjo, 1993)

NOTE:
If water evaporation is not considered, let H_c =0.

3.1.4 Determination of Ice and Hydraulic Conductivity Reduction

It is necessary to develop an advanced algorithm describing the ice change rate during soil freezing and thawing. The following analysis is a simple approach to estimate ice based on SWCC and SFCC. At any time, the ice content can be expressed as

$$\theta_i=\frac{\rho_w}{\rho_i}(\theta-\theta_u),\ if\ \theta>\theta_u$$
$$\theta_i=0 \qquad otherwise \quad [71]$$

where:

θ = volumetric water content at soil temperatures above freezing point, m^3/m^3,

θ_u = volumetric unfrozen water content at soil temperatures blow the freezing point, m^3/m^3,

θ_i = volumetric ice content, m^3/m^3,

ρ_l = water density, kg/m^3, and

ρ_i = ice density, kg/m^3.

When the soil temperature is above the soil freezing point, the soil water content, θ, is uniquely determined by matric suction through using the Soil Water Characteristic Curve (SWCC). When the soil temperature is going down to the soil freezing point, the unfrozen water uniquely depends on the soil temperature through Soil Freezing Characteristic Curve (SFCC). The relationship between SWCC and SFCC is realized through the Clapeyron as defined in Equation [34].

In the frozen soil regime, soil matric suction is calculated based on the negative soil temperature, and the soil hydraulic conductivity can be calculated using this matric suction. It can be seen from the Equation [34] that when the soil temperature goes down, the soil matric suction is dramatically increased. Consequently, the hydraulic conductivity is significantly reduced in the frozen soil region. This behavior will be discussed in the section of Material Properties of this document.

3.2 COUPLED MODEL OF MOISTURE AND HEAT FLOW

By the default neither the vapor flow is included in SVFLUX, nor thermal convection included in SVHEAT. To include the vapor flow in the analysis of moisture migration, the climate boundary including evaporation should be applied with SVFLUX. More details see the **SVFLUX theory manual**. In addition, to take account of the thermal convection into the thermal flow, the convection option should be explicitly selected in SVHEAT model settings. In addition, the pore air in the soil is assumed to connect to the atmosphere, i.e., $u_a = 0$.

3.2.1 Transient-State Coupled Model for Moisture and Heat Flow

- **1D Horizontal**

h:
$$\frac{\partial}{\partial x}\left[k^x_{11}\frac{\partial(u_w)}{\partial x}+k^x_{12}\frac{\partial T}{\partial x}\right]+S_{\sin k}=\frac{\partial\theta_u}{\partial t}+\frac{\rho_i}{\rho_w}\frac{\partial\theta_i}{\partial t} \qquad [\ 72\ ]$$

T:
$$\frac{\partial}{\partial x}\left(k^x_{21}\frac{\partial u_w}{\partial x}+k^x_{22}\frac{\partial T}{\partial x}\right)-\left(C_w q^L_x+C_v q^v_x\right)\frac{\partial T}{\partial x}+Q_{\sin k}= \left(C+L_f m^i_2+L_v m^v_2\right)\frac{\partial T}{\partial t}-L_v m^{vh}_2\frac{\partial(u_a-u_w)}{\partial t} \qquad [\ 73\ ]$$

$$k^x_{11}=\frac{k^w_x+k^{vh}}{\gamma_w},\quad k^x_{12}=k^{LT}_x+k^{vT},\quad k^{LT}_x=m^{\varphi}_2\frac{k^w_x}{\gamma_w} \qquad [\ 74\ ]$$

$$k^x_{21}=\frac{L_f k^w_x+L_v k^{vh}}{\gamma_w},\quad k^x_{22}=\lambda_x+L_v k^{vT}+L_f k^{LT}_x$$

- **1D Vertical**

h:
$$\frac{\partial}{\partial y}\left[k^y_{11}\frac{\partial(u_w)}{\partial y}+k^y_{12}\frac{\partial T}{\partial y}+k^w_y\right]+S_{\sin k}=\frac{\partial\theta_u}{\partial t}+\frac{\rho_i}{\rho_w}\frac{\partial\theta_i}{\partial t} \qquad [\ 75\ ]$$

T:
$$\frac{\partial}{\partial y}\left(k^y_{21}\frac{\partial u_w}{\partial y}+k^y_{22}\frac{\partial T}{\partial y}+L_f k^w_y\right)-\left(C_w q^L_y+C_v q^v_y\right)\frac{\partial T}{\partial y}+Q_{\sin k} =\left(C+L_f m^i_2+L_v m^v_2\right)\frac{\partial T}{\partial t}-L_v m^{vh}_2\frac{\partial(u_a-u_w)}{\partial t} \qquad [\ 76\ ]$$

$$k^y_{11}=\frac{k^w_y+k^{vh}}{\gamma_w},\quad k^y_{12}=k^{LT}_y+k^{vT},\quad k^{LT}_y=m^{\varphi}_2\frac{k^w_y}{\gamma_w}$$
$$k^y_{21}=\frac{L_f k^w_y+L_v k^{vh}}{\gamma_w},\quad k^y_{22}=\lambda_y+L_v k^{vT}+L_f k^{LT}_y \qquad [\ 77\ ]$$

- **2D**

h:
$$\frac{\partial}{\partial x}\left[k^x_{11}\frac{\partial(u_w)}{\partial x}+k^x_{12}\frac{\partial T}{\partial x}\right]+\frac{\partial}{\partial y}\left[k^y_{11}\frac{\partial(u_w)}{\partial y}+k^y_{12}\frac{\partial T}{\partial y}+k^w_y\right]+S_{\sin k}=\frac{\partial\theta_u}{\partial t}+\frac{\rho_i}{\rho_w}\frac{\partial\theta_i}{\partial t} \qquad [\ 78\ ]$$

T:
$$\frac{\partial}{\partial x}\left[k^x_{21}\frac{\partial(u_w)}{\partial x}+k^x_{22}\frac{\partial T}{\partial x}\right]+\frac{\partial}{\partial y}\left[k^y_{21}\frac{\partial(u_w)}{\partial y}+k^y_{22}\frac{\partial T}{\partial y}+L_f k^w_y\right] -\left[C_w q^L_x+C_v q^v_x\right]\frac{\partial T}{\partial x}-\left[C_w q^L_y+q^v_y\right]\frac{\partial T}{\partial y}+Q_{\sin k} =\left(C+L_f m^i_2+L_v m^v_2\right)\frac{\partial T}{\partial t}-L_v m^{vh}_2\frac{\partial(u_a-u_w)}{\partial t} \qquad [\ 79\ ]$$

$$k_{11}^{x} = \frac{k_{x}^{w} + k^{vh}}{\gamma_w}, \quad k_{11}^{y} = \frac{k_{y}^{w} + k^{vh}}{\gamma_w} \qquad [\ 80\ ]$$

$$k_{12}^{x} = k_{x}^{LT} + k^{vT}, \quad k_{12}^{y} = k_{y}^{LT} + k^{vT} \qquad [\ 81\ ]$$

$$k_{21}^{x} = \frac{L_f k_{x}^{w} + L_v k^{vh}}{\gamma_w}, \quad k_{21}^{y} = \frac{L_f k_{y}^{w} + L_v k^{vh}}{\gamma_w} \qquad [\ 82\ ]$$

$$k_{22}^{x} = \lambda_x + L_v k^{vT} + L_f k_{x}^{LT}, \quad k_{22}^{y} = \lambda_y + L_v k^{vT} + L_f k_{y}^{LT} \qquad [\ 83\ ]$$

$$k_{x}^{LT} = m_2^{\varphi} \frac{k_{x}^{w}}{\gamma_w}, \quad k_{y}^{LT} = m_2^{\varphi} \frac{k_{y}^{w}}{\gamma_w} \qquad [\ 84\ ]$$

- **Plane**

h:

$$\frac{\partial}{\partial x}\left[k_{11}^{x}\frac{\partial(u_w)}{\partial x} + k_{12}^{x}\frac{\partial T}{\partial x}\right] + \frac{\partial}{\partial y}\left[k_{11}^{y}\frac{\partial(u_w)}{\partial y} + k_{12}^{x}\frac{\partial T}{\partial y}\right] + S_{\sin k} = \frac{\partial \theta_u}{\partial t} + \frac{\rho_i}{\rho_w}\frac{\partial \theta_i}{\partial t} \qquad [\ 85\ ]$$

T:

$$\begin{aligned}&\frac{\partial}{\partial x}\left[k_{21}^{x}\frac{\partial(u_w)}{\partial x} + k_{22}^{x}\frac{\partial T}{\partial x}\right] + \frac{\partial}{\partial y}\left[k_{21}^{y}\frac{\partial(u_w)}{\partial y} + k_{22}^{y}\frac{\partial T}{\partial y}\right]\\ &-\left[C_w q_x^L + C_v q_x^v\right]\frac{\partial T}{\partial x} - \left[C_w q_y^L + q_y^v\right]\frac{\partial T}{\partial y} + Q_{\sin k}\\ &= \left(C + L_f m_2^i + L_v m_2^v\right)\frac{\partial T}{\partial t} - L_v m_2^{vh}\frac{\partial(u_a - u_w)}{\partial t}\end{aligned} \qquad [\ 86\ ]$$

$$k_{11}^{x} = \frac{k_{x}^{w} + k^{vh}}{\gamma_w}, \quad k_{11}^{y} = \frac{k_{y}^{w} + k^{vh}}{\gamma_w} \qquad [\ 87\ ]$$

$$k_{12}^{x} = k_{x}^{LT} + k^{vT}, \quad k_{12}^{y} = k_{y}^{LT} + k^{vT} \qquad [\ 88\ ]$$

$$k_{21}^{x} = \frac{L_f k_{x}^{w} + L_v k^{vh}}{\gamma_w}, \quad k_{21}^{y} = \frac{L_f k_{y}^{w} + L_v k^{vh}}{\gamma_w} \qquad [\ 89\ ]$$

$$k_{22}^{x} = \lambda_x + L_v k^{vT} + L_f k_{x}^{LT}, \quad k_{22}^{y} = \lambda_y + L_v k^{vT} + L_f k_{y}^{LT} \qquad [\ 90\ ]$$

$$k_{x}^{LT} = m_2^{\varphi} \frac{k_{x}^{w}}{\gamma_w}, \quad k_{y}^{LT} = m_2^{\varphi} \frac{k_{y}^{w}}{\gamma_w} \qquad [\ 91\ ]$$

- **Axis-Symmetric**

h:

$$\begin{aligned}&\frac{\partial}{\partial r}\left[k_{11}^{r}\frac{\partial(u_w)}{\partial r} + k_{12}^{r}\frac{\partial T}{\partial r}\right] + \frac{k_{11}^{r}}{r}\frac{\partial u_w}{\partial r} + \frac{k_{12}^{r}}{r}\frac{\partial T}{\partial r} +\\ &\frac{\partial}{\partial z}\left[k_{11}^{z}\frac{\partial(u_w)}{\partial z} + k_{12}^{z}\frac{\partial T}{\partial z} + k_{z}^{w}\right] + S_{\sin k} = \frac{\partial \theta_u}{\partial t} + \frac{\rho_i}{\rho_w}\frac{\partial \theta_i}{\partial t}\end{aligned} \qquad [\ 92\ ]$$

T:

$$\begin{aligned}&\frac{\partial}{\partial r}\left[k_{21}^{r}\frac{\partial(u_w)}{\partial r} + k_{22}^{r}\frac{\partial T}{\partial r}\right] + \frac{k_{21}^{r}}{r}\frac{\partial u_w}{\partial r} + \frac{k_{22}^{r}}{r}\frac{\partial T}{\partial r} + \frac{\partial}{\partial z}\left[k_{21}^{z}\frac{\partial(u_w)}{\partial z} + k_{22}^{z}\frac{\partial T}{\partial z} + L_f k_{z}^{w}\right]\\ &-\left[C_w q_r^L + C_w q_r^v\right]\frac{\partial T}{\partial r} - \left[C_v q_z^L + C_v q_z^v\right]\frac{\partial T}{\partial z} + Q_{\sin k}\\ &= \left(C + L_f m_2^i + L_v m_2^v\right)\frac{\partial T}{\partial t} - L_v m_2^{vh}\frac{\partial(u_a - u_w)}{\partial t}\end{aligned} \qquad [\ 93\ ]$$

$$k_{11}^{r} = \frac{k_{r}^{w} + k^{vh}}{\gamma_w}, \quad k_{11}^{z} = \frac{k_{z}^{w} + k^{vh}}{\gamma_w} \qquad [\ 94\ ]$$

$$k_{12}^{r} = k_{r}^{LT} + k^{vT}, \quad k_{12}^{z} = k_{z}^{LT} + k^{vT} \qquad [\ 95\ ]$$

$$k_{21}^{r} = \frac{L_f k_r^w + L_v k^{vh}}{\gamma_w}, \quad k_{21}^{z} = \frac{L_f k_z^w + L_v k^{vh}}{\gamma_w} \qquad [\ 96\ ]$$

$$k_{22}^{r} = \lambda_r + L_v k^{vT} + L_f k_r^{LT}, \quad k_{22}^{z} = \lambda_z + L_v k^{vT} + L_f k_z^{LT} \qquad [\ 97\ ]$$

$$k_r^{LT} = m_2^{\varphi} \frac{k_r^w}{\gamma_w}, \quad k_z^{LT} = m_2^{\varphi} \frac{k_z^w}{\gamma_w} \qquad [\ 98\ ]$$

- **3D**

h:

$$\frac{\partial}{\partial x}\left[k_{11}^{x} \frac{\partial(u_w)}{\partial x} + k_{12}^{x} \frac{\partial T}{\partial x}\right] + \frac{\partial}{\partial y}\left[k_{11}^{y} \frac{\partial(u_w)}{\partial y} + k_{12}^{y} \frac{\partial T}{\partial y}\right] + \frac{\partial}{\partial z}\left[k_{11}^{z} \frac{\partial(u_w)}{\partial z} + k_{12}^{z} \frac{\partial T}{\partial z} + k_z\right]$$
$$+ S_{\sin k} = \frac{\partial \theta_u}{\partial t} + \frac{\rho_i}{\rho_w} \frac{\partial \theta_i}{\partial t} \qquad [\ 99\ ]$$

T:

$$\frac{\partial}{\partial x}\left[k_{21}^{x} \frac{\partial(u_w)}{\partial x} + k_{22}^{x} \frac{\partial T}{\partial x}\right] + \frac{\partial}{\partial y}\left[k_{21}^{y} \frac{\partial(u_w)}{\partial y} + k_{22}^{y} \frac{\partial T}{\partial y}\right] + \frac{\partial}{\partial z}\left[k_{21}^{z} \frac{\partial(u_w)}{\partial z} + k_{22}^{z} \frac{\partial T}{\partial z} + L_f k_z\right]$$
$$-\left(C_w q_x^L + C_v q_x^v\right)\frac{\partial T}{\partial x} - \left(C_w q_y^L + C_v q_y^v\right)\frac{\partial T}{\partial y} - \left(C_w q_z^L + C_v q_z^v\right)\frac{\partial T}{\partial z} + Q_{\sin k} \qquad [\ 100\ ]$$
$$== \left(C + L_f m_2^i + L_v m_2^v\right)\frac{\partial T}{\partial t} - L_v m_2^{vh} \frac{\partial(u_a - u_w)}{\partial t}$$

$$k_{11}^{x} = \frac{k_x^w + k^{vh}}{\gamma_w}, \quad k_{11}^{y} = \frac{k_y^w + k^{vh}}{\gamma_w}, \quad k_{11}^{z} = \frac{k_z^w + k^{vh}}{\gamma_w} \qquad [\ 101\ ]$$

$$k_{12}^{x} = k_x^{LT} + k^{vT}, \quad k_{12}^{y} = k_y^{LT} + k^{vT}, \quad k_{12}^{z} = k_z^{LT} + k^{vT} \qquad [\ 102\ ]$$

$$k_{21}^{x} = \frac{L_f k_x^w + L_v k^{vh}}{\gamma_w}, \quad k_{21}^{y} = \frac{L_f k_y^w + L_v k^{vh}}{\gamma_w}, \quad k_{21}^{z} = \frac{L_f k_z^w + L_v k^{vh}}{\gamma_w} \qquad [\ 103\ ]$$

$$k_{22}^{x} = \lambda_x + L_v k^{vT} + L_f k_x^{LT}, \quad k_{22}^{y} = \lambda_y + L_v k^{vT} + L_f k_y^{LT}, \quad k_{22}^{z} = \lambda_z + L_v k^{vT} + L_f k_z^{LT} \qquad [\ 104\ ]$$

$$k_x^{LT} = m_2^{\varphi} \frac{k_x^w}{\gamma_w}, \quad k_y^{LT} = m_2^{\varphi} \frac{k_y^w}{\gamma_w}, \quad k_z^{LT} = m_2^{\varphi} \frac{k_z^w}{\gamma_w} \qquad [\ 105\ ]$$

where:

u_w	= pore water pressure due to hydraulic head, *kPa*,
T	= material temperature, *°C*,
t	= time, *s*,
k_x^w, k_y^w, k_z^w, k_r^w	= hydraulic conductivity in *x*, *y*, *z*, or *r*-directions, *m/s*. For a homogenous material, $k = k_x^w = k_y^w = k_z^w = k_r^w$,
k^{vh}	= pore-water vapor conductivity by vapor diffusion within the air phase, *m/s*, see equation [47]
k^{vT}	= vapor diffusion due to temperature gradient, *m/s,* see equation [48],
γ_w	= unit weight of water, kN/m^3,
$\lambda_x, \lambda_y, \lambda_z, \lambda_r$	= thermal conductivity in *x*, *y*, *z*, or *r*-directions, *J/(s-m-°C),* For a homogenous material, $\lambda_x = \lambda_y = \lambda_z = \lambda_r$,
q_x^L, q_y^L, q_z^L, q_r^L	= pore-water flow rate (Darcian velocity) in the *x, y, z, or r*-direction across a unit area of the soil due to the hydraulic head gradient, *m/s*, see equation [27],
q_x^v, q_y^v, q_z^v, q_r^v	= water vapor flow rate (Darcian velocity) in the *x, y, z, or r*-direction across a unit area of the soil due to the hydraulic head gradient, *m/s*, see equation [46],
L_v	= volumetric latent heat of water vaporization or condensation, see equation [62], J/m^3,

L_f	=	volumetric latent heat of water freezing or thawing, as given in equation [63], J/m^3,
C_w	=	volumetric heat capacity of water, $J/(m^3\text{-}°C)$,
C_v	=	volumetric heat capacity of vapour, $J/(m^3\text{-}°C)$,
C	=	volumetric heat capacity of soil, $J/(m^3\text{-}°C)$,
θ_v	=	volumetric water vapour content, m^3/m^3,
m_2^i	=	slope of soil Freezing characteristic curve,
m_2^φ	=	slope of the relation of soil matric suction to the temperature,
m_2^v	=	defined in equation [60], and
m_2^{vh}	=	defined in equation [61].

NOTE:
The water vaporization factor is included only when a vaporization climate boundary condition is applied. Otherwise, $k_{vT} = 0$, and $k_{vh} = 0$.
If the water flow induced by temperature gradient is neglected, let $k_{LT} = 0$.

3.2.2 Steady-State Coupled Model of Moisture and Heat Flow

- **1D Horizontal**

h:
$$\frac{\partial}{\partial x}\left[k_{11}^{x}\frac{\partial(u_w)}{\partial x}+k_{12}\frac{\partial T}{\partial x}\right]+S_{\sin k}=0 \qquad [\ 106\ ]$$

T:
$$\frac{\partial}{\partial x}\left(k_{21}^{x}\frac{\partial u_w}{\partial x}+k_{22}^{x}\frac{\partial T}{\partial x}\right)-\left(C_w q_x^L+C_v q_x^v\right)\frac{\partial T}{\partial x}+Q_{\sin k}=0 \qquad [\ 107\ ]$$

$$k_{11}^{x}=\frac{k_x^w+k^{vh}}{\gamma_w},\quad k_{12}^{x}=k_x^{LT}+k^{vT},\quad k_x^{LT}=m_2^{\varphi}\frac{k_x^w}{\gamma_w}$$
$$k_{21}^{x}=\frac{L_f k_x^w+L_v k^{vh}}{\gamma_w},\quad k_{22}^{x}=\lambda_x+L_v k^{vT}+L_f k_x^{LT} \qquad [\ 108\ ]$$

- **1D Vertical**

h:
$$\frac{\partial}{\partial y}\left[k_{11}^{y}\frac{\partial(u_w)}{\partial y}+k_{12}\frac{\partial T}{\partial y}+k_y^w\right]+S_{\sin k}=0 \qquad [\ 109\ ]$$

T:
$$\frac{\partial}{\partial y}\left(k_{21}^{y}\frac{\partial u_w}{\partial y}+k_{22}^{y}\frac{\partial T}{\partial y}+L_f k_y^w\right)-\left(C_w q_y^L+C_v q_y^v\right)\frac{\partial T}{\partial y}+Q_{\sin k}=0 \qquad [\ 110\ ]$$

$$k_{11}^{y}=\frac{k_y^w+k^{vh}}{\gamma_w},\quad k_{12}^{y}=k_y^{LT}+k^{vT},\quad k_y^{LT}=m_2^{\varphi}\frac{k_y^w}{\gamma_w}$$
$$k_{21}^{y}=\frac{L_f k_y^w+L_v k^{vh}}{\gamma_w},\quad k_{22}^{y}=\lambda_y+L_v k^{vT}+L_f k_y^{LT} \qquad [\ 111\ ]$$

- **2D**

h:
$$\frac{\partial}{\partial x}\left[k_{11}^{x}\frac{\partial(u_w)}{\partial x}+k_{12}^{x}\frac{\partial T}{\partial x}\right]+\frac{\partial}{\partial y}\left[k_{11}^{y}\frac{\partial(u_w)}{\partial y}+k_{12}^{y}\frac{\partial T}{\partial y}+k_y^w\right]+S_{\sin k}=0 \qquad [\ 112\ ]$$

T:
$$\frac{\partial}{\partial x}\left[k_{21}^{x}\frac{\partial(u_w)}{\partial x}+k_{22}^{x}\frac{\partial T}{\partial x}\right]+\frac{\partial}{\partial y}\left[k_{21}^{y}\frac{\partial(u_w)}{\partial y}+k_{22}^{y}\frac{\partial T}{\partial y}+L_f k_y^w\right]+Q_{\sin k}$$
$$-\left[C_w q_x^L+C_v q_x^v\right]\frac{\partial T}{\partial x}-\left[C_w q_y^L+q_y^v\right]\frac{\partial T}{\partial y}=0 \qquad [\ 113\ ]$$

$$k_{11}^{x}=\frac{k_x^w+k^{vh}}{\gamma_w},\quad k_{11}^{y}=\frac{k_y^w+k^{vh}}{\gamma_w} \qquad [\ 114\ ]$$

$$k_{12}^{x} = k_{x}^{LT} + k^{vT}, \quad k_{12}^{y} = k_{y}^{LT} + k^{vT} \qquad [\ 115\ ]$$

$$k_{21}^{x} = \frac{L_f k_x^w + L_v k^{vh}}{\gamma_w}, \quad k_{21}^{y} = \frac{L_f k_y^w + L_v k^{vh}}{\gamma_w} \qquad [\ 116\ ]$$

$$k_{22}^{x} = \lambda_x + L_v k^{vT} + L_f k_x^{LT}, \quad k_{22}^{y} = \lambda_y + L_v k^{vT} + L_f k_y^{LT} \qquad [\ 117\ ]$$

$$k_x^{LT} = m_2^{\varphi} \frac{k_x^w}{\gamma_w}, \quad k_y^{LT} = m_2^{\varphi} \frac{k_y^w}{\gamma_w} \qquad [\ 118\ ]$$

- **Plane**

h:

$$\frac{\partial}{\partial x}\left[k_{11}^{x} \frac{\partial(u_w)}{\partial x} + k_{12}^{x} \frac{\partial T}{\partial x}\right] + \frac{\partial}{\partial y}\left[k_{11}^{y} \frac{\partial(u_w)}{\partial y} + k_{12}^{y} \frac{\partial T}{\partial y}\right] + S_{\sin k} = 0 \qquad [\ 119\ ]$$

T:

$$\begin{aligned} &\frac{\partial}{\partial x}\left[k_{21}^{x} \frac{\partial(u_w)}{\partial x} + k_{22}^{x} \frac{\partial T}{\partial x}\right] + \frac{\partial}{\partial y}\left[k_{21}^{y} \frac{\partial(u_w)}{\partial y} + k_{22}^{y} \frac{\partial T}{\partial y}\right] \\ &- \left[C_w q_x^L + C_v q_x^v\right]\frac{\partial T}{\partial x} - \left[C_w q_y^L + q_y^v\right]\frac{\partial T}{\partial y} + Q_{\sin k} = 0 \end{aligned} \qquad [\ 120\ ]$$

$$k_{11}^{x} = \frac{k_x^w + k^{vh}}{\gamma_w}, \quad k_{11}^{y} = \frac{k_y^w + k^{vh}}{\gamma_w} \qquad [\ 121\ ]$$

$$k_{12}^{x} = k_{x}^{LT} + k^{vT}, \quad k_{12}^{y} = k_{y}^{LT} + k^{vT} \qquad [\ 122\ ]$$

$$k_{21}^{x} = \frac{L_f k_x^w + L_v k^{vh}}{\gamma_w}, \quad k_{21}^{y} = \frac{L_f k_y^w + L_v k^{vh}}{\gamma_w} \qquad [\ 123\ ]$$

$$k_{22}^{x} = \lambda_x + L_v k^{vT} + L_f k_x^{LT}, \quad k_{22}^{y} = \lambda_y + L_v k^{vT} + L_f k_y^{LT} \qquad [\ 124\ ]$$

$$k_x^{LT} = m_2^{\varphi} \frac{k_x^w}{\gamma_w}, \quad k_y^{LT} = m_2^{\varphi} \frac{k_y^w}{\gamma_w} \qquad [\ 125\ ]$$

- **Axis-Symmetric**

h:

$$\frac{\partial}{\partial r}\left[k_{11}^{r} \frac{\partial(u_w)}{\partial r} + k_{12}^{r} \frac{\partial T}{\partial r}\right] + \frac{k_{11}^{r}}{r}\frac{\partial u_w}{\partial r} + \frac{k_{12}^{r}}{r}\frac{\partial T}{\partial r} + \frac{\partial}{\partial z}\left[k_{11}^{y} \frac{\partial(u_w)}{\partial z} + k_{12}^{z} \frac{\partial T}{\partial z}\right] + S_{\sin k} = 0 \qquad [\ 126\ ]$$

T:

$$\begin{aligned} &\frac{\partial}{\partial r}\left[k_{21}^{r} \frac{\partial(u_w)}{\partial r} + k_{22}^{r} \frac{\partial T}{\partial r}\right] + \frac{k_{21}^{r}}{r}\frac{\partial u_w}{\partial r} + \frac{k_{22}^{r}}{r}\frac{\partial T}{\partial r} + \frac{\partial}{\partial z}\left[k_{21}^{z} \frac{\partial(u_w)}{\partial z} + k_{22}^{z} \frac{\partial T}{\partial z}\right] \\ &- \left[C_w q_r^L + C_w q_r^v\right]\frac{\partial T}{\partial r} - \left[C_v q_z^L + C_v q_z^v\right]\frac{\partial T}{\partial z} + Q_{\sin k} = 0 \end{aligned} \qquad [\ 127\ ]$$

$$k_{11}^{r} = \frac{k_r^w + k^{vh}}{\gamma_w}, \quad k_{11}^{z} = \frac{k_z^w + k^{vh}}{\gamma_w} \qquad [\ 128\ ]$$

$$k_{12}^{r} = k_{r}^{LT} + k^{vT}, \quad k_{12}^{z} = k_{z}^{LT} + k^{vT} \qquad [\ 129\ ]$$

$$k_{21}^{r} = \frac{L_f k_r^w + L_v k^{vh}}{\gamma_w}, \quad k_{21}^{z} = \frac{L_f k_z^w + L_v k^{vh}}{\gamma_w} \qquad [\ 130\ ]$$

$$k_{22}^{r} = \lambda_r + L_v k^{vT} + L_f k_r^{LT}, \quad k_{22}^{z} = \lambda_z + L_v k^{vT} + L_f k_z^{LT} \qquad [\ 131\ ]$$

$$k_r^{LT} = m_2^{\varphi} \frac{k_r^w}{\gamma_w}, \quad k_z^{LT} = m_2^{\varphi} \frac{k_z^w}{\gamma_w} \qquad [\ 132\ ]$$

- **3D**

h:
$$\frac{\partial}{\partial x}\left[k_{11}^{x}\frac{\partial(u_w)}{\partial x}+k_{12}^{x}\frac{\partial T}{\partial x}\right]+\frac{\partial}{\partial y}\left[k_{11}^{y}\frac{\partial(u_w)}{\partial y}+k_{12}^{y}\frac{\partial T}{\partial y}\right]+\frac{\partial}{\partial z}\left[k_{11}^{z}\frac{\partial(u_w)}{\partial z}+k_{12}^{z}\frac{\partial T}{\partial z}+k_z\right]+S_{\sin k}=0 \quad [133]$$

T:
$$\frac{\partial}{\partial x}\left[k_{21}^{x}\frac{\partial(u_w)}{\partial x}+k_{22}^{x}\frac{\partial T}{\partial x}\right]+\frac{\partial}{\partial y}\left[k_{21}^{y}\frac{\partial(u_w)}{\partial y}+k_{22}^{y}\frac{\partial T}{\partial y}\right]+\frac{\partial}{\partial z}\left[k_{21}^{z}\frac{\partial(u_w)}{\partial z}+k_{22}^{z}\frac{\partial T}{\partial z}+L_f k_z\right]-\left(C_w q_x^L+C_v q_x^v\right)\frac{\partial T}{\partial x}-\left(C_w q_y^L+C_v q_y^v\right)\frac{\partial T}{\partial y}-\left(C_w q_z^L+C_v q_z^v\right)\frac{\partial T}{\partial z}+Q_{\sin k}=0 \quad [134]$$

$$k_{11}^{x}=\frac{k_x^w+k^{vh}}{\gamma_w},\quad k_{11}^{y}=\frac{k_y^w+k^{vh}}{\gamma_w},\quad k_{11}^{z}=\frac{k_z^w+k^{vh}}{\gamma_w} \quad [135]$$

$$k_{12}^{x}=k_x^{LT}+k^{vT},\quad k_{12}^{y}=k_y^{LT}+k^{vT},\quad k_{12}^{z}=k_z^{LT}+k^{vT} \quad [136]$$

$$k_{21}^{x}=\frac{L_f k_x^w+L_v k^{vh}}{\gamma_w},\quad k_{21}^{y}=\frac{L_f k_y^w+L_v k^{vh}}{\gamma_w},\quad k_{21}^{z}=\frac{L_f k_z^w+L_v k^{vh}}{\gamma_w} \quad [137]$$

$$k_{22}^{x}=\lambda_x+L_v k^{vT}+L_f k_x^{LT},\quad k_{22}^{y}=\lambda_y+L_v k^{vT}+L_f k_y^{LT},\quad k_{22}^{z}=\lambda_z+L_v k^{vT}+L_f k_z^{LT} \quad [138]$$

$$k_x^{LT}=m_2^{\varphi}\frac{k_x^w}{\gamma_w},\quad k_y^{LT}=m_2^{\varphi}\frac{k_y^w}{\gamma_w},\quad k_z^{LT}=m_2^{\varphi}\frac{k_z^w}{\gamma_w} \quad [139]$$

3.3 COUPLED MODEL FOR HEAT AND AIR FLOW

If moisture flow is not considered, the Henry's air solubility coefficient, H_c = 0, and the water evaporation is neglected. The governing equations for air flow and heat flow are simplified as described in the following sections.

3.3.1 Transient-State Coupled Model of Heat Flow and Air Flow

- **1D Horizontal**

u_a:
$$\frac{\partial}{\partial x}\left(k_x^a\frac{\partial u_a}{\partial x}\right)=\frac{g\omega_a}{R(273.15+T)}\left[\theta_a\frac{\partial u_a}{\partial t}-\frac{\theta_a(u_a+u_{atm})}{273.15+T}\frac{\partial T}{\partial t}\right] \quad [140]$$

T:
$$\frac{\partial}{\partial x}\left(\lambda_x\frac{\partial T}{\partial x}\right)-\left(C_a q_x^a\right)\frac{\partial T}{\partial x}+Q_{\sin k}=\left(C+L_f m_2^i\right)\frac{\partial T}{\partial t} \quad [141]$$

- **1D Vertical**

u_a:
$$\frac{\partial}{\partial y}\left(k_y^a\frac{\partial u_a}{\partial y}+\gamma_a k_y^a\right)=\frac{g\omega_a}{R(273.15+T)}\left[\theta_a\frac{\partial u_a}{\partial t}-\frac{\theta_a(u_a+u_{atm})}{273.15+T}\frac{\partial T}{\partial t}\right] \quad [142]$$

T:
$$\frac{\partial}{\partial y}\left(\lambda_y\frac{\partial T}{\partial y}\right)-\left(C_a q_y^a\right)\frac{\partial T}{\partial y}+Q_{\sin k}=\left(C+L_f m_2^i\right)\frac{\partial T}{\partial t} \quad [143]$$

- **2D**

u_a:
$$\frac{\partial}{\partial x}\left(k_x^a\frac{\partial u_a}{\partial x}\right)+\frac{\partial}{\partial y}\left(k_y^a\frac{\partial u_a}{\partial y}+\gamma_a k_y^a\right)=\frac{g\omega_a}{R(273.15+T)}\left[\theta_a\frac{\partial u_a}{\partial t}-\frac{\theta_a(u_a+u_{atm})}{273.15+T}\frac{\partial T}{\partial t}\right] \quad [144]$$

T:
$$\frac{\partial}{\partial x}\left(\lambda_x\frac{\partial T}{\partial x}\right)+\frac{\partial}{\partial y}\left(\lambda_y\frac{\partial T}{\partial y}\right)-\left(C_a q_x^a\right)\frac{\partial T}{\partial x}-\left(C_a q_y^a\right)\frac{\partial T}{\partial y}+Q_{\sin k}=\left(C+L_f m_2^i\right)\frac{\partial T}{\partial t} \quad [145]$$

- **Plane**

u_a:

$$\frac{\partial}{\partial x}\left(k_x^a \frac{\partial u_a}{\partial x}\right)+\frac{\partial}{\partial y}\left(k_y^a \frac{\partial u_a}{\partial y}\right)=\frac{g\omega_a}{R(273.15+T)}\left[\theta_a \frac{\partial u_a}{\partial t}-\frac{\theta_a(u_a+u_{atm})}{273.15+T}\frac{\partial T}{\partial t}\right] \quad [146]$$

T:

$$\frac{\partial}{\partial x}\left(\lambda_x \frac{\partial T}{\partial x}\right)+\frac{\partial}{\partial y}\left(\lambda_y \frac{\partial T}{\partial y}\right)-\left(C_a q_x^a\right)\frac{\partial T}{\partial x}-\left(C_a q_y^a\right)\frac{\partial T}{\partial y}+Q_{\sin k} = \left(C+L_f m_2^i\right)\frac{\partial T}{\partial t} \quad [147]$$

- **Axisymmetric**

u_a:

$$\frac{\partial}{\partial r}\left(k_r^a \frac{\partial u_a}{\partial r}\right)+\frac{k_r^a}{r}\frac{\partial u_a}{\partial r}+\frac{\partial}{\partial z}\left(k_z^a \frac{\partial u_a}{\partial z}+\gamma_a k_z^a\right)= \frac{g\omega_a}{R(273.15+T)}\left[\theta_a \frac{\partial u_a}{\partial t}-\frac{\theta_a(u_a+u_{atm})}{273.15+T}\frac{\partial T}{\partial t}\right] \quad [148]$$

T:

$$\frac{\partial}{\partial r}\left(\lambda_r \frac{\partial T}{\partial r}\right)+\frac{\lambda_r}{r}\frac{\partial T}{\partial r}+\frac{\partial}{\partial z}\left(\lambda_z \frac{\partial T}{\partial z}\right)-\left(C_a q_r^a\right)\frac{\partial T}{\partial r} -\left(C_a q_z^a\right)\frac{\partial T}{\partial z}+Q_{\sin k}=\left(C+L_f m_2^i\right)\frac{\partial T}{\partial t} \quad [149]$$

- **Three-Dimensional**

u_a:

$$\frac{\partial}{\partial x}\left(k_x^a \frac{\partial u_a}{\partial x}\right)+\frac{\partial}{\partial y}\left(k_y^a \frac{\partial u_a}{\partial y}\right)+\frac{\partial}{\partial z}\left(k_z^a \frac{\partial u_a}{\partial z}+\gamma_a k_z^a\right)= \frac{g\omega_a}{R(273.15+T)}\left[\theta_a \frac{\partial u_a}{\partial t}-\frac{\theta_a(u_a+u_{atm})}{273.15+T}\frac{\partial T}{\partial t}\right] \quad [150]$$

T:

$$\frac{\partial}{\partial x}\left(\lambda_x \frac{\partial T}{\partial x}\right)+\frac{\partial}{\partial y}\left(\lambda_y \frac{\partial T}{\partial y}\right)+\frac{\partial}{\partial z}\left(\lambda_z \frac{\partial T}{\partial z}\right) -\left(C_a q_x^a\right)\frac{\partial T}{\partial x}-\left(C_a q_y^a\right)\frac{\partial T}{\partial y}-\left(C_a q_z^a\right)\frac{\partial T}{\partial z}+Q_{\sin k}=\left(C+L_f m_2^i\right)\frac{\partial T}{\partial t} \quad [151]$$

where:

u_a	= pore-air pressure, *kPa*,
k_x^a, k_y^a k_z^a, k_r^a	= air conductivity of the material in the *x, y, z, or r*-directions, *m/s*. For homogenous material, $k_x^a = k_y^a = k_z^a = k_r^a$,
γ_a	= unit of air weight, kN/m^3,
n	= porosity, dimensionless,
θ_w	= volumetric water content of a material, m^3/m^3,
ω_a	= average molecular weight of air 0.0288 *kg/mol*,
g	= acceleration due to gravity, 9.81 m/s^2,
R	= universal gas constant, 8.3144 *J/mol-K*,
T	= temperature, °*C*,
λ_x, λ_y, λ_z, λ_z	= thermal conductivity in *x*, *y*, *z*, or *r*-direction, *J/(s-m-°C)*. For a homogenous material, $\lambda_x = \lambda_y, = \lambda_z, = \lambda_r$,
q_x^a, q_y^a, q_z^a, q_r^a	= pore-air flow velocity (Darcian velocity) in the *x, y, z, or r*-direction across a unit area of the soil due to the air pressure gradient or the temperature gradient, *m/s*,
L_f	= volumetric latent heat of water freezing or thawing, J/m^3, $L_f = 3.334\text{x}10^8\ J/m^3$ if $T_{ef} > T > T_{ep}$, otherwise = *0.*
T_{ef}	= temperature at soil freezing point, °*C*,
T_{ep}	= temperature at the end of phase change during freezing, °*C* ,
C_a	= volumetric heat capacity of air, $J/(m^3\text{-°}C)$,
C	= volumetric heat capacity of the soil, $J/(m^3\text{-°}C)$,
m_2^i	= slope of soil Freezing characteristic curve, and

Q_{sink} = heat source or sink, $J/s\text{-}m^3$.

3.3.2 Steady-State Coupled Model of Heat Flow and Air Flow

- **1D Horizontal**

u_a:
$$\frac{\partial}{\partial x}\left(k_x^a \frac{\partial u_a}{\partial x}\right) = 0 \qquad [152]$$

T:
$$\frac{\partial}{\partial x}\left(\lambda_x \frac{\partial T}{\partial x}\right) - \left(C_a q_x^a\right)\frac{\partial T}{\partial x} + Q_{\sin k} = 0 \qquad [153]$$

- **1D Vertical**

u_a:
$$\frac{\partial}{\partial y}\left(k_y^a \frac{\partial u_a}{\partial y} + \gamma_a k_y^a\right) = 0 \qquad [154]$$

T:
$$\frac{\partial}{\partial y}\left(\lambda_y \frac{\partial T}{\partial y}\right) - \left(C_a q_y^a\right)\frac{\partial T}{\partial y} + Q_{\sin k} = 0 \qquad [155]$$

- **2D**

u_a:
$$\frac{\partial}{\partial x}\left(k_x^a \frac{\partial u_a}{\partial x}\right) + \frac{\partial}{\partial y}\left(k_y^a \frac{\partial u_a}{\partial y} + \gamma_a k_y^a\right) = 0 \qquad [156]$$

T:
$$\frac{\partial}{\partial x}\left(\lambda_x \frac{\partial T}{\partial x}\right) + \frac{\partial}{\partial y}\left(\lambda_y \frac{\partial T}{\partial y}\right) - \left(C_a q_x^a\right)\frac{\partial T}{\partial x} - \left(C_a q_y^a\right)\frac{\partial T}{\partial y} + Q_{\sin k} = 0 \qquad [157]$$

- **Plane**

u_a:
$$\frac{\partial}{\partial x}\left(k_x^a \frac{\partial u_a}{\partial x}\right) + \frac{\partial}{\partial y}\left(k_y^a \frac{\partial u_a}{\partial y}\right) = 0 \qquad [158]$$

T:
$$\frac{\partial}{\partial x}\left(\lambda_x \frac{\partial T}{\partial x}\right) + \frac{\partial}{\partial y}\left(\lambda_y \frac{\partial T}{\partial y}\right) - \left(C_a q_x^a\right)\frac{\partial T}{\partial x} - \left(C_a q_y^a\right)\frac{\partial T}{\partial y} + Q_{\sin k} = 0 \qquad [159]$$

- **Axisymmetric**

u_a:
$$\frac{\partial}{\partial r}\left(k_r^a \frac{\partial u_a}{\partial r}\right) + \frac{k_r^a}{r}\frac{\partial u_a}{\partial r} + \frac{\partial}{\partial z}\left(k_z^a \frac{\partial u_a}{\partial z} + \gamma_a k_z^a\right) = 0 \qquad [160]$$

T:
$$\frac{\partial}{\partial r}\left(\lambda_r \frac{\partial T}{\partial r}\right) + \frac{\lambda_r}{r}\frac{\partial T}{\partial r} + \frac{\partial}{\partial z}\left(\lambda_z \frac{\partial T}{\partial z}\right) - \left(C_a q_r^a\right)\frac{\partial T}{\partial r} - \left(C_a q_z^a\right)\frac{\partial T}{\partial z} + Q_{\sin k} = 0 \qquad [161]$$

- **Three-Dimensional**

u_a:
$$\frac{\partial}{\partial x}\left(k_x^a \frac{\partial u_a}{\partial x}\right) + \frac{\partial}{\partial y}\left(k_y^a \frac{\partial u_a}{\partial y}\right) + \frac{\partial}{\partial z}\left(k_z^a \frac{\partial u_a}{\partial z} + \gamma_a k_z^a\right) = 0 \qquad [162]$$

T:
$$\begin{aligned}&\frac{\partial}{\partial x}\left(\lambda_x \frac{\partial T}{\partial x}\right) + \frac{\partial}{\partial y}\left(\lambda_y \frac{\partial T}{\partial y}\right) + \frac{\partial}{\partial z}\left(\lambda_z \frac{\partial T}{\partial z}\right)\\ &- \left(C_a q_x^a\right)\frac{\partial T}{\partial x} - \left(C_a q_y^a\right)\frac{\partial T}{\partial y} - \left(C_a q_z^a\right)\frac{\partial T}{\partial z} + Q_{\sin k} = 0\end{aligned} \qquad [163]$$

3.3.3 Heat Flow and Air Flow due to Natural Convection

This section presents the governing equations of air flow due to thermo-buoyant or natural convection. The air density is assumed to be incompressible in the natural convection, and it can be applicable with Oberbeck-Boussinesq approximation as follows (Nield and Bejan, 2006):

$$\rho_a = \rho_{a0}\left[1-\beta_a(T-T_0)\right] = \beta\rho_{a0} \qquad [\ 164\ ]$$

$$\beta = \frac{\rho_a}{\rho_{a0}}$$

where:

ρ_a	= pore air density at the given temperature, *kg/m³*,
ρ_{a0}	= pore air density at the reference temperature, *kg/m³*,
T	= temperature, *°C*,
T_0	= reference temperature, *°C*, and
β_a	= air expansion coefficient, *1/°C*.

The thermal expansion coefficient varies with temperature. Please see the following web site for reference: http://www.engineeringtoolbox.com/air-properties-d_156.html

The air flow governing equation [68] is simplified as:

$$\frac{\partial}{\partial z}\left(k_a\frac{\partial u_a}{\partial y} + \gamma_a k_a\right) = 0 \qquad [\ 165\ ]$$

$$\gamma_a = \frac{g\rho_a}{C_u} = \frac{g\rho_{a0}\left[1-\beta(T-T_0)\right]}{C_u} \qquad [\ 166\ ]$$

The following presents the heat and air flow equations in the process of natural convection under different coordinates:

- **1D Horizontal**

u_a:

$$\frac{\partial}{\partial x}\left(k_x^a\frac{\partial u_a}{\partial x}\right) = 0 \qquad [\ 167\ ]$$

T:

$$\frac{\partial}{\partial x}\left(\lambda_x\frac{\partial T}{\partial x}\right) - \left(C_a q_x^a\right)\frac{\partial T}{\partial x} + Q_{\sin k} = \left(C + L_f m_2^i\right)\frac{\partial T}{\partial t} \qquad [\ 168\ ]$$

- **1D Vertical**

u_a:

$$\frac{\partial}{\partial y}\left(k_y^a\frac{\partial u_a}{\partial y} + \gamma_a k_y^a\right) = 0 \qquad [\ 169\ ]$$

T:

$$\frac{\partial}{\partial y}\left(\lambda_y\frac{\partial T}{\partial y}\right) - \left(C_a q_y^a\right)\frac{\partial T}{\partial y} + Q_{\sin k} = \left(C + L_f m_2^i\right)\frac{\partial T}{\partial t} \qquad [\ 170\ ]$$

- **2D**

u_a:

$$\frac{\partial}{\partial x}\left(k_x^a\frac{\partial u_a}{\partial x}\right) + \frac{\partial}{\partial y}\left(k_y^a\frac{\partial u_a}{\partial y} + \gamma_a k_y^a\right) = 0 \qquad [\ 171\ ]$$

T:

$$\frac{\partial}{\partial x}\left(\lambda_x \frac{\partial T}{\partial x}\right)+\frac{\partial}{\partial y}\left(\lambda_y \frac{\partial T}{\partial y}\right)-\left(C_a q_x^a\right)\frac{\partial T}{\partial x}-\left(C_a q_y^a\right)\frac{\partial T}{\partial y}+Q_{\sin k} = \left(C+L_f m_2^i\right)\frac{\partial T}{\partial t} \quad [172]$$

- **Plane**

u_a:

$$\frac{\partial}{\partial x}\left(k_x^a \frac{\partial u_a}{\partial x}\right)+\frac{\partial}{\partial y}\left(k_y^a \frac{\partial u_a}{\partial y}\right)=0 \quad [173]$$

T:

$$\frac{\partial}{\partial x}\left(\lambda_x \frac{\partial T}{\partial x}\right)+\frac{\partial}{\partial y}\left(\lambda_y \frac{\partial T}{\partial y}\right)-\left(C_a q_x^a\right)\frac{\partial T}{\partial x}-\left(C_a q_y^a\right)\frac{\partial T}{\partial y}+Q_{\sin k} = \left(C+L_f m_2^i\right)\frac{\partial T}{\partial t} \quad [174]$$

- **Axisymmetric**

u_a:

$$\frac{\partial}{\partial r}\left(k_r^a \frac{\partial u_a}{\partial r}\right)+\frac{k_r^a}{r}\frac{\partial u_a}{\partial r}+\frac{\partial}{\partial z}\left(k_z^a \frac{\partial u_a}{\partial z}+\gamma_a k_z^a\right)=0 \quad [175]$$

T:

$$\frac{\partial}{\partial r}\left(\lambda_r \frac{\partial T}{\partial r}\right)+\frac{\lambda_r}{r}\frac{\partial T}{\partial r}+\frac{\partial}{\partial z}\left(\lambda_z \frac{\partial T}{\partial z}\right)-\left(C_a q_r^a\right)\frac{\partial T}{\partial r}-\left(C_a q_z^a\right)\frac{\partial T}{\partial z} + Q_{\sin k} = \left(C+L_f m_2^i\right)\frac{\partial T}{\partial t} \quad [176]$$

- **Three-Dimensional**

u_a:

$$\frac{\partial}{\partial x}\left(k_x^a \frac{\partial u_a}{\partial x}\right)+\frac{\partial}{\partial y}\left(k_y^a \frac{\partial u_a}{\partial y}\right)+\frac{\partial}{\partial z}\left(k_z^a \frac{\partial u_a}{\partial z}+\gamma_a k_z^a\right)=0 \quad [177]$$

T:

$$\frac{\partial}{\partial x}\left(\lambda_x \frac{\partial T}{\partial x}\right)+\frac{\partial}{\partial y}\left(\lambda_y \frac{\partial T}{\partial y}\right)+\frac{\partial}{\partial z}\left(\lambda_z \frac{\partial T}{\partial z}\right) -\left(C_a q_x^a\right)\frac{\partial T}{\partial x}-\left(C_a q_y^a\right)\frac{\partial T}{\partial y}-\left(C_a q_z^a\right)\frac{\partial T}{\partial z}+Q_{\sin k} = \left(C+L_f m_2^i\right)\frac{\partial T}{\partial t} \quad [178]$$

3.4 FULLY COUPLED MODEL OF MOISTURE, AIR, AND HEAT FLOW

The following is the governing equations coupled with the moisture (liquid and vapor) flow, air flow and heat flow under the different coordinates.

- **1D Horizontal**

h:

$$\frac{\partial}{\partial x}\left[k_{11}^x \frac{\partial u_w}{\partial x}+k_{12}^x \frac{\partial T}{\partial x}+k_{13}^x \frac{\partial u_a}{\partial x}\right]+S_{\sin k}=\frac{\partial \theta_u}{\partial t}+\frac{\rho_i}{\rho_w}\frac{\partial \theta_i}{\partial t} \quad [179]$$

T:

$$\frac{\partial}{\partial x}\left(k_{21}^x \frac{\partial u_w}{\partial x}+k_{22}^x \frac{\partial T}{\partial x}+k_{23}^x \frac{\partial u_a}{\partial x}\right)-\left(C_w q_x^L+C_v q_x^v+C_a q_x^a\right)\frac{\partial T}{\partial x}+Q_{\sin k} = \left(C+L_f m_2^i+L_v m_2^v\right)\frac{\partial T}{\partial t}-L_v m_2^{vh}\frac{\partial (u_a-u_w)}{\partial t} \quad [180]$$

u_a:

$$\frac{\partial}{\partial x}\left[k_{31}^x \frac{\partial u_w}{\partial x}+k_{32}^x \frac{\partial T}{\partial x}+k_{33}^x \frac{\partial u_a}{\partial x}\right] = \frac{g\omega_a}{R(273.15+T)}\left[\left(\theta_a\right)\frac{\partial u_a}{\partial t}+(u_a+u_{atm})\frac{\partial}{\partial t}\left(\theta_a\right)-\frac{\left(\theta_a\right)\left(u_a+u_{atm}\right)}{273.15+T}\frac{\partial T}{\partial t}\right] \quad [181]$$

$$k_{11}^{x} = \frac{k_x^w + k^{vh}}{\gamma_w}, \quad k_{12}^{x} = k_x^{LT} + k^{vT}, \quad k_{13}^{x} = -\frac{k^{vh}}{\gamma_w} \qquad [\ 182\ ]$$

$$k_{21}^{x} = \frac{L_f k_x^w + L_v k^{vh}}{\gamma_w}, \quad k_{22}^{x} = \lambda_x + L_v k^{vT} + L_f k_x^{LT}, \quad k_{23}^{x} = -\frac{L_v k^{vh}}{\gamma_w} \qquad [\ 183\ ]$$

$$k_{31}^{x} = \frac{\gamma_a H_c k_x^w}{\gamma_w}, \quad k_{32}^{x} = 0, \quad k_{33}^{x} = k_x^a \qquad [\ 184\ ]$$

$$k_x^{LT} = m_2^{\varphi} \frac{k_x^w}{\gamma_w} \qquad [\ 185\ ]$$

- **1D Vertical**

h:

$$\frac{\partial}{\partial y}\left[k_{11}^{y}\frac{\partial u_w}{\partial y} + k_{12}^{y}\frac{\partial T}{\partial y} + k_{13}^{y}\frac{\partial u_a}{\partial y} + k_y^w\right] + S_{\sin k} = \frac{\partial \theta_u}{\partial t} + \frac{\rho_i}{\rho_w}\frac{\partial \theta_i}{\partial t} \qquad [\ 186\ ]$$

T:

$$\frac{\partial}{\partial y}\left(k_{21}^{y}\frac{\partial u_w}{\partial x} + k_{22}^{y}\frac{\partial T}{\partial x} + k_{23}^{y}\frac{\partial u_a}{\partial x} + L_f k_y^w\right) - \left(C_w q_y^L + C_v q_y^v + C_a q_y^a\right)\frac{\partial T}{\partial y}$$
$$+ Q_{\sin k} = \left(C + L_f m_2^i + L_v m_2^v\right)\frac{\partial T}{\partial t} - L_v m_2^{vh}\frac{\partial (u_a - u_w)}{\partial t} \qquad [\ 187\ ]$$

u_a:

$$\frac{\partial}{\partial y}\left[k_{31}^{y}\frac{\partial u_w}{\partial y} + k_{32}^{y}\frac{\partial T}{\partial y} + k_{33}^{y}\frac{\partial u_a}{\partial y} + \gamma_a (k_y^a + H_c k_y^w)\right] =$$
$$\frac{g\omega_a}{R(273.15+T)}\left[(\theta_a)\frac{\partial u_a}{\partial t} + (u_a + u_{atm})\frac{\partial}{\partial t}(\theta_a) - \frac{(\theta_a)(u_a + u_{atm})}{273.15+T}\frac{\partial T}{\partial t}\right] \qquad [\ 188\ ]$$

$$k_{11}^{y} = \frac{k_y^w + k^{vh}}{\gamma_w}, \quad k_{12}^{y} = k_y^{LT} + k^{vT}, \quad k_{13}^{y} = -\frac{k^{vh}}{\gamma_w} \qquad [\ 189\ ]$$

$$k_{21}^{y} = \frac{L_f k_y^w + L_v k^{vh}}{\gamma_w}, \quad k_{22}^{y} = \lambda_y + L_v k^{vT} + L_f k_y^{LT}, \quad k_{23}^{y} = -\frac{L_v k^{vh}}{\gamma_w}, \qquad [\ 190\ ]$$

$$k_{31}^{y} = \frac{\gamma_a H_c k_y^w}{\gamma_w}, \quad k_{32}^{y} = 0, \quad k_{33}^{y} = k_y^a, \qquad [\ 191\ ]$$

$$k_y^{LT} = m_2^{\varphi} \frac{k_y^w}{\gamma_w} \qquad [\ 192\ ]$$

- **2D**

h:

$$\frac{\partial}{\partial x}\left[k_{11}^{x}\frac{\partial u_w}{\partial x} + k_{12}^{x}\frac{\partial T}{\partial x} + k_{13}^{x}\frac{\partial u_a}{\partial x}\right]$$
$$+ \frac{\partial}{\partial y}\left[k_{11}^{y}\frac{\partial u_w}{\partial y} + k_{12}^{y}\frac{\partial T}{\partial y} + k_{13}^{y}\frac{\partial u_a}{\partial y} + k_y^w\right] + S_{\sin k} = \frac{\partial \theta_u}{\partial t} + \frac{\rho_i}{\rho_w}\frac{\partial \theta_i}{\partial t} \qquad [\ 193\ ]$$

T:

$$\frac{\partial}{\partial x}\left(k_{21}^{x}\frac{\partial u_w}{\partial x} + k_{22}^{x}\frac{\partial T}{\partial x} + k_{23}^{x}\frac{\partial u_a}{\partial x}\right) + \frac{\partial}{\partial y}\left(k_{21}^{y}\frac{\partial u_w}{\partial x} + k_{22}^{y}\frac{\partial T}{\partial x} + k_{23}^{y}\frac{\partial u_a}{\partial x} + L_f k_y^w\right)$$
$$-\left(C_w q_x^L + C_v q_x^v + C_a q_x^a\right)\frac{\partial T}{\partial x} - \left(C_w q_y^L + C_v q_y^v + C_a q_y^a\right)\frac{\partial T}{\partial y} + Q_{\sin k} \qquad [\ 194\ ]$$
$$= \left(C + L_f m_2^i + L_v m_2^v\right)\frac{\partial T}{\partial t} - L_v m_2^{vh}\frac{\partial (u_a - u_w)}{\partial t}$$

u_a:

$$\frac{\partial}{\partial x}\left[k_{31}^{x}\frac{\partial u_w}{\partial x}+k_{32}^{x}\frac{\partial T}{\partial x}+k_{33}^{x}\frac{\partial u_a}{\partial x}\right]+$$
$$\frac{\partial}{\partial y}\left[k_{31}^{y}\frac{\partial u_w}{\partial y}+k_{32}^{y}\frac{\partial T}{\partial y}+k_{33}^{y}\frac{\partial u_a}{\partial y}+\gamma_a(k_y^a+H_c k_y^w)\right]= \quad \textbf{[195]}$$
$$\frac{g\omega_a}{R(273.15+T)}\left[(\theta_a)\frac{\partial u_a}{\partial t}+(u_a+u_{atm})\frac{\partial}{\partial t}(\theta_a)-\frac{(\theta_a)(u_a+u_{atm})}{273.15+T}\frac{\partial T}{\partial t}\right]$$

$$k_{11}^{x}=\frac{k_x^w+k^{vh}}{\gamma_w},\quad k_{12}^{x}=k_x^{LT}+k^{vT},\quad k_{13}^{x}=-\frac{k^{vh}}{\gamma_w}, \quad \textbf{[196]}$$

$$k_{11}^{y}=\frac{k_y^w+k^{vh}}{\gamma_w},\quad k_{12}^{y}=k_y^{LT}+k^{vT},\quad k_{13}^{y}=-\frac{k^{vh}}{\gamma_w}, \quad \textbf{[197]}$$

$$k_{21}^{x}=\frac{L_f k_x^w+L_v k^{vh}}{\gamma_w},\quad k_{22}^{x}=\lambda_x+L_v k^{vT}+L_f k_x^{LT},\quad k_{23}^{x}=-\frac{L_v k^{vh}}{\gamma_w}, \quad \textbf{[198]}$$

$$k_{21}^{y}=\frac{L_f k_y^w+L_v k^{vh}}{\gamma_w},\quad k_{22}^{y}=\lambda_y+L_v k^{vT}+L_f k_y^{LT},\quad k_{23}^{y}=-\frac{L_v k k^{vh}}{\gamma_w}, \quad \textbf{[199]}$$

$$k_{31}^{x}=\frac{\gamma_a H_c k_x^w}{\gamma_w},\quad k_{32}^{x}=0,\quad k_{33}^{x}=k_x^a, \quad \textbf{[200]}$$

$$k_{31}^{y}=\frac{\gamma_a H_c k_y^w}{\gamma_w},\quad k_{32}^{y}=0,\quad k_{33}^{y}=k_y^a, \quad \textbf{[201]}$$

$$k_x^{LT}=m_2^{\varphi}\frac{k_x^w}{\gamma_w},\quad k_y^{LT}=m_2^{\varphi}\frac{k_y^w}{\gamma_w} \quad \textbf{[202]}$$

- **2D-Plan**

h:

$$\frac{\partial}{\partial x}\left[k_{11}^{x}\frac{\partial u_w}{\partial x}+k_{12}^{x}\frac{\partial T}{\partial x}+k_{13}^{x}\frac{\partial u_a}{\partial x}\right]+\frac{\partial}{\partial y}\left[k_{11}^{y}\frac{\partial u_w}{\partial y}+k_{12}^{y}\frac{\partial T}{\partial y}+k_{13}^{y}\frac{\partial u_a}{\partial y}\right]$$
$$+S_{\sin k}=\frac{\partial\theta_u}{\partial t}+\frac{\rho_i}{\rho_w}\frac{\partial\theta_i}{\partial t} \quad \textbf{[203]}$$

T:

$$\frac{\partial}{\partial x}\left(k_{21}^{x}\frac{\partial u_w}{\partial x}+k_{22}^{x}\frac{\partial T}{\partial x}+k_{23}^{x}\frac{\partial u_a}{\partial x}\right)+\frac{\partial}{\partial y}\left(k_{21}^{y}\frac{\partial u_w}{\partial x}+k_{22}^{y}\frac{\partial T}{\partial x}+k_{23}^{y}\frac{\partial u_a}{\partial x}\right)$$
$$-\left(C_w q_x^L+C_v q_x^v+C_a q_x^a\right)\frac{\partial T}{\partial x}-\left(C_w q_y^L+C_v q_y^v+C_a q_y^a\right)\frac{\partial T}{\partial y}+Q_{\sin k} \quad \textbf{[204]}$$
$$=\left(C+L_f m_2^i+L_v m_2^v\right)\frac{\partial T}{\partial t}-L_v m_2^{vh}\frac{\partial(u_a-u_w)}{\partial t}$$

u_a:

$$\frac{\partial}{\partial x}\left[k_{31}^{x}\frac{\partial u_w}{\partial x}+k_{32}^{x}\frac{\partial T}{\partial x}+k_{33}^{x}\frac{\partial u_a}{\partial x}\right]+\frac{\partial}{\partial y}\left[k_{31}^{y}\frac{\partial u_w}{\partial y}+k_{32}^{y}\frac{\partial T}{\partial y}+k_{33}^{y}\frac{\partial u_a}{\partial y}\right]=$$
$$\frac{g\omega_a}{R(273.15+T)}\left[(\theta_a)\frac{\partial u_a}{\partial t}+(u_a+u_{atm})\frac{\partial}{\partial t}(\theta_a)-\frac{(\theta_a)(u_a+u_{atm})}{273.15+T}\frac{\partial T}{\partial t}\right] \quad \textbf{[205]}$$

$$k_{11}^{x}=\frac{k_x^w+k^{vh}}{\gamma_w},\quad k_{12}^{x}=k_x^{LT}+k^{vT},\quad k_{13}^{x}=-\frac{k^{vh}}{\gamma_w}, \quad \textbf{[206]}$$

$$k_{11}^{y}=\frac{k_y^w+k^{vh}}{\gamma_w},\quad k_{12}^{y}=k_y^{LT}+k^{vT},\quad k_{13}^{y}=-\frac{k^{vh}}{\gamma_w}, \quad \textbf{[207]}$$

$$k_{21}^{x}=\frac{L_f k_x^w+L_v k^{vh}}{\gamma_w},\quad k_{22}^{x}=\lambda_x+L_v k^{vT}+L_f k_x^{LT},\quad k_{23}^{x}=-\frac{L_v k^{vh}}{\gamma_w}, \quad \textbf{[208]}$$

$$k_{21}^{y}=\frac{L_f k_y^w+L_v k^{vh}}{\gamma_w},\quad k_{22}^{y}=\lambda_Y+L_v k^{vT}+L_f k_y^{LT},\quad k_{23}^{y}=-\frac{L_v k_{vh}}{\gamma_w}, \quad \textbf{[209]}$$

$$k_{31}^{x} = \frac{\gamma_a H_c k_x^w}{\gamma_w}, \quad k_{32}^{x} = 0, \quad k_{33}^{x} = k_x^a, \qquad \textbf{[210]}$$

$$k_{31}^{y} = \frac{\gamma_a H_c k_y^w}{\gamma_w}, \quad k_{32}^{y} = 0, \quad k_{33}^{y} = k_y^a, \qquad \textbf{[211]}$$

$$k_x^{LT} = m_2^{\varphi} \frac{k_x^w}{\gamma_w}, \quad k_y^{LT} = m_2^{\varphi} \frac{k_y^w}{\gamma_w}, \qquad \textbf{[212]}$$

- **Axis-Symmetric**

h:

$$\frac{\partial}{\partial r}\left[k_{11}^{r}\frac{\partial(u_w)}{\partial r} + k_{12}^{r}\frac{\partial T}{\partial r} + k_{13}^{r}\frac{\partial u_a}{\partial r}\right] + \frac{k_{11}^{r}}{r}\frac{\partial u_w}{\partial r} + \frac{k_{12}}{r}\frac{\partial T}{\partial r} + \frac{k_{13}}{r}\frac{\partial u_a}{\partial r}$$
$$+ \frac{\partial}{\partial z}\left[k_{11}^{z}\frac{\partial(u_w)}{\partial z} + k_{12}^{z}\frac{\partial T}{\partial z} + k_{13}^{z}\frac{\partial u_a}{\partial z} + k_z^w\right] + S_{\sin k} = \frac{\partial \theta_u}{\partial t} + \frac{\rho_i}{\rho_w}\frac{\partial \theta_i}{\partial t} \qquad \textbf{[213]}$$

T:

$$\frac{\partial}{\partial r}\left[k_{21}^{r}\frac{\partial(u_w)}{\partial r} + k_{22}^{r}\frac{\partial T}{\partial r} + k_{23}^{r}\frac{\partial u_a}{\partial r}\right] + \frac{k_{21}^{r}}{r}\frac{\partial u_w}{\partial r} + \frac{k_{22}^{r}}{r}\frac{\partial T}{\partial r} + \frac{k_{23}^{r}}{r}\frac{\partial u_a}{\partial r}$$
$$+ \frac{\partial}{\partial z}\left[k_{21}^{z}\frac{\partial(u_w)}{\partial y} + k_{22}^{z}\frac{\partial T}{\partial z} + k_{23}^{z}\frac{\partial u_a}{\partial z} + L_f k_z^w\right]$$
$$-\left(C_w q_r^L + C_v q_r^v + C_a q_r^a\right)\frac{\partial T}{\partial r} - \left(C_w q_z^L + C_v q_z^v + C_a q_z^a\right)\frac{\partial T}{\partial z} + Q_{\sin k} \qquad \textbf{[214]}$$
$$= \left(C + L_f m_2^i + L_v m_2^v\right)\frac{\partial T}{\partial t} - L_v m_2^{vh}\frac{\partial(u_a - u_w)}{\partial t}$$

u_a:

$$\frac{\partial}{\partial r}\left[k_{31}^{r}\frac{\partial u_w}{\partial r} + k_{32}^{r}\frac{\partial T}{\partial r} + k_{33}^{r}\frac{\partial u_a}{\partial r}\right] + \frac{k_{31}^{r}}{r}\frac{\partial u_w}{\partial r} + \frac{k_{32}^{r}}{r}\frac{\partial T}{\partial r} + \frac{k_{33}^{r}}{r}\frac{\partial u_a}{\partial r}$$
$$+ \frac{\partial}{\partial z}\left[k_{31}^{z}\frac{\partial u_w}{\partial z} + k_{32}^{z}\frac{\partial T}{\partial z} + k_{33}^{z}\frac{\partial u_a}{\partial z} + \gamma_a(k_z^a + H_c k_z^w)\right] = \qquad \textbf{[215]}$$
$$\frac{g\omega_a}{R(273.15+T)}\left[(\theta_a)\frac{\partial u_a}{\partial t} + (u_a + u_{atm})\frac{\partial}{\partial t}(\theta_a) - \frac{(\theta_a)(u_a + u_{atm})}{273.15+T}\frac{\partial T}{\partial t}\right]$$

$$k_{11}^{r} = \frac{k_r^w + k^{vh}}{\gamma_w}, \quad k_{12}^{r} = k_r^{LT} + k^{vT}, \quad k_{13}^{r} = -\frac{k^{vh}}{\gamma_w},$$

$$k_{11}^{z} = \frac{k_z^w + k^{vh}}{\gamma_w}, \quad k_{12}^{z} = k_z^{LT} + k^{vT}, \quad k_{13}^{z} = -\frac{k^{vh}}{\gamma_w}, \qquad \textbf{[216]}$$

$$k_{21}^{r} = \frac{L_f k_r^w + L_v k^{vh}}{\gamma_w}, \quad k_{22}^{r} = \lambda_r + L_v k^{vT} + L_f k_r^{LT}, \quad k_{23}^{r} = -\frac{L_v k^{vh}}{\gamma_w}, \qquad \textbf{[217]}$$

$$k_{21}^{z} = \frac{L_f k_z^w + L_v k^{vh}}{\gamma_w}, \quad k_{22}^{z} = \lambda_z + L_v k^{vT} + L_f k_z^{LT}, \quad k_{23}^{z} = -\frac{L_v k^{vh}}{\gamma_w}, \qquad \textbf{[218]}$$

$$k_{31}^{r} = \frac{\gamma_a H_c k_r^w}{\gamma_w}, \quad k_{32}^{r} = 0, \quad k_{33}^{r} = k_r^a, \qquad \textbf{[219]}$$

$$k_{31}^{z} = \frac{\gamma_a H_c k_z^w}{\gamma_w}, \quad k_{32}^{z} = 0, \quad k_{33}^{z} = k_z^a, \qquad \textbf{[220]}$$

$$k_r^{LT} = m_2^{\varphi}\frac{k_r^w}{\gamma_w}, \quad k_z^{LT} = m_2^{\varphi}\frac{k_z^w}{\gamma_w} \qquad \textbf{[221]}$$

- **3D**

h:

$$\frac{\partial}{\partial x}\left[k_{11}^{x}\frac{\partial u_w}{\partial x}+k_{12}^{x}\frac{\partial T}{\partial x}+k_{13}^{x}\frac{\partial u_a}{\partial x}\right]+\frac{\partial}{\partial y}\left[k_{11}^{y}\frac{\partial u_w}{\partial y}+k_{12}^{y}\frac{\partial T}{\partial y}+k_{13}^{y}\frac{\partial u_a}{\partial y}\right]$$
$$+\frac{\partial}{\partial z}\left[k_{11}^{z}\frac{\partial (u_w)}{\partial z}+k_{12}^{z}\frac{\partial T}{\partial z}+k_{13}^{z}\frac{\partial u_a}{\partial z}+k_{z}^{w}\right]+S_{\sin k}=\frac{\partial \theta_u}{\partial t}+\frac{\rho_i}{\rho_w}\frac{\partial \theta_i}{\partial t} \quad [222]$$

T:

$$\frac{\partial}{\partial x}\left(k_{21}^{x}\frac{\partial u_w}{\partial x}+k_{22}^{x}\frac{\partial T}{\partial x}+k_{23}^{x}\frac{\partial u_a}{\partial x}\right)+\frac{\partial}{\partial y}\left(k_{21}^{y}\frac{\partial u_w}{\partial x}+k_{22}^{y}\frac{\partial T}{\partial x}+k_{23}^{y}\frac{\partial u_a}{\partial x}\right)$$
$$+\frac{\partial}{\partial z}\left[k_{21}^{z}\frac{\partial (u_w)}{\partial y}+k_{22}^{z}\frac{\partial T}{\partial z}+k_{23}^{z}\frac{\partial u_a}{\partial z}+L_f k_z^w\right]$$
$$-\left(C_w q_x^L+C_v q_x^v+C_a q_x^a\right)\frac{\partial T}{\partial x}-\left(C_w q_y^L+C_v q_y^v+C_a q_y^a\right)\frac{\partial T}{\partial y} \quad [223]$$
$$-\left(C_w q_z^L+C_v q_z^v+C_a q_z^a\right)\frac{\partial T}{\partial z}+Q_{\sin k}=\left(C+L_f m_2^i+L_v m_2^v\right)\frac{\partial T}{\partial t}-L_v m_2^{vh}\frac{\partial (u_a-u_w)}{\partial t}$$

u_a:

$$\frac{\partial}{\partial x}\left[k_{31}^{x}\frac{\partial u_w}{\partial x}+k_{32}^{x}\frac{\partial T}{\partial x}+k_{33}^{x}\frac{\partial u_a}{\partial x}\right]+\frac{\partial}{\partial y}\left[k_{31}^{y}\frac{\partial u_w}{\partial y}+k_{32}^{y}\frac{\partial T}{\partial y}+k_{33}^{y}\frac{\partial u_a}{\partial y}\right]$$
$$+\frac{\partial}{\partial z}\left[k_{31}^{z}\frac{\partial u_w}{\partial z}+k_{32}^{z}\frac{\partial T}{\partial z}+k_{33}^{z}\frac{\partial u_a}{\partial z}+\gamma_a(k_z^a+H_c k_z^w)\right]= \quad [224]$$
$$\frac{g\omega_a}{R(273.15+T)}\left[(\theta_a)\frac{\partial u_a}{\partial t}+(u_a+u_{atm})\frac{\partial}{\partial t}(\theta_a)-\frac{(\theta_a)(u_a+u_{atm})}{273.15+T}\frac{\partial T}{\partial t}\right]$$

$$k_{11}^{x}=\frac{k_x^w+k^{vh}}{\gamma_w},\quad k_{12}^{x}=k_x^{LT}+k^{vT},\quad k_{13}^{x}=-\frac{k^{vh}}{\gamma_w}, \quad [225]$$

$$k_{11}^{y}=\frac{k_y^w+k^{vh}}{\gamma_w},\quad k_{12}^{y}=k_y^{LT}+k^{vT},\quad k_{13}^{y}=-\frac{k^{vh}}{\gamma_w}, \quad [226]$$

$$k_{11}^{z}=\frac{k_z^w+k^{vh}}{\gamma_w},\quad k_{12}^{z}=k_z^{LT}+k^{vT},\quad k_{13}^{z}=-\frac{k^{vh}}{\gamma_w}, \quad [227]$$

$$k_{21}^{x}=\frac{L_f k_x^w+L_v k^{vh}}{\gamma_w},\quad k_{22}^{x}=\lambda_x+L_v k^{vT}+L_f k_x^{LT},\quad k_{23}^{x}=-\frac{L_v k^{vh}}{\gamma_w}, \quad [228]$$

$$k_{21}^{y}=\frac{L_f k_y^w+L_v k^{vh}}{\gamma_w},\quad k_{22}^{y}=\lambda_y+L_v k^{vT}+L_f k_y^{LT},\quad k_{23}^{y}=-\frac{L_v k^{vh}}{\gamma_w}, \quad [229]$$

$$k_{21}^{z}=\frac{L_f k_z^w+L_v k^{vh}}{\gamma_w},\quad k_{22}^{z}=\lambda_z+L_v k^{vT}+L_f k_z^{LT},\quad k_{23}^{z}=-\frac{L_v k^{vh}}{\gamma_w}, \quad [230]$$

$$k_{31}^{x}=\frac{\gamma_a H_c k_x^w}{\gamma_w},\quad k_{32}^{x}=0,\quad k_{33}^{x}=k_x^a, \quad [231]$$

$$k_{31}^{y}=\frac{\gamma_a H_c k_y^w}{\gamma_w},\quad k_{32}^{y}=0,\quad k_{33}^{y}=k_y^a, \quad [232]$$

$$k_{31}^{z}=\frac{\gamma_a H_c k_z^w}{\gamma_w},\quad k_{32}^{z}=0,\quad k_{33}^{z}=k_z^a, \quad [233]$$

$$k_x^{LT}=m_2^{\varphi}\frac{k_x^w}{\gamma_w},\quad k_y^{LT}=m_2^{\varphi}\frac{k_y^w}{\gamma_w},\quad k_z^{LT}=m_2^{\varphi}\frac{k_z^w}{\gamma_w} \quad [234]$$

where:

u_w = pore water pressure due to hydraulic head, *kPa*,

u_a = pore air pressure, *kPa*,

T = temperature, °*C*,

k_x^w, k_y^w, = hydraulic conductivity in *x*, *y*, *z*, or *r*-direction, m/s. For a homogenous material, $k = k_x^w = k_y^w = k_z^w = k_r^w$,

k_z^w, k_r^w	
k^{vh}	= pore-water vapor conductivity by vapor diffusion within the air phase, as defined in equation [47], *m/s*,
k^{vT}	= pore-water vapor conductivity induced by temperature gradient, as defined in equation [48],
k^{LT}	= hydraulic conductivity introduced by the temperature gradient, *m/s*,
k_x^a,k_y^a k_z^a, k_r^a	= air conductivity of the soil in the *x, y, z, or r*-direction, *m/s*. For homogenous material, $k_x^a = k_y^a = k_z^a = k_r^a$,
λ_x, λ_y, λ_z, λ_r	= thermal conductivity of the soil in the *x*, *y*, *z*, or *r*-direction, *J/(s-m-°C)*. For a homogenous material, $\lambda_x = \lambda_y = \lambda_z = \lambda_r$,
q_x^L, q_y^L, q_z^L, q_r^L	= pore-water flow rate (Darcian velocity) in the *x, y, z, or r*-direction across a unit area of the soil due to hydraulic head gradients defined in equation [27], *m/s*,
q_x^v, q_y^v, q_z^v, q_r^v	= pore-water vapor flow rate (Darcian velocity) in the *x, y, z, or r*-direction across a unit area of the soil due to vapor diffusion defined in equation [46], *m/s*,
q_x^a, q_y^a, q_z^a, q_r^a	= pore-air flow velocity (Darcian velocity) in the *x, y, z, or r*-direction across a unit area of the soil due to air pressure gradient defined in equation [66], *m/s*,
θ_u	= volumetric unfrozen water content (including liquid and vapor) of the soil that is determined by soil freezing characteristic curve, m^3/m^3,
θ_i	= volumetric ice content of the soil defined in equation [71], m^3/m^3,
θ_v	= volumetric pore-water vapor content of the defined in equation [39], m^3/m^3,
γ_w	= unit weight of water, kN/m^3,
γ_a	= unit of air weight, kN/m^3, $\gamma_a = g\rho_a/C_u$,
ρ_a	= air density, kg/m^3,
C_u	= unit conversion coefficient, $C_u = 1000$ for Metric, and $C_u = 1$ for Imperial,
n	= porosity, dimensionless,
H_c	= Henry's volumetric coefficient of air solubility in the water, m^3/m^3,
ω_a	= average molecular weight of air 0.0288 *kg/mol*,
g	= acceleration due to gravity, 9.81 m/s^2,
R	= universal gas constant, 8.3144 *J/mol-K*,
L_v	= volumetric latent heat of water vaporization, J/m^3, as defined in equation [62],
L_f	= volumetric latent heat of water freezing or thawing, J/m^3, as defined in equation [63],
C_a	= volumetric heat capacity of dry air, $J/(m^3\text{-}°C)$,
C_w	= volumetric heat capacity of water, $J/(m^3\text{-}°C)$,
C_v	= volumetric heat capacity of water vapour, $J/(m^3\text{-}°C)$,
C	= volumetric heat capacity of a material, calculated with equation [53] , $J/(m^3\text{-}°C)$,
m_2^i	= slope of soil Freezing characteristic curve,
m_2^φ	= slope of the relation of soil matric suction to the soil temperature, *kPa/°C*,
Q_{sink}	= heat source or sink, J/s-m^3,
m_2^v	= defined in equation [60], and
m_2^{vh}	= defined in equation [61].

4 MATERIAL THERMAL PROPERTIES

Thermal conductivity, heat capacity, and soil freezing characteristic curve (SFCC) are three major thermal properties in heat transfer during the soil freezing and thawing process. The thermal conductivity of ice is almost 4 times higher than water, but water has a higher value of heat capacity than ice. The ice content in a frozen soil depends on both volumetric water content in unfrozen soil, and unfrozen water content in frozen soil. The unfrozen water content is uniquely determined by soil freezing characteristic curve. The following sections describe how to estimate or calculate the thermal conductivity, heat capacity, and SFCC.

4.1 THERMAL CONDUCTIVITY CURVE

The three main factors affecting the thermal conductivity of a material include 1) the thermal conductivity of constituent material, 2) the fraction of the material volume each material represents, and 3) the "connectedness" of each of the constituent materials. The "connectedness" refers to the completeness of paths that are available for movement of heat through a material Pentland (2000). Heat is conducted to individual soil particles through discrete contact points, as the area of these discrete points increases the conductivity of the soil increases. Therefore, as the "connectedness" increases, so does the thermal conductivity.

4.1.1 Johansen Approach (1973)

The Johansen (1973) and Farouki, (1981) approach has been used widely to calculate thermal conductivity based on soil state, type, fraction of soil components, and thermal conductivity of water, ice, and solid components. It is recommended to use this method to estimate soil thermal conductivity, especially in a coupled seepage and heat model, where ice content in the frozen soil is changeable due to moisture migration. The Johansen method is applicable for both unfrozen and frozen soils. The method is based on dry and saturated thermal conductivity at a given dry density as follows:

- **Fine and Coarse Soils**

$$\lambda = (\lambda_{sat} - \lambda_{dry})\lambda_e + \lambda_{dry} \qquad [\ 235\ ]$$

where

λ = soil thermal conductivity, *J/s-m-°C,*

λ_{sat} = the saturated thermal conductivity, *J/s-m-°C,*

λ_{dry} = the thermal conductivity of dry soil, *J/s-m-°C,* and

λ_e = the Kerstern number (normalized thermal conductivity), which is related to saturation.

$$\lambda_{dry} = \frac{0.135\gamma_d + 64.7}{2700 - 0.947\gamma_d} \pm 20\%, \text{ for dry nature soils} \qquad [\ 236\ ]$$

$$\lambda_{dry} = 0.039n^{-2.2}, \text{ for dry crushed rock materials} \qquad [\ 237\ ]$$

$$\lambda_{sat} = (\lambda_s)^{1-n}(\lambda_w)^n, \text{ for saturated unfrozen soil} \qquad [\ 238\ ]$$

$$\lambda_{sat} = (\lambda_s)^{1-n}(\lambda_i)^{n-w_u}(\lambda_w)^{w_u}, \text{ for saturated frozen soil} \qquad [\ 239\ ]$$

$$\lambda_s = 7.7^q(2.0)^{1-q} \quad \textit{if } q > 0.20$$
$$\lambda_s = 7.7^q(3.0)^{1-q} \quad \text{if } q <= 0.20 \qquad [\ 240\ ]$$

$$\lambda_e = 0.7\log(S_r) + 1.0, \text{ for unfrozen coarse grained soil} \qquad [\ 241\ ]$$

$$\lambda_e = \log(S_r) + 1.0, \text{ for unfrozen fine grained soil} \qquad [\ 242\ ]$$

$$\lambda_e = S_r, \text{ for frozen soil} \qquad [\ 243\ ]$$

where:

γ_d = dry density of soil, *kg/m³*,

n = soil porosity,

λ_s = thermal conductivity of soil particles, *J/s-m-°C,*

q = quartz content,

λ_w = thermal conductivity of water, *J/s-m-°C,*

λ_i = thermal conductivity of ice, *J/s-m-°C*

w_u = volumetric unfrozen water content, m^3/m^3, and

S_r = soil saturation.

- **Peaty Soils (Peats)**

Generally, peat has a lower thermal conductivity than other mineral soils (fine and coarse soils). The portion of water and ice have a major influence on the thermal properties of peats. Water content in peats can be as high as 2100 % (Pihlainen, 1963, cited in Farouki, 1981). Frozen thermal conductivity of peats is usually about four times larger than unfrozen thermal conductivity, which is similar to the ratio between water and ice. Thermal conductivity equations are:

Unfrozen peat

$$\sqrt{\lambda} - \sqrt{\lambda_{dry}} = S_r\left(\sqrt{\lambda_{sat(u)}} - \sqrt{\lambda_{dry}}\right) \quad \textbf{[244]}$$

Frozen peat

$$\lambda = \lambda_{dry}\left(\frac{\lambda_{sat(f)}}{\lambda_{dry}}\right)^{S_r} \quad \textbf{[245]}$$

These equations are a result of fitting Kersten's measured data (Kersten, 1949). By combining these equations with equation [235], the resulting equations are the relation between the Kerstern number and degree of saturation (Cote and Conrad, 2005):

Unfrozen peat

$$\lambda_e = 0.54\,S_r^2 + 0.46\,S_r \quad \textbf{[246]}$$

Frozen peat

$$\lambda_e = 0.029\left(36^{S_r} - 1\right) \quad \textbf{[247]}$$

The inputs for calculating peat thermal conductivity are λ_{dry}, $\lambda_{sat(u)}$, and $\lambda_{sat(f)}$. Johansen suggested values for these inputs of 0.05, 0.55, and 1.8 *W/m-°C* for λ_{dry}, $\lambda_{sat(u)}$, and $\lambda_{sat(f)}$, respectively.

Table 1 is the thermal conductivity of some common materials.

Table 1 Typical Values of Thermal conductivity

Material	Thermal Conductivity (*J/s-m-°C*)
Quartz	**8.8**
Clay Minerals	**2.9**
Organic Matter	**0.25**
Water	**0.57**
Ice	**2.2**
Air	**0.025**

Table 2 lists the quartz content *q* for the common soils:

Table 2 Quartz content of common soils (Tarnawski et al., 2009)

Chinese Soil (Lu el al., 2007)		**Kersten's soil (Tarnawski et al., 2009)**	
Soil name	***Quartz content (%)***	***Soil name***	***Quartz content (%)***
Sand 1	75	Lowell sand	77
Sand 2	53	Northway fine sand	23
Sandy loam 3	65	Northway sand	5.0
Loam 4	54	Fairbanks sand	84
Loam 11	56	Dakota sandy loam	73

Silt loam 5	49	Ramsey sandy loam	53
Silt loam 6	60	Northway silt loam	2.0
Silty clay loam 7	34	Fairbanks silt loam	40
Silty clay loam 8	33	Fairbanks silty clay loam	28
Clay loam 9	39	Healy clay	31

Tarnawski et al., 2009 analyzed the relationship between the quartz content and the contents of sand and gravel, as shown in Figure 4. The quartz content can be estimated with the following expression:

$$q = 0.339 + 0.417\, m_{co} \qquad [\ 248\ ]$$

where:

q = quartz content, *and*

m_{co} = contents of sand and gravel.

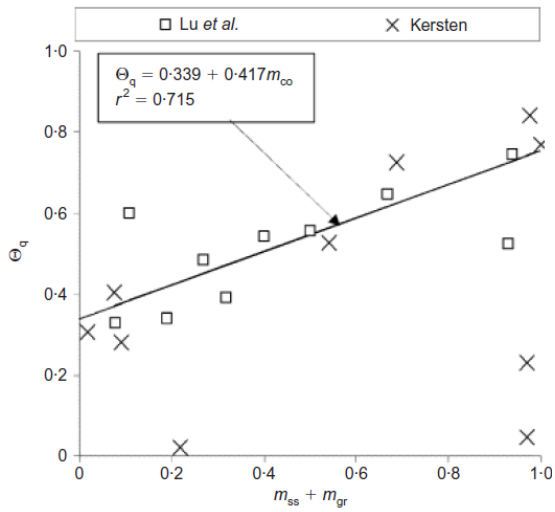

Figure 4 Relationship between quartz content and sand and gravel contents

The thermal conductivity for ice is related to the temperature. According to the data presented in the website http://www.engineeringtoolbox.com/ice-thermal-properties-d_576.html, the ice thermal conductivity can be approximated with the following data fitting equation:

$$\lambda_i = 2.1932 - 0.0097\, T + 0.00003\, T^2 \qquad [\ 249\ ]$$

where:

λ_i = ice thermal conductivity, *w/m-°C*, and

T = ice temperature, *°C*.

The comparison of measured data with the calculation of ice thermal conductivity with the equation is illustrated in Figure 5.

Figure 6 is the Johansen model prediction of thermal conductivity as the function of temperature and volumetric water content for sand. Due to the ice existence in the frozen soil, the thermal conductivity of frozen soils has larger values than the conductivity of unfrozen soil. Figure 7 and Figure 8 demonstrate the calculation of thermal conductivity for sand and clay loam changing with the water content and dry density. It can be seen from the Figure 8 that Johansen model cannot predict the thermal conductivity at the very low water content, because the Kerstern number, λ_e, is negative in that case.

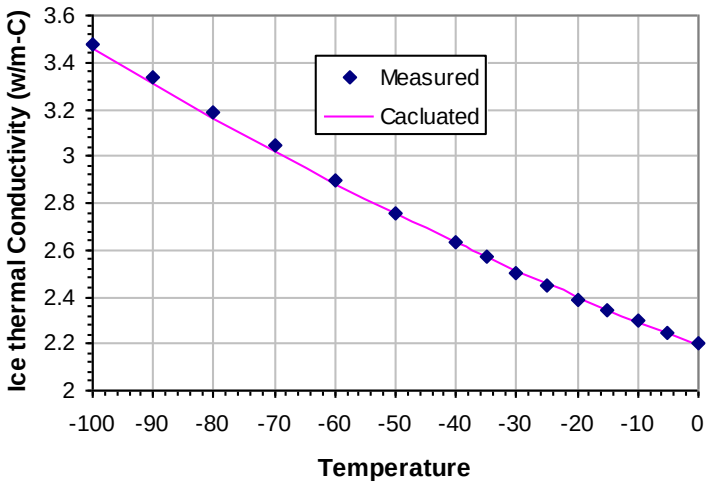

Figure 5 Temperature effect on the ice thermal conductivity

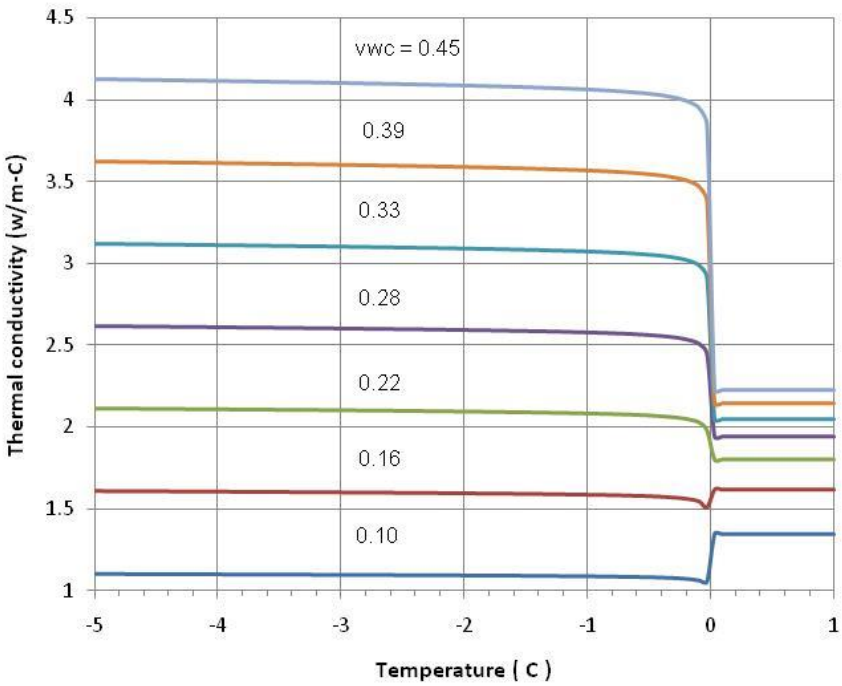

Figure 6 Thermal conductivity calculated with Johansen approach at different temperatures and volumetric water contents for sand (quartz content = 74 %)

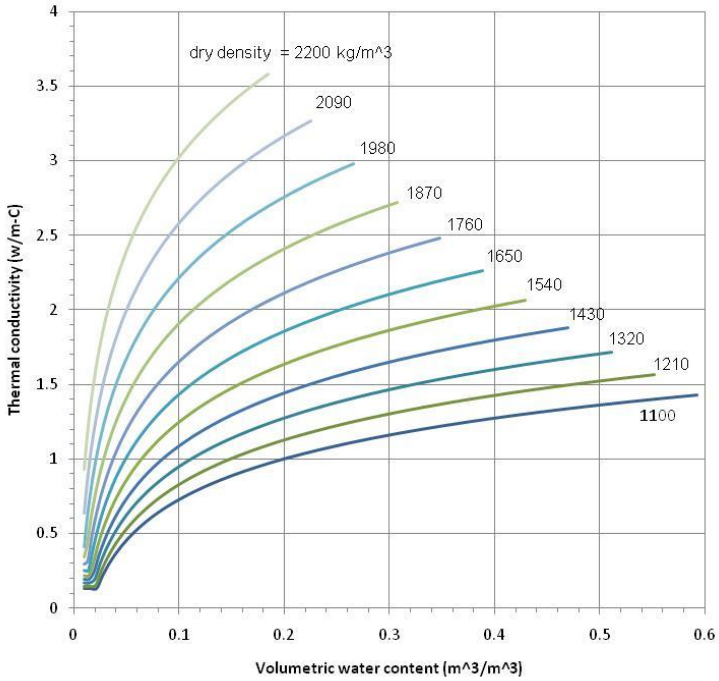

Figure 7 Thermal conductivity calculated with Johansen approach at different volumetric water contents and dry densities for sand (quartz content = 74 %)

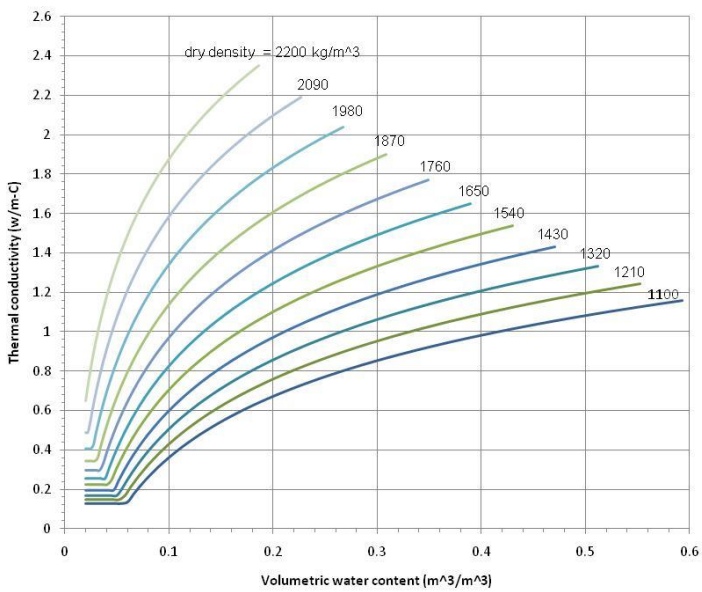

Figure 8 Thermal conductivity calculated with Johansen approach at different volumetric water contents and dry densities for clay loam (quartz content = 36 %)

4.1.2 Improved Johansen – Lu et al., (2007)

Lu et al., (2007) improved the Johansen model in the calculation of dry thermal conductivity, λ_{dry}, (i.e. equation [236]), and the Kerstern number, λ_e, (i.e. equation [241] or equation [242]). The main limitation of Johansen model is that the Kerstern number, λ_e, will be negative for a soil having very low degrees of water saturation. The improved equation [250] is used to describe the Kerstern number, λ_e, in the Lu et al., (2007) model:

$$\lambda_e = Exp\left\{\alpha\left[1 - S_r^{(\alpha-\beta)}\right]\right\}, \text{ for the unfrozen soil} \qquad \textbf{[250]}$$

where:

α = parameter related to soil texture. $\alpha = 0.96$ for the coarse soil, and $\alpha = 0.27$ for the fine soil,

β = shape parameter, $\beta = 1.33$, and

S_r = the degree of water saturation.

The dry thermal conductivity, λ_{dry}, is expressed as a linear expression:

$$\lambda_{dry} = -0.56n + 0.51 \quad \textbf{[251]}$$

where:

n = porosity of soil.

In the above model, the value for the parameters of α and β are obtained according to the sand content of a soil. The calculation of thermal conductivity for sand is over predicted if using sand content (Lu et al., 2007). Tarnawski et al., (2009) analyzed the effect of quartz content on the prediction of the thermal conductivity using the Lu et al., (2007) model. Based on the quartz content, the following values for the parameter α and β are obtained:

Table 3 Values of parameter α and β

Material Type	α	β
Coarse	0.728	1.165
Fine	0.370	1.29

SVHEAT implements Lu et al., (2007) model based on the values as given in Table 3.

As indicated in the Figure 10, the Lu et al., (2007) model has improved the prediction of thermal conductivity at the very low water content compared to the Johansen model (see Figure 8).

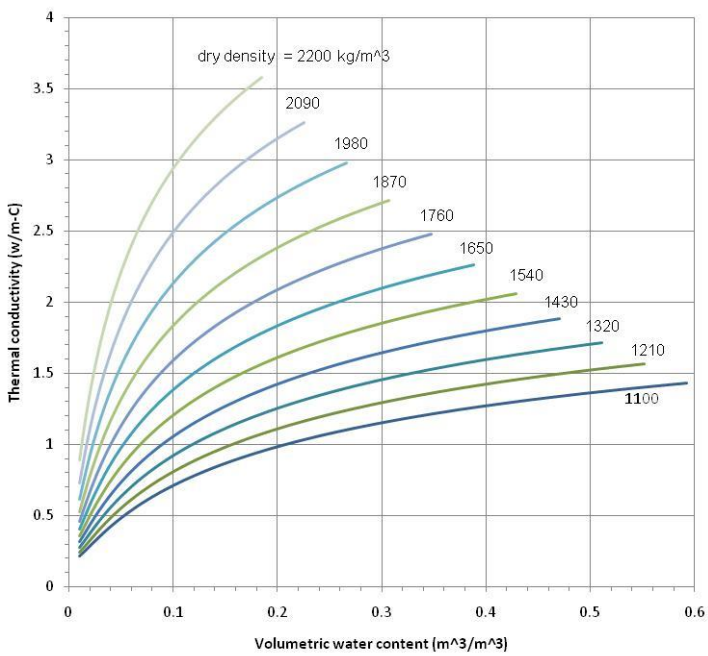

Figure 9 Thermal conductivity calculated with Lu at al approach at different volumetric water contents and dry densities for sand (quartz content = 74 %)

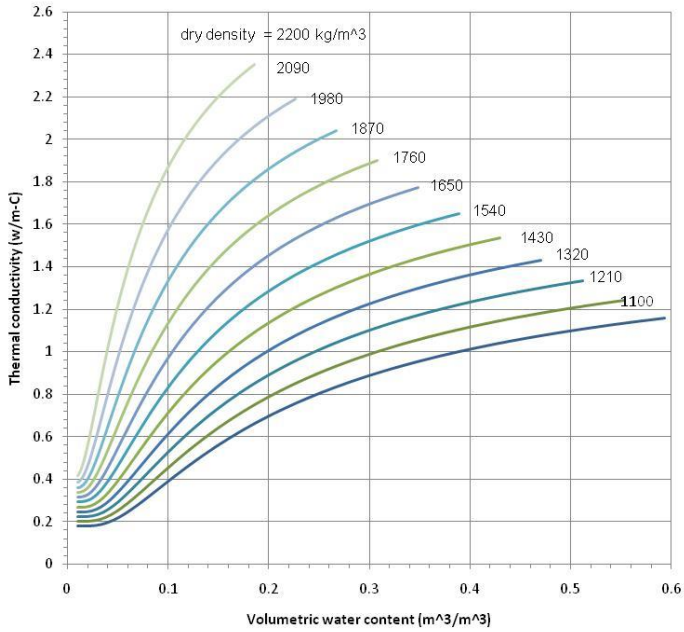

Figure 10 Thermal conductivity calculated with Lu at al approach at different volumetric water contents and dry densities for clay loam (quartz content = 36 %)

4.1.3 De Vries Approach (1963)

De Vries (1963) reviewed some of the formulas by which the thermal conductivity of soil is estimated based on the fraction and thermal conductivity of its constituents. The De Vries model (Tang et al., 2008) is expressed as:

$$\lambda_{unfrozen} = \frac{\theta_w \lambda_w + F_a (n-\theta_w)\lambda_a + F_s (1-n)\lambda_s}{\theta_w + F_a (n-\theta_w) + F_s (1-n)} \quad [252]$$

$$\lambda_{frozen} = \frac{\theta_i \lambda_i + \theta_u \lambda_w + F_a (n-\theta_w)\lambda_a + F_s (1-n)\lambda_s}{\theta_w + F_a (n-\theta_w) + F_s (1-n)}$$

$$F_a = \frac{1}{3}\left\{ \frac{2}{1+g_a\left(\frac{\lambda_a}{\lambda_w}-1\right)} + \frac{1}{1+g_c\left(\frac{\lambda_a}{\lambda_w}-1\right)} \right\} \quad [253]$$

$$F_s = \frac{1}{3}\left\{ \frac{2}{1+0.125\left(\frac{\lambda_s}{\lambda_w}-1\right)} + \frac{1}{1+0.75\left(\frac{\lambda_s}{\lambda_w}-1\right)} \right\} \quad [254]$$

$$g_a = 0.035 + 0.298 S_r$$

$$g_c = 1 - 2 g_a$$

where:

$\lambda_{unfrozen}$ = the thermal conductivity of unfrozen soil, *J/s-m-°C,*

λ_{frozen} = the thermal conductivity of frozen soil, *J/s-m-°C,*

λ_w = thermal conductivity of water, *J/s-m-°C*,

λ_a = thermal conductivity of air, *J/s-m-°C*,

λ_s = thermal conductivity of solid particles, *J/s-m-°C*,

λ_i = thermal conductivity of ice, *J/s-m-°C*,

θ_w = volumetric water content, m^3/m^3,

θ_w = volumetric ice content, m^3/m^3,

θ_u = volumetric unfrozen water content, m^3/m^3, and

S_r = degree of water saturation.

The unfrozen water content is determined by the approaches as described in the section of SFCC.

Figure 11 and Figure 12 illustrate the thermal conductivity predicted with the De Vries model for the sand and clay loam.

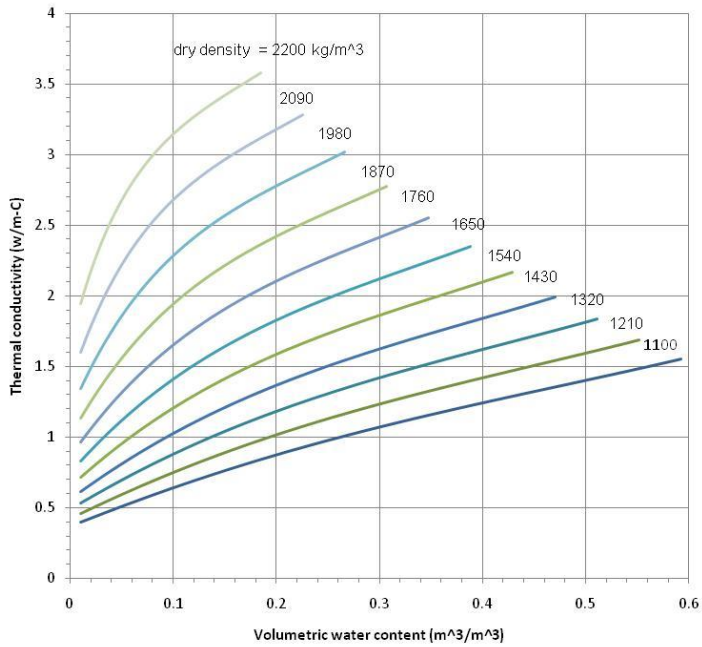

Figure 11 Thermal conductivity calculated with De Vries approach at different volumetric water contents and dry densities for sand (quartz content = 74 %)

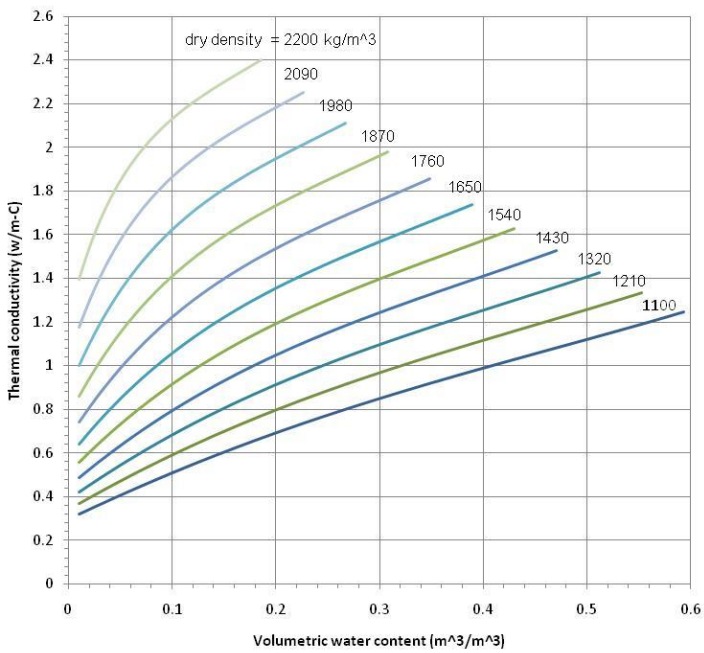

Figure 12 Thermal conductivity calculated with De Vries al approach at different volumetric water contents and dry densities for clay loam (quartz content = 36 %)

4.1.4 Côté and Konrad (2005)

Côté and Konrad (2005) study were based on nearly 200 experimental samples of thermal conductivity measurements and they proposed a generalized method to calculate thermal conductivity. The main point of this method is the relation between normalized thermal conductivity (or the Kerstern number in section 4.1.1) and the degree of saturation for different soil types and textures. This method is based on the normalized thermal conductivity concept shown in [235].

$$\lambda_e = \frac{\kappa S_r}{1+(\kappa-1)S_r} \qquad [\ 255\ ]$$

where

κ = an empirical parameters accounting for soil types shown in Table 4.

Other parameters in the above equation were defined in section 4.1.1.

The thermal conductivity of dry soil is determined using the following equation.

$$\lambda_{dry} = \chi \times 10^{-\eta n} \qquad [\ 256\ ]$$

where

χ = an empirical value accounting for soil types, W/m-°C (Table 5)

η = an empirical constant (Table 5).

n = soil porosity

Table 4 Typical Values of κ (Côté and Konrad, 2005)

Material	κ Unfrozen	κ Frozen
Gravels and coarse sands	4.60	1.70
Medium and fine sands	3.55	0.95
Silty and clayey soils	1.90	0.85
Organic fibrous soils (peat)	0.60	0.25

Table 5 Typical Values of χ and η (Côté and Konrad, 2005)

Material	χ (W/m-°C)	η
Crushed rock and gravels	1.70	1.80
Natural mineral soils	0.75	1.20
Organic fibrous soils (peat)	0.30	0.87

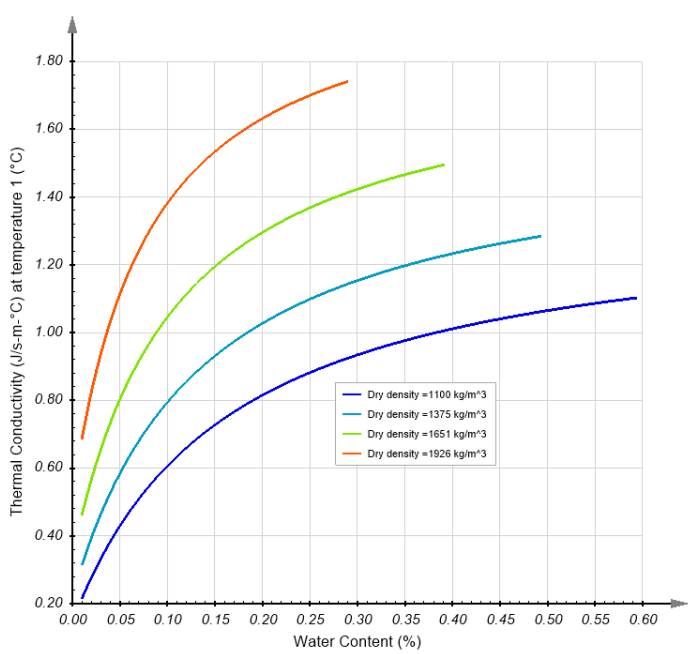

Figure 13 Thermal conductivity of crushed granite calculated with Côté and Konrad (2005) method with λ_s = 2.69 W/m-°C, n = 0.29.

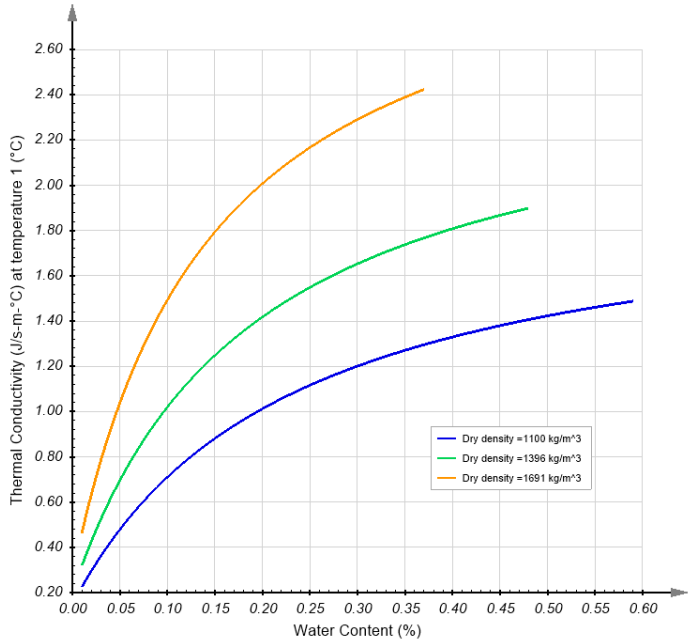

Figure 14 Thermal conductivity of Lowell sand calculated with Côté and Konrad (2005) method with λ_s = 5.5 W/m-°C, n = 0.37.

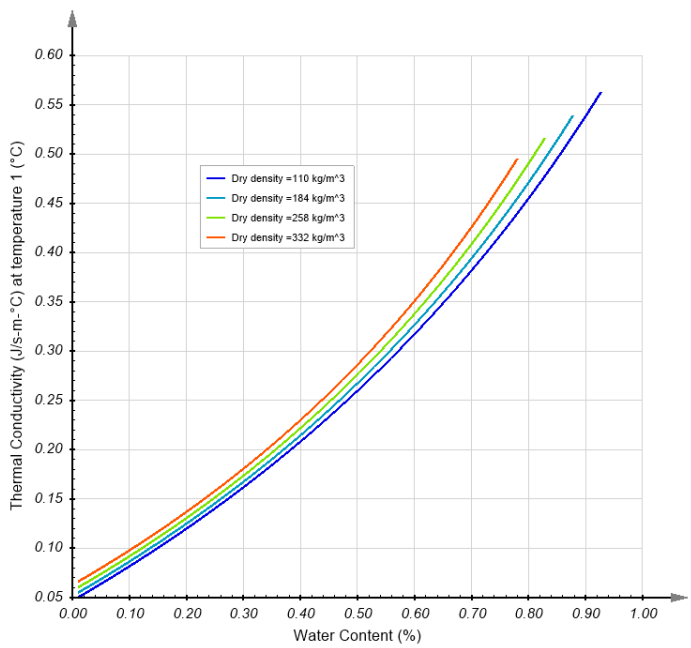

Figure 15 Thermal conductivity of Fairbanks peat calculated with Côté and Konrad (2005) method with λ_s = 0.25 W/m-°C, n = 0.78.

4.1.5 Comparison of Thermal Conductivity Calculated with Johansen, Lu et al., and De Vries Approach

Lu et al., (2007) presented the experimental data of thermal conductivity for different soils in laboratory. The calculated thermal conductivity with Johansen, Lu et al. (2007), and De Vries (1963) methods are compared in the Figure 13 for metric units and the Figure 14 for imperial units.

It can be seen from the figures below that the Johansen and Lu et al., (2007), approach is very similar, but Lu et al., (2007) approach can predict the thermal conductivity changing with the full range of water content. The De Vries (1963) approach can predict thermal conductivity at the mediate water content.

NOTE:

SVHEAT recommends Lu et al., (2007) or Johansen approach to estimate the thermal conductivity.

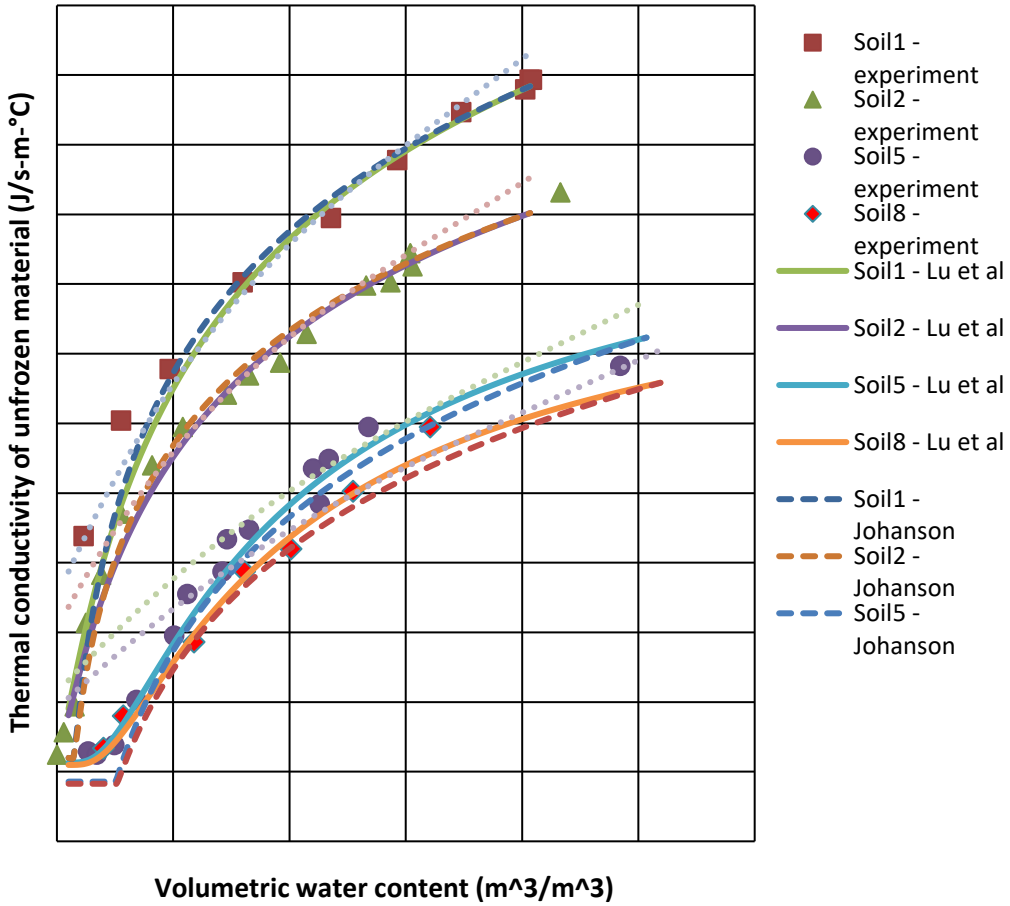

Figure 16 Comparison of thermal conductivity calculated with different approaches for unfrozen soils in metric units (experimental data from Lu et al., 2007)

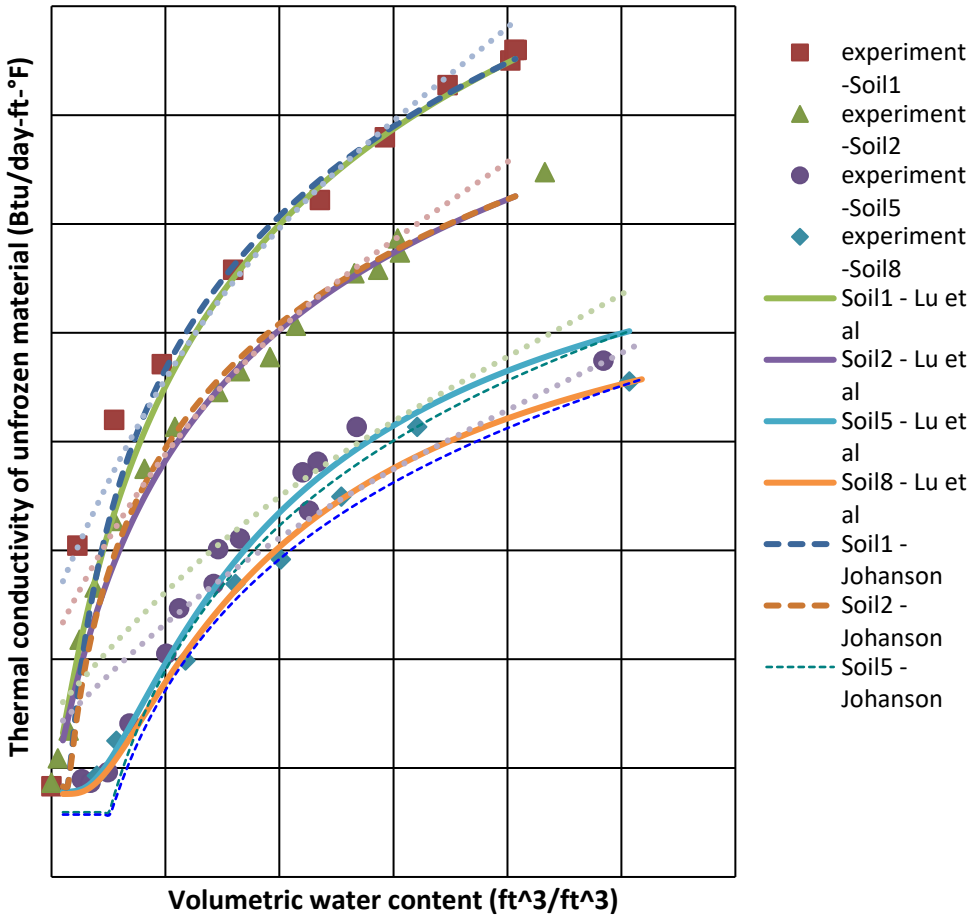

Figure 17 Comparison of thermal conductivity calculated with different approaches for unfrozen soils in imperial units (experimental data from Lu et al., 2007)

4.1.6 Measured by Experimental Data

Thermal conductivity may be provided with experimental data as a function of soil temperature. SVHEAT implements thermal conductivity curves through the use of table files. A table file is created using two columns of data, temperature versus thermal conductivity. The SVHEAT solver uses linear interpolation to estimate thermal conductivities between data points. Therefore, including more points will minimize the error in the estimation between points. As a general rule, it is good to use at least ten points to describe each thermal conductivity curve.

Below is a typical thermal conductivity curve. It can be seen that as the material freezes the thermal conductivity increases. This is due to the large difference between the thermal conductivity of water and ice.

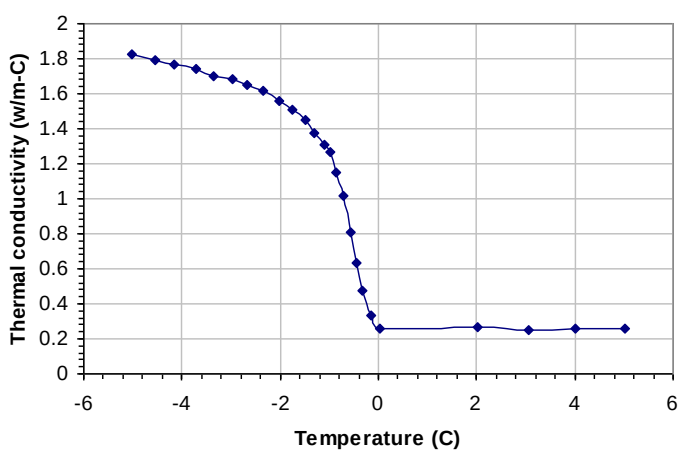

Figure 18 Typical thermal conductivity curve

Figure 16 to Figure 21 are the measured thermal conductivity for different soils at the different water contents. Table 4 lists the thermal conductivity for the common materials.

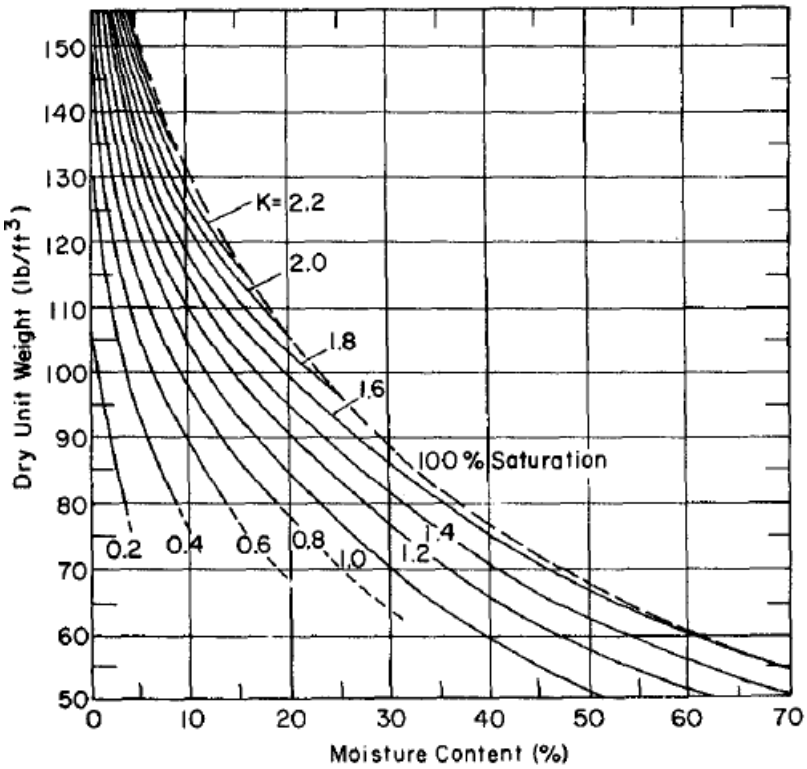

Figure 19 Average thermal conductivity for frozen sands and gravel **(Note: Thermal conductivity in Btu/ ft^{2}-hr-ºF-ft, from U.S. Army Corps of Engineers)**

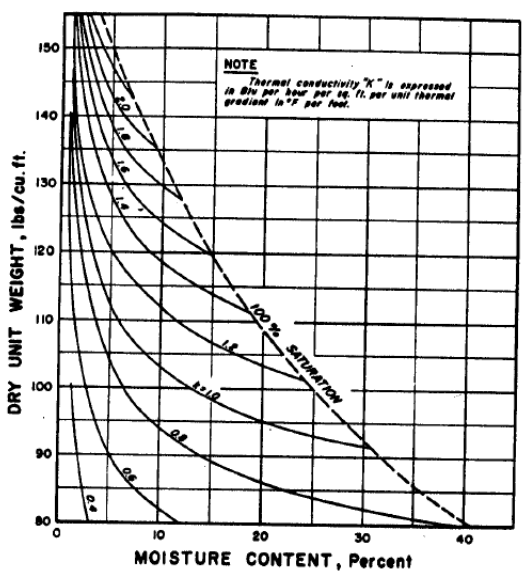

Figure 20 Average thermal conductivity for unfrozen sand and gravels **(Note: Thermal conductivity in Btu/ ft^{2}-hr-ºF-ft, from U.S. Army Corps of Engineers)**

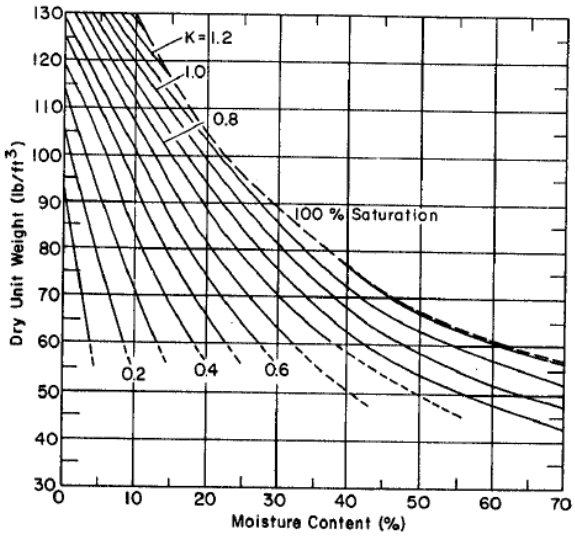

γ_d	w 90	120	100% saturated
50	N/A	N/A	1.20
40	1.00	N/A	1.23
30		0.98	1.26
20		0.61	1.26
pure ice			1.26

Figure 21 Average thermal conductivity for frozen silt and clay soils (Note: Thermal conductivity in Btu/ ft^2-hr-ºF-ft, from U.S. Army Corps of Engineers)

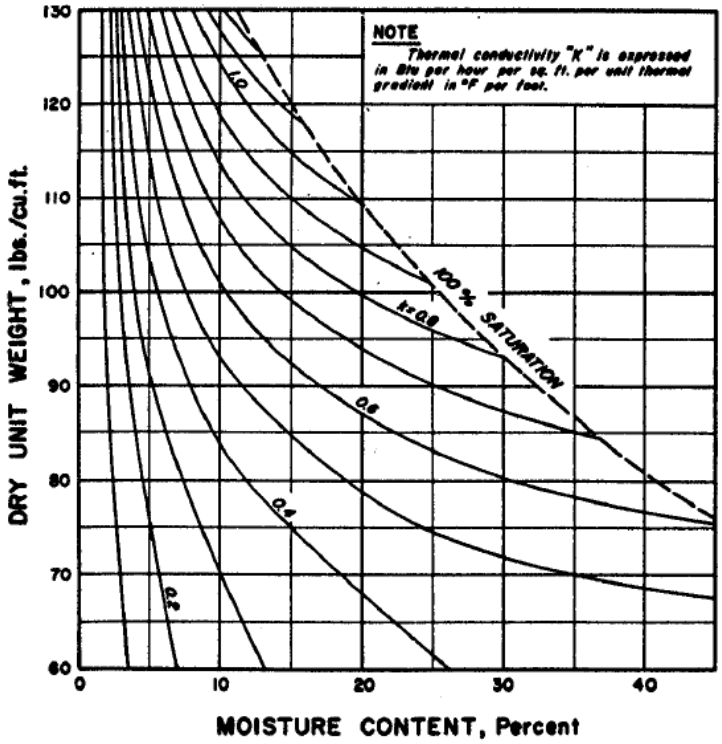

Figure 22 Average thermal conductivity for unfrozen silt and clay soils (Note: Thermal conductivity in Btu/ ft^2-hr-ºF-ft, from U.S. Army Corps of Engineers)

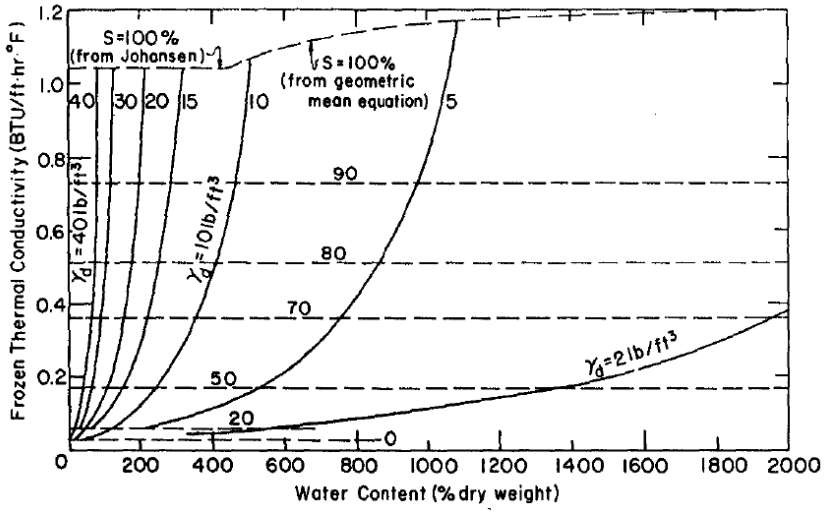

Figure 23 Thermal conductivity for frozen peat (from U.S. Army Corps of Engineers)

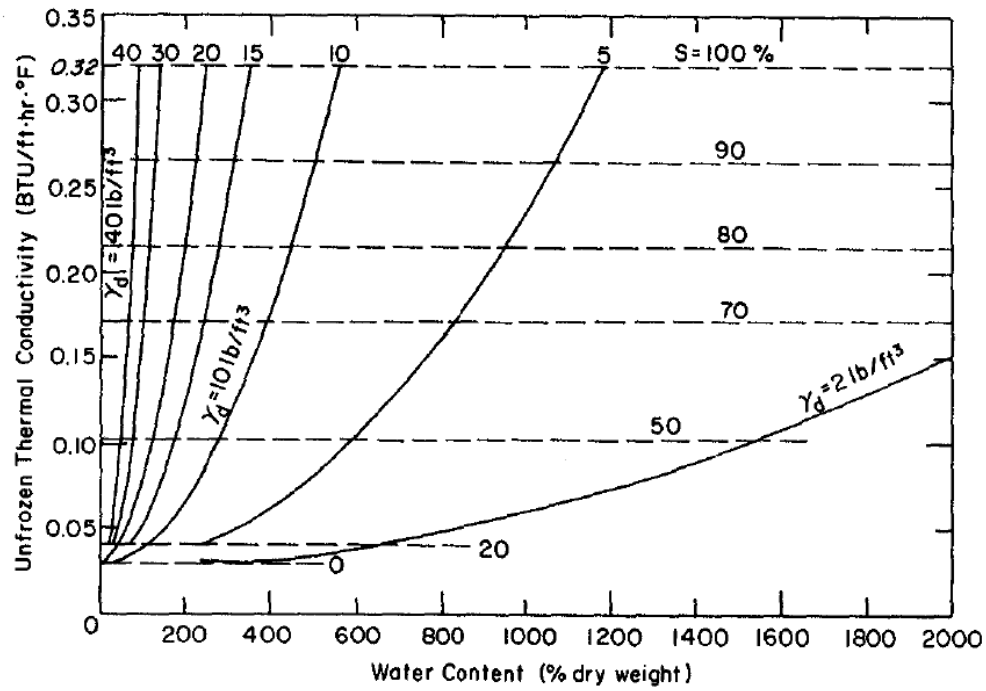

Figure 24 Thermal conductivity for unfrozen peat (from U.S. Army Corps of Engineers)

Table 6 Thermal conductivity for the common materials

Type of material	Description	Unit weight (lb/ft^3)	Thermal conductivity (Btu/ft^2-hr-^{o}F per in)	Thermal conductivity (Btu/hr-ft-^{o}F)
Asphalt paving Mixture	Mix with 6% by weight cutback asphalt	138	10.3	0.86
concrete	With sand and gravel for stone aggregate (oven-dried)	140	9	0.75
Concrete	With sand and gravel for stone aggregate (not dried)	140	12.0	1.0
Concrete	With lightweight aggregates,	120	5.2	0.43
Concrete	With expanded shale, clay, or slate	100	3.6	0.30
Concrete	With Expended slags, cinders	60	1.7	0.14
Concrete	With Pumice, perlite	40	1.15	0.096
Concrete	With vermiculite	30	0.90	0.075
Cellular concrete		20	0.7	0.058

Wood	Maple, Oak and similar hardwoods	45	1.10	0.092
Wood	Fir, pine, and similar soft woods	32	0.8	0.067
Building boards	Asbestos-cement board	120	4.0	0.33
Building boards	Plywood, fiberboard	34	0.8	0.067
	Laminated or homogeneous	26.33	0.42 - 0.55	0.035 – 0.046
	Wood fiber-hardboard type	65	1.4	0.12
Blanket and batt insulation	Mineral wool, fibrous form, processed from rock, slag, or glass	1.5 - 4.0	0.27	0.022
Board and slab insulation	Cellular glass corkboard (without added binder)	6.5-8.0	0.27	0.022
Insulation	Glass fiber wood or cane fiber interior finish (plank, tile, lath)	15.0	0.35	0.029
	Expanded polystyrene	1.6	0.29	0.024
	Expanded ureaformal-dyhyde	1.0	0.25	--
	Expanded perlite	9.5-11.5	0.34	--
	Polyurethane foam	1.5-3.0	0.34	--
	Mineral wool with resin binder	15.0	0.28	0.023
	Mineral wool with asphalt binder	15.0	0.31	0.026
Loose fill insulation	Cork, granulated	5-12	0.25-0.36	--
	Expanded perite	3-4	0.28	--
	Mineral wool (glass, slag, or rock)	2-5	0.30	--
	Sawdust or shavings	8- 15	0.45	0.37
	Vermiculite (expanded)	7.0-8.2	0.48	0.040
	Wood fiber: redwood, hemlock or fir	2.0-3.5	0.30	0.025
Miscellaneous	Aluminum	168	1416	118
	Copper	549	2640	220
	Ductile iron	468	360	30
	glass	164	5.5	0.46
ice	ice	57	15.4	0.46
Snow	Snow, new, loose	5.3	0.6	0.05
	Snow on ground	18.7	1.58	0.13
	Snow, drifted and compacted	18.7	1.58	0.13
Steel		487	310	25.8
water	average	62.4	4.2	0.35

Reference: Arctic and subarctic construction calculation methods for determination of depths of freeze and thaw in soils. Departments of the Army and the air force, January, 1988.

4.1.7 Estimated by Empirical Expression

SVHEAT provides an approach that allows users to specify the empirical expression as a function of temperature or water content.

4.1.8 Thermal Conductivity of Snow

The thermal conductivity of snow is primarily related to the snow density and it is estimated with the Yen equation (Yen, 1969):

$$\lambda_{sn} = 2.86\left(\frac{\rho_{sn}}{\rho_w}\right)^2 \qquad [\ 257\ ]$$

where:

λ_{sn} = thermal conductivity of snow, *J/s-m-°C*,

2.86 = parameter, *J/s-m-°C*,

ρ_{sn} = density of snow, *kg/m³*, and

ρ_w = density of water, *kg/m³*.

The density of snow varies depending on snow age as shown in Figure 22. The data analysis from Figure 22 indicates that the mean density of snow is about 298.66 *kg/m³*, or 18.64 *lb/ft³*. Therefore, the mean thermal conductivity calculated with the equation [255] is around 0.255 *J/s-m-°C*.

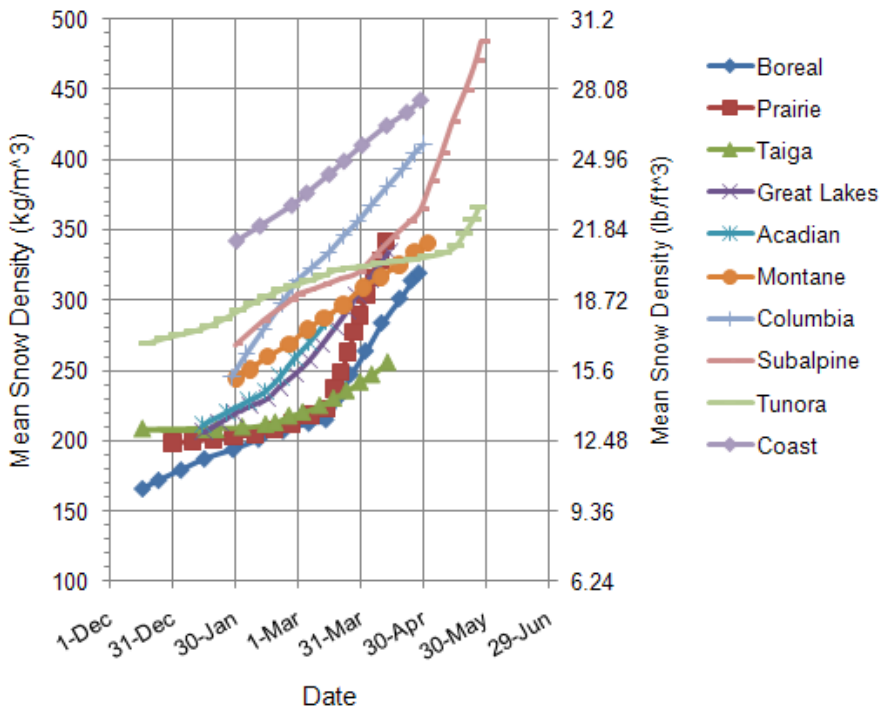

Figure 25 The density of snow (from MacKay and Findlay 1971, Hwang 1976)

4.2 VOLUMETRIC HEAT CAPACITY

The capacity for heat storage is made up of two parts. The first part is the volumetric heat capacity of a material. The second part is a term included to account for the energy released or adsorbed due to phase change. In general, it can be expressed as given in equation [4]. Please note that the term of heat capacity used in this document is referred to as the first part of volumetric heat capacity. The energy release or absorption in phase change will be discussed in the section of soil freezing characteristic curve (SFCC). The following two sections describe these formulations in detail.

4.2.1 Constant Formulation

The constant method for volumetric heat capacity requires the user to enter frozen and unfrozen volumetric heat capacity.

$$C = C_u \text{ if } T > T_{ef}$$
$$C = C_f \text{ otherwise} \qquad [\ 258\ ]$$

where:

T	= temperature, *°C*,
T_{ef}	= the temperature at soil freezing point, *°C*,
C	= volumetric heat capacity, *J/m³-°C*,
C_u	= unfrozen volumetric heat capacity, *J/m³-°C*, and
C_f	= frozen volumetric heat capacity, *J/m³-°C*.

The following table lists the heat capacity of the common materials:

Table 7 Mass specific heat capacity of various materials (U.S. Army Corps of Engineers)

Material	Temperature (°C)	Specific heat (J/kg-°C)	Temperature (°F)	Specific heat (Btu/lb-°F)
Aluminum	-33.00	837.35	-27.4	0.20
Asbestos fibers		1046.68		0.25
Concrete (avg. stone)		837.35		0.20
Concrete (dams)		921.08		0.22
Copper	7.00	837.35	44.6	0.20

Corkboard	32.78	1214.15	91	0.29
	-28.33	1214.15	-19	0.29
Cork, granulated		1758.43		0.42
Fiberglas board	43.89	1004.82	111	0.24
	-30.00	795.48	-22	0.19
Foamglas	-28.89	669.88	-20	0.16
Glass block, expanded	44.44	753.61	112	0.18
Glass sheets		837.35		0.20
Glass wool		669.88		0.16
ice	0.00	2009.63	32	0.48
iron (alpha)	7.00	460.54	44.6	0.11
iron (alpha)	7.00	460.54	44.6	0.11
Masonry		921.08		0.22
Mineral wool		921.08		0.22
Perlite, expanded		921.08		0.22
Plystyrene, cellular foam		1130.42		0.27
Ployurethane foam		1046.68		0.25
Sawdust		2512.038		0.60
Snow		2093.37		0.50
Steel		502.41		0.12
Straw		1465.36		0.35
Water		4186.73		1.00
Woods (avg.)	20.00	1381.62	68	0.33
Woods (fibraboard)	64.44	1423.49	148	0.34

Reference: Arctic and subarctic construction calculation methods for determination of depths of freeze and thaw in soils. Departments of the Army and the air force, January, 1988.

4.2.2 Jame-Newman Formulation

Jame (1977) and Newman (1995) provided a formulation that uses commonly measured values including dry density and volumetric water content for the computation of volumetric heat capacity. The function neglects the specific heat capacity of air, which are orders of magnitude lower than solid, liquid, and ice components.

$$C = \gamma_d [c_s + c_w w_u + c_i w_i] \qquad \textbf{[259]}$$

where:

C = volumetric heat capacity, J/m^3-°C,

γ_d = dry unit weight of soil, kN/m^3,

C_s = mass specific heat of soil solids, J/kg-°C

C_w = mass specific heat of unfrozen water, 4184 J/kg-°C,

c_i = mass specific heat of ice, 2100 J/kg-°C,

W_u = gravimetric unfrozen water content of the soil, and

W_i = gravimetric ice content of the soil.

The volumetric unfrozen water content can be determined by soil freezing characteristic curve. Using volume-mass relations from Fredlund and Rahardjo (1993), the gravimetric water content can be calculated from the volumetric water content as follows:

$$w = \frac{\theta_w \rho_w}{\gamma_d} \qquad \textbf{[260]}$$

where:

ρ_w = density of water, 1000 kg/m^3,

θ_w = volumetric water content, and

γ_d = dry unit weight of soil, kN/m^3.

4.2.3 Curve Comparison

The following function describes how energy is stored in a material as temperature changes. A point on the curve describes the amount of energy required to keep the material at a given temperature. The part of the curve that has a steep slope describes the energy loss from the material, as there is a phase change from liquid to ice.

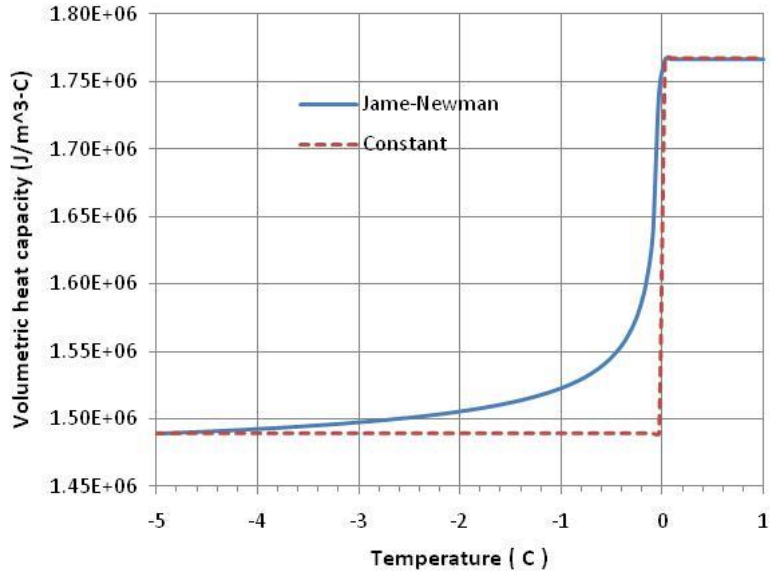

Figure 26 Newman versus Constant Formulation

In the constant formulation the user is required to enter the temperature at which the water will change phases from water to ice. In the above figure it can be seen that using constants to describe the volumetric heat capacity in the frozen and unfrozen states causes severe discontinuities at the phase change temperature. Discontinuities such as these may cause convergence problems in finite element solutions. The Jame-Newman formulation has been included with the SVHEAT software to alleviate such convergence problems. The Jame-Newman formulation provides a method for describing the volumetric heat capacity with a smooth transition between the frozen and unfrozen states. In a seepage and heat coupled model, Jame-Newman formula is recommended to estimate heat capacity.

Table 8 Typical values of mass specific heat capacity and density

Material	Density (kg/m^3)	Mass Specific Heat Capacity (J/kg-°C)
Quartz	2660	755
Clay Minerals	2650	755
Organic Matter	1300	1930
Water	1000	4184
Ice	920	2100
Air	1.25	1000

4.3 SOIL FREEZING CHARACTERISTIC CURVE (SFCC)

As a material freezes, the water within the material does not freeze at a uniform temperature. This phenomenon known to some as freezing point depression is caused due to the formation of ice. Ice formation in materials causes suction. This suction acting on the water phase causes it to remain unfrozen at temperatures below the freezing point. In fine-grained soils, it is possible that water will remain unfrozen at temperatures of -20 °C. For a given soil, unfrozen water content is uniquely determined by the negative temperature, regardless how much initial water content before freezing. This significant behavior of between unfrozen water content and temperature is referred to as soil freezing characteristic curve (SFCC). It is similar to the behavior of soil water content as the function of suction in soil water characteristic curve (SWCC).

SFCC plays four roles in SVHEAT calculation:

- Determining unfrozen water content at a given temperature below freezing point,
- Calculate ice content for a given water content above freezing point, and a given temperature,
- Calculate energy release or absorption during phase change,
- Calculate hydraulic conductivity reduction in soil freezing-frozen regime.

Ice content and unfrozen water content have a major effect on thermal conductivity and heat capacity, as indicated in equation [235], equation[252], and equation [256]. Due to huge amount of latent heat of water ($3.34X10^8$ J/m^3), a little

ice segregation will generate a large amount of energy released during freezing. Therefore, it is very important to determine or estimate SFCC in calculation of thermal conductivity, heat capacity, and phase change. The following sections describe how to determine or estimate SFCC with SVHEAT.

4.3.1 Estimated SFCC with SWCC

Many researchers have suggested that SFCC is very similar to the SWCC in shape. SVHEAT provides the approach using SWCC to estimate SFCC, in which the soil suction under the temperature is calculated with Clapeyron equation [34]. Using SWCC equation as described in the SVFLUX Theory Manual, the unfrozen water content can be obtained.

4.3.2 Estimated SFCC by Empirical Expression

As another option, SFCC can be calculated using empirical expression. SVHEAT allows user to specify the SFCC expression and m_2^i expression, which is the slope or a derivate of SFCC. For example, Tice et al., (1976) proposed an expression of unfrozen water content as the function of temperature:

$$w_u = \begin{cases} w_w & if\ \ T > T_{ef} \\ a|T|^{-b} & else \end{cases} \qquad \textbf{[261]}$$

where:

w_u	= gravimetric unfrozen water content,
w_w	= gravimetric water content of unfrozen soil,
$\|T\|$	= absolute value of the negative temperature, *°C,*
T_{ef}	= Soil freezing point, *°C*, and
a and *b*	= experimental parameters.

In SVHEAT the water content is expressed as the volumetric water content, so that the equation [259] is modified as the equation [260]:

$$\theta_u = \begin{cases} \theta_w & if\ \ T > T_{ef} \\ \dfrac{\gamma_d}{\rho_w} a|T|^{-b} & else \end{cases} \qquad \textbf{[262]}$$

$$m_2^i = \begin{cases} 0 & if\ \ T > T_{ef} \\ \dfrac{\gamma_d}{\rho_w} ab|T|^{-(b+1)} & else \end{cases} \qquad \textbf{[263]}$$

where:

θ_u	= volumetric unfrozen water content, m^3/m^3,
θ_w	= volumetric water content of unfrozen soil, m^3/m^3,
γ_d	= soil dry density, kg/m^3,
ρ_w	= water density, kg/m^3, and
m_2^i	= the slope of SFCC.

The values of *parameter a* and parameter *b* in the equation [260] for the common soils are provided as a reference in the following table:

Table 9 Experimental parameters, *a* and *b*, used in equation [260]

Soil Type	Specific surface area	Parameter *a*	Parameter b
Morin Clay	60	0.096	0.406
Caen silt	-	0.095	0.227
Calgary silt	-	0.096	0.364
Manchester silt	-	0.025	0.864
Kaolin	-	0.104	0.425
Allendale clay	-	0.157	0.187
Inuvik clay	-	0.145	0.254
Tomokomai clay	54	0.195	0.305
Suffield clay	140	0.139	0.315
Fairbanks silt	40	0.048	0.326
Illite	50.6	0.332	0.273
Undisturbed Fairbanks silt	-	0.058	0.439
China silt	6	0.014	1.46
Japanese clay (45%)	-	0.128	0.402
West Lebanon Gravel	15	0.021	0.408

Manchester silt	18	0.025	0.515
Kaolin (KCa-1)	23	0.058	0.864
China silt	40	0.032	0.531
Leda clay	58	0.108	0.649
Morin clay	60	0.095	0.479
O'Brien clay	61	0.104	0.484
Goodrich clay	68	0.0864	0.456
Tuto clay	78	0.128	0.603
Sweden 478 clay	113	0.271	0.472
Suffield silty clay	148	0.111	0.254
Frederick clay	159	0.140	0.279
Elleworth clay	184	0.112	0.293
Regina clay	291	0.211	0.238
Niagara silt	37	0.066	0.410
Norway LE-1 clay	52	0.099	0.523
Kaolin No7	72	0.198	0.689
Athena silt Loam	83	0.06	0.301
Sweden 201 clay	419	0.197	0.492
Hectorie	419	0.384	0.369
Volcanic Ash	474	0.031	0.097
Hawaiian clay	382	0.3242	0.243
Umiat bentonite	800	0.6755	0.343
Wyoming bentonite	800	0.5599	0.29
Basalt	6	0.0345	1.13
Morin clay	60	0.131	0.505

Figure 24 and Figure 25 illustrate the SFCC and m_2^i estimated by the Tice and Anderson approach at the water content = 0.5, 0.3, and 0.15. The temperature at the end of phase change (i.e., T_{ep} parameter used in SFCC) can be determined using the relationship between m_2^i and the temperature. For example, according to the Figure 25 when $T < -3\ ^oC$, $m_2^i = 0$. Therefore T_{ep} can be chosen as -3 ^oC.

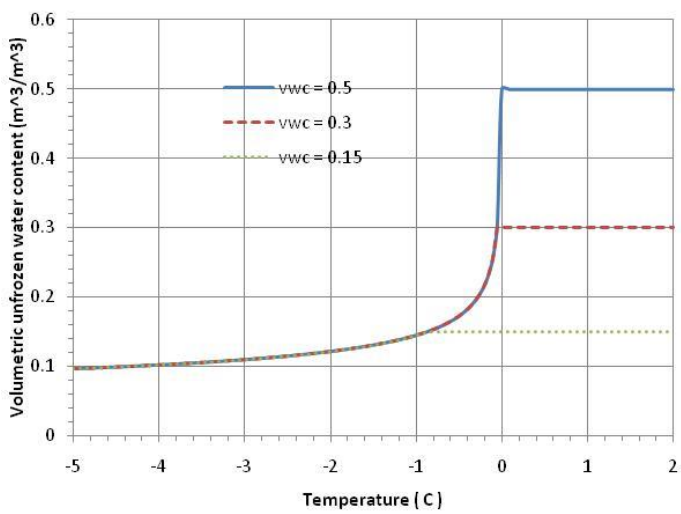

Figure 27 SFCC with Tice and Anderson (1976) approach

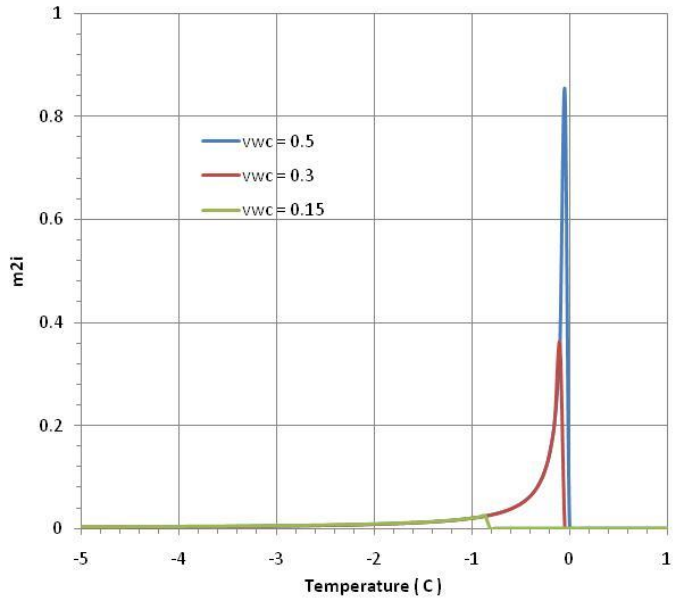

Figure 28 m2i with Tice and Anderson (1976) SFCC approach

NOTE:

In the SVHEAT software usek the "m2i Graph" to display m_2^i changing with the temperature, and then determine the T_{ep} value that is required for the SFCC.

4.3.3 Exponential Expression of SFCC

Mackenzie et al., (2006), Lebeau and Konrad (2009) use an exponential expression to describe SFCC:

$$\theta_u = (\theta_w - \theta_r)\exp\left[-\left(\frac{T - T_{ef}}{\zeta}\right)^2\right] + \theta_r \quad if\ T < T_{ef} \qquad [\ 264\ ]$$

$$m_2^i = -2(\theta_w - \theta_r)\frac{T - T_{ef}}{\zeta^2}\exp\left[-\left(\frac{T - T_{ef}}{\zeta}\right)^2\right] = -2(\theta_u - \theta_r)\frac{T - T_{ef}}{\zeta^2} \quad if\ T < T_{ef} \qquad [\ 265\ ]$$

where:

θ_u	= unfrozen water content, m^3/m^3,
θ_w	= volumetric water content of unfrozen soil, i.e., $T >= T_{ef}$,
θ_r	= residual water content after the temperature $T < T_{ep}$, m^3/m^3,
T_{ef}	= soil freezing point, or liquidus temperature, ^oC,
T_{ep}	= temperature at the end of ice phase change, or solidus temperature, ^oC, and
ζ	= an empirical parameter, approximated with the value of $(T_{ef} - T_{ep})/2$.

The parameter ζ is used to control the shape of SFCC in the exponential expression. Figure 26 and Figure 27 show the impact of the parameter ζ on the shape of SFCC and m_2^i.

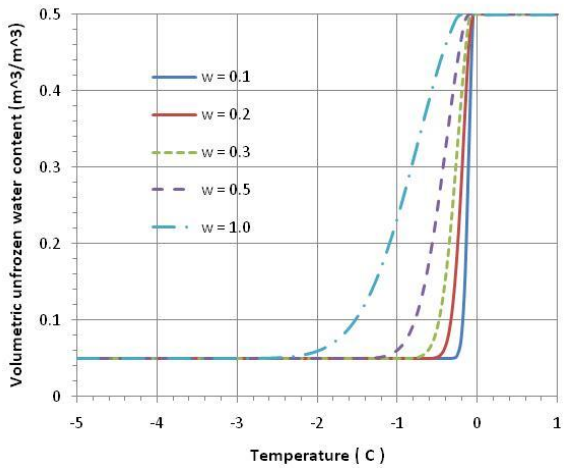

Figure 29 SFCC with exponential expression

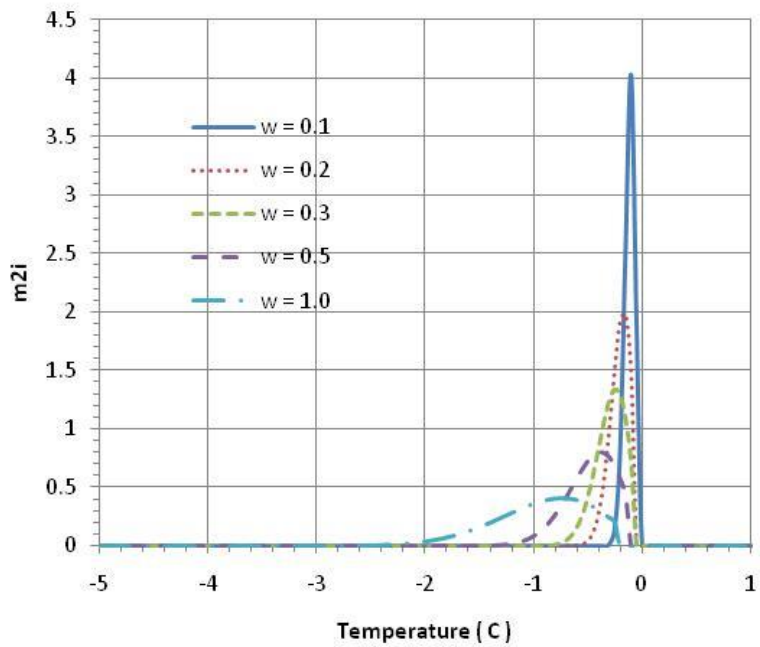

Figure 30 m2i with exponential expression

4.3.4 Determine SFCC with Multi-lines

In a simplified case it can be assumed that unfrozen water content is decreased linearly with temperature decreasing, such that SFCC and m_2^i can be expressed as

$$\theta_u = \theta_w,\ if\ T > T_{ef}$$
$$\theta_u = \theta_{res} + \frac{\theta_i}{T_{ef} - T_{ep}}(T - T_{ep}),\ \ if\ T_{ef} >= T >= T_{ep} \qquad [\ 266\ ]$$
$$\theta_u = \theta_{res},\ if\ T < T_{ep}$$

$$m_2^i = \frac{\theta_w}{T_{ef} - T_{ep}} \qquad [\ 267\ ]$$

where:

θ_u	= unfrozen water content, m^3/m^3,
θ_{res}	= the remaining unfrozen water content after phase change is completed, m^3/m^3,
θ_w	= volumetric water content before freezing, m^3/m^3,
T_{ef}	= soil freezing temperature, ^oC, *and*

T_{ep} = the temperature at the end of soil phase change, ^oC

With this method, m_2^i is a constant value, and decreases with the decrease in the value of T_{ep}. In other words, the phase change can be relaxed by adjusting the value of T_{ep} as shown in Figure 28 and Figure 29. This feature may be useful in some cases to ensure a model running stability with the phase change.

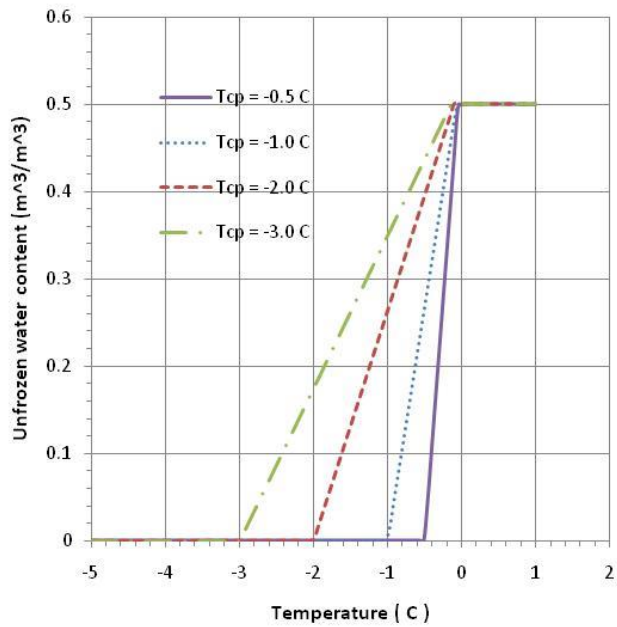

Figure 31 SFCC with multi-line estimation

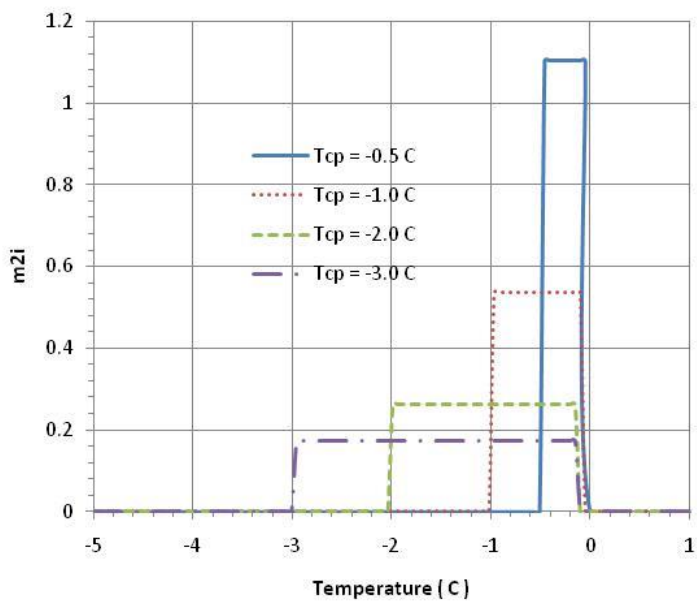

Figure 32 m2i with the multi-line estimation

4.3.5 Determine SFCC by Experimental Data

If a user can obtain experimental data of unfrozen water content, it would be a better way to reach a high precision in FEM calculation. SVHEAT provides a data table, allowing for user to specify the unfrozen water content as the function of temperature.

SVHEAT uses the derivative of the unfrozen water content curve to calculate the change in the latent heat component of the energy storage term of Equation [5]. The equations needed to describe the derivative of most unfrozen water content curves can be quite complex. Therefore, table files have been used to describe the necessary functions to the SVHEAT solver.

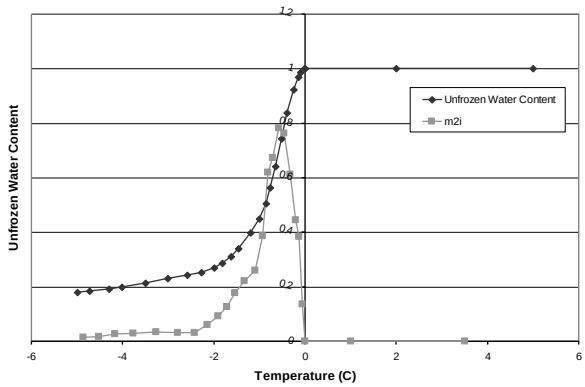

Figure 33 Typical unfrozen water content and m_2^i curves

4.4 HYDRAULIC CONDUCTIVITY REDUCTION

In the seepage and heat coupled model, hydraulic conductivity in freezing or frozen regime is significantly reduced. Two approaches are implemented in SVHEAT to consider the hydraulic conductivity reduction in frozen soil.

4.4.1 Impedance Factor (Jame, 1977)

Jame originally proposed an empirical expression to account for the ice existence of ice effect on the hydraulic conductivity. The equation is

$$k_f = 10^{-ES_i} k_u \qquad [\ 268\ ]$$

where:

E	= impedance factor, a dimensionless and empirical constant,
S_i	= the degree of ice saturation, $S_i = \theta_i/\theta_{ws}$,
θ_i	= volumetric ice content, m^3/m^3,
θ_{ws}	= volumetric saturated water content, m^3/m^3,
k_u	= hydraulic conductivity of unfrozen soil, m/s, and
k_f	= hydraulic conductivity of frozen soil, m/s

The approaches to determine hydraulic conductivity of unfrozen soil please see the SVFLUX Theory Manual.

4.4.2 Estimated by SWCC

SVHEAT employs Clapeyron equation [34] to calculate the pore water suction for the given temperature below freezing point, and then uses the relationship between hydraulic conductivity and suction to calculate hydraulic conductivity.

5 BOUNDARY CONDITIONS

SVHEAT implements the use of Temperature (Dirichlet), Gradient (Neumann), and convection (Robin) boundary conditions. In addition, SVHEAT provides special boundary conditions named as Climate boundary, and Thermal Insulation boundary.

- A Temperature boundary condition forces the solution of temperature in the governing partial differential to the value defined by an expression on a continuous series of one or more boundary segments. The expression may be an explicit specification value, involving only constants and coordinates, or it may be an implicit relationship involving values and derivatives of system variables (FlexPDE User's Manual, 2001).
- The Gradient boundary condition represents a generalized flux boundary condition derived from the divergence theorem. The expression may be an explicit specification, involving only constants and coordinates, or it may be an implicit relation involving values and derivatives of system variables. The Gradient boundary condition is a generalization of the concept of a flux boundary condition (FlexPDE User's Manual, 2001).
- Convection and radiation boundary condition applies to a boundary exposed to moving fluid, for example, air temperature. In SVHEAT, the convection and radiation boundary condition is implemented as one of climate condition, but it can be applied to outer and inner boundary.
- Climate boundary condition is used to specify boundary condition related to the climate data, including air temperature, wind, sun radiation, snow cover, or thermosyphon, etc.
- Thermal insulation boundary condition is implemented for easy to use the very thin layer of thermal insulation in the model simulation.

5.1 RULES TO SPECIFY BOUNDARY CONDITIONS

SVHEAT provides an interface allowing user to specify a constant value or expression of temperature or thermal flux. To build an expression of temperature or thermal flux, the system variable may be used.

NOTE:
The main system variables in SVHEAT include *Te* (Temperature), *t* (Time), *x* (*x*-coordinate), *y* (*y*-coordinate), and *z* (*z*-coordinate).
The variable of soil freezing point, *Tef*, and temperature at phase change finished, *Tep*, are available for freezing/thawing process.

FlexPDE uses integration by parts to reduce the order of second derivative terms in the system equations. Application of this technique over a two-dimensional computation cell produces an interior area integral term and a boundary line integral term. Forming the same integral in two adjacent computation cells produces the same boundary integral at their interface, except that the direction of integration is opposite in the two cells. If the integrals are added together to form the total integral, the shared boundary integrals cancel (FlexPDE User's Manual, 2001).

Applied to the term *Dx(f)*, where *f* is an expression containing further derivative terms, integration by parts yields:

$$\int \frac{\partial f}{\partial x} \cdot \partial V = \int f \cdot c \cdot \partial s \qquad [\ 269\ ]$$

where *c* denotes the *x*-component of the outward surface-normal unit vector and *dS* is the differential surface element (FlexPDE User's Manual, 2001). (*y*- and *z*- derivative terms are handled similarly, with *c* replaced by the appropriate unit-vector component).

Applied to the term *Dxx(f)*, where *f* denotes a scalar quantity, integration by parts yields:

$$\int \frac{\partial^2 f}{\partial x^2} \cdot \partial V = \int \frac{\partial f}{\partial x} \cdot c \cdot \partial s \qquad [\ 270\ ]$$

where *c* denotes the *x*-component of the outward surface-normal unit vector and *dS* is the differential surface element FlexPDE (2001). (*y*- and *z*- derivative terms are handled similarly, with *c* replaced by the appropriate unit-vector component).

FlexPDE performs these integrations in 3 dimensions, including the volume and surface elements appropriate to the geometry. In 2D Cartesian geometry, the volume cell is extended one unit in the *z* direction. This technique forms the basis of the treatment of exterior boundary conditions and interior material interface behavior in (FlexPDE User's Manual, 2001).

NOTE:
If statements will be of the form *IF* expression *THEN* expression *ELSE* expression. The *THEN* or *ELSE* expression may contain nested *IF...THEN...ELSE* expressions. Each *ELSE* will bind to the nearest *IF.*

NOTE:
See the User's Manual for more a more detailed discussion on each specific system of boundary condition usage.

5.2 CLIMATE BOUNDARY CONDITIONS

The temperature and thermal flux applied to the boundary may be associated with the climate temperature and conditions. SVHEAT implements the following approaches to determine the soil temperature at the ground surface based on the climate temperature.

- Approximated with air temperature
- Empirical based N-Factor
- Thermal balance based
- Thermosyphon
- User specified thermal convection and radiation.

5.2.1 Equal to Air Temperature

In the simple case if no snow existence, the soil temperature at the applied boundary is approximated with the air temperature, i.e.

$$T\big|_{surface} = T_a \qquad [\ 271\ ]$$

5.2.2 N-Factor

The soil temperature at the applied boundary is estimated using the following empirical equation:

$$T\big|_{surface} = NF(T_a - T_{ef}) + T_{ef} \qquad [\ 272\ ]$$

where:

NF	= empirical value of N-factor,
T_a	= air temperature, ℃, and
T_{ef}	= temperature at soil freezing point, ℃.

The N-Factor can be specified as a global value or daily basis in SVHEAT. Daily basis allows user to specify the different values day-by-day. Use the below table for N-Factor values for various surfaces.

Table 10 N-Factor values for common surfaces

Surface Type	Freezing (n_f)	Thawing (n_t)
Soil Surface - spruce trees, brush, moss over peat	0.29 (under snow)	0.37
Soil Surface - brush, moss over peat	0.25 (under snow)	0.73
Turf	0.5 (under snow)	1.0
Snow	1.0	-
	0.6 - 1.0	1.3 - 2
Probable range for northern conditions	0.9 - 0.95	-
Asphalt pavement	0.29 - 1.0 or greater	1.4 - 2.3
Probable range for northern conditions	0.9 - 0.95	-
Concrete Pavement	0.25 - 0.95	1.3 - 2.1
Probable range for northern conditions	0.7 - 0.9	-

The Food and Agriculture Organization of the United Nations presents good information on weather analysis at: http://www.fao.org//docrep/x0490e/x0490e07.htm

5.2.3 Boundary with Snow Cover

If the surface of the applied boundary is covered with snow, the snow cover is regarded as a virtual layer. There is thermal resistance to the heat flow from the surface of snow cover to the soil. Figure 31 is a conceptual model with the boundary A-B

covered with snow. Because snow has a lower value of thermal conductivity the temperature at the ground surface, T_g, will be different from the temperature at the snow surface, T_{sn}. The magnitude of the difference will depend on the snow depth.

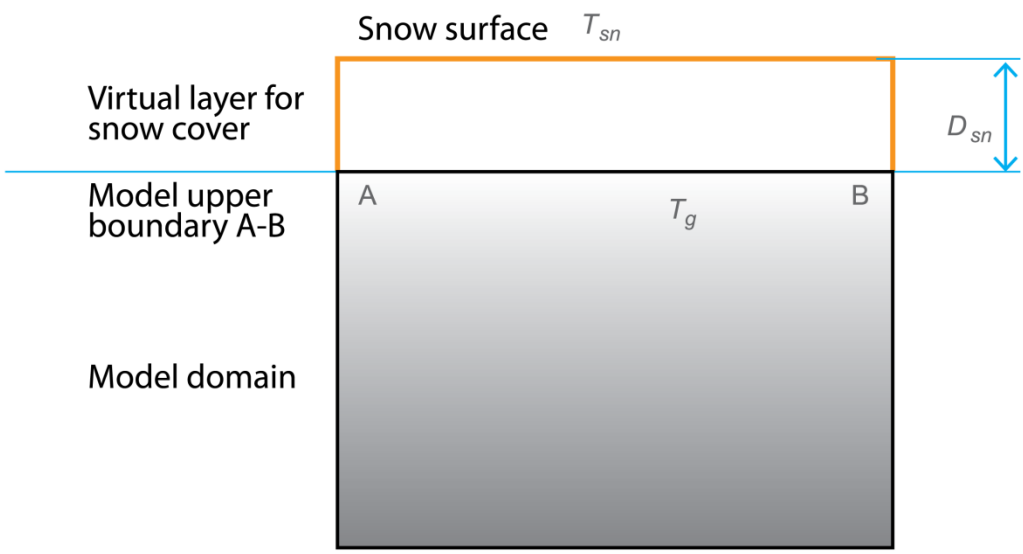

Figure 34 Boundary condition with snow cover

In the case without consideration of heat storage in the snow cover, the heat flux through the snow cover must be equal to the heat flux at the ground surface, that is,

$$\lambda_{sn}\frac{T_{sn}-T_g}{D_{sn}}=q_{Tg} \qquad [\ 273\ ]$$

$$q_{Tg}=\lambda\frac{\partial T}{\partial Z}-L_v q_v-\left(C_w q_L+C_v q_v+C_a q_a\right)\left(T-T_{in}\right) \qquad [\ 274\ ]$$

where:

T_{sn}	= temperature at the snow surface, *°C*,
T_g	= temperature at the ground surface, *°C*
D_{sn}	= snow depth, *m*,
λ_s	= thermal conductivity of snow, *J/s-m-°C*,
λ	= thermal conductivity of soil, *J/s-m-°C*,
q_{Tg}	= soil heat flux at the applied boundary, *J/s-m²*,
L_v	= latent of heat for water evaporation, *J/m³*,
q_v	= vapour water in soil flow velocity, *m/s*,
q_L	= liquid water in soil flow velocity, *m/s*,
q_a	= dry air in soil flow velocity, *m/s*,
C_w	= heat capacity of water, *J/m³-°C*,
C_v	= heat capacity of water vapour, *J/m³-°C*,
C_a	= heat capacity of dry air, *J/m³-°C*, and
T_{in}	= temperature of water, vapour, or air.

Therefore, the temperature applied to the boundary can be expressed in term of snow depth and the temperature at the snow surface:

$$T\big|_{surface}=T_g=T_{sn}-\frac{D_{sn}}{\lambda_s}q_{Tg} \qquad [\ 275\ ]$$

The temperature at the snow surface can be determined using the equation [271], or [272]. It can be seen from equation [273] that when the snow depth, D_{sn} = 0, the equation [273] simplifies to equation [271], or [272]. The thermal conductivity can be calculated with equation [273]. The snow depth can be determined by measured values or estimated according to precipitation accumulation. The theories related to snow accumulation, compaction and melt are addressed in the SVFLUX theory manual.

Snow cover densification

A seasonal ground thermal regime under snow conver is usually simulated using a homogneous snow layer with constant snow density and thermal conductivity. However, in nature the snow cover constains layers of snow and each with its own density. The snow cover is compacted and densified by its own weight and climatically metamorphic processes. Therefore, the snow cover density and snow thermal conductivity change contininously during the winter season.

Goodrich (1982) presented a theory to simulate snow cover densification processes. The theory assumes that the compaction of the snow cover is due to the over-burden pressure.

$$\sigma = \int_0^{Z(t,t_o)} \rho(Z,t,t_o)\,dZ = \int_{t_o}^{t} A(t)\,dt \qquad [\ 276\ ]$$

where:

$Z(t,t_o)$ = depth below the surface at time *t* of snow deposited at time t_o,

$\rho(Z,t,t_o)$ = snow density, it is a function of *Z, t,* t_o and

$A(t)$ = accumulation rate.

A constant mass of the snow cover is assumed (Goodrich, 1982) and the vertical strain rate is defined as:

$$\dot{\varepsilon} = -\frac{\partial Z/\partial t}{Z} = \frac{\partial \rho/\partial t}{\rho} \qquad [\ 277\ ]$$

where:

$\dot{\varepsilon} = \frac{d\varepsilon}{dt}$ = vertical strain rate in snow cover

A linear stress-strain rate relation is usually used for snow cover:

$$\dot{\varepsilon} == \frac{\sigma}{\eta} \qquad [\ 278\ ]$$

where:

η = compactive viscosity factor

The compactive viscosity factor, η, is a function of snow density and temperature.

$$\eta = \eta_0 e^{q\rho} e^{A/RT} \qquad [\ 279\ ]$$

where:

η_0 and q = imperical coefficients depending on snow type (Goodrich, 1982)

A, R and *T* = Activation energy for snow, universal gas constant and absolute temperature

The imperical coefficient, η_0, is between 6 kg-day/m^2 and 15 kg-day/m^2 for dry old snow at temperatures between 0 °C and -5 °C (Goodrich, 1982).

The imperical coefficient, *q*, varies from 15.8 m^3/ton to 21.7 m^3/ton for natural densification at sites in Greenland and Antartica (Goodrich, 1982).

Measured values of activation energy for snow, *A*, are between 29 and 105 kJ/mole (Goodrich, 1982). For snow density of 0.17 ton/m^3, a typical activation energy, *A*, value of 38 kJ/mole is used (Goodrich, 1982).

Equations [277], [278] and [279] are used to solve for snow layer thickness and snow density.

5.2.4 Energy Balance

With this method, the applied thermal boundary condition is based on thermal flux balance at the ground surface, i.e.,

$$Q\big|_{surface} = Q_G = Q_N - Q_H - Q_L \qquad [\ 280\ ]$$

where:

Q_N = net radiation flux, *J/(m^2-day)*,

Q_H = sensible heat flux, *J/(m^2-day),* and

Q_L = latent heat flux, *J/(m^2-day)*.

For historic reasons, the net radiation flux, sensible heat flux, and latent heat flux are obtained or calculated in $m^3/(m^2 day)$, or *m/day*. In this case, the equation [280] is changed into the follows:

$$Q\big|_{surface} = C_e(Q_n - Q_h - Q_l) \qquad \textbf{[281]}$$

where:

Q_n	= net radiation flux, *m/day*,
Q_h	= sensible heat flux, *m/day,*
Q_l	= latent heat flux, *m/day*, and
C_e	= conversion factor to covert *m/day* into $J/(m^2\text{-}day)$.

NOTE:
In current SVFLUX or SVHEAT version, volumetric latent heat of water vaporization, L_v, is used as C_e (i.e., $C_e = L_v = 2.5\times10^9\ J/m^3$). This approach may be improved in future versions of SVFLUX or SVHEAT.

Net radiation at the water surface, Q_n, can be measured or approximated using the Penman equation (Penman, 1948), which is as follows,

$$Q_n = (1-r)R_c - \sigma(273.5+T_a)^4\left(0.56 - 0.92\left(u_{vsat}^{air}\right)^{0.5}\right)(0.10 + 0.90n/N) \qquad \textbf{[282]}$$

where:

Q_n	= net radiation, *m/day*,
r	= reflection coefficient,
R_c	= 0.95 R_a(0.18 + 0.55n/N) = shortwave radiation, *m/day*,
0.95	= coefficient suggested by Penman for evaporation from a wet and bare soil as compared to evaporation from an open water surface,
R_a	= solar radiation, $MJ/m^2\text{-}day$,
σ	= Stefan Boltzmann's constant, $W\text{-}m^2\text{-}K^4$,
T_a	= air temperature, ^oC,
u_{vsat}^{air}	= vapor pressure of the air above the surface, *mmHg*, and
n/N	= sunshine ratio (actual/possible hours of bright sunshine).

NOTE:
u_{vsat}^{air} in the above equation must be in *mmHg*.

The sensible heat component, Q_h, reflected from the ground surface to the air is described as follows (Penman, 1948; Gray, 1970; Wilson, 1990):

$$Q_h = C_f\,\eta\, f(u)(T_s - T_a) \qquad \textbf{[283]}$$

where:

Q_h	= sensible heat, *m/day*,
C_f	= conversion factor, (i.e., 1 *kPa* = 0.0075 *mHg*),
η	= psychometric constant, 0.06733 $kPa/^oC$ at 20 ^oC,
$f(u)$	= function depending on wind speed, $f(u)$ = 0.35(1+ 0.146 W_w),
W_w	= wind speed, *km/hr*,
T_s	= soil temperature at the ground surface, and
T_a	= air temperature overlying the ground surface.

The latent heat, Q_l, is mainly associated with liquid evaporation. It can be described by actual evaporation, *AE*. Please see SVFLUX theory manual describes several approaches to estimate or calculate the actual evaporation.

If the boundary covered with snow, the thermal flux applied to the boundary condition is approximated with the following expression:

$$Q\big|_{surface} = \begin{cases} Q_G & if\ D_{sn} = 0 \\ \lambda_{sn}\dfrac{T_{sn} - T_g}{D_{sn}} & if\ D_{sn} > 0 \end{cases} \qquad \textbf{[284]}$$

The temperature at the snow surface is assumed to equal to air temperature.

5.2.5 Thermosyphon

The thermosyphon climate boundary method allows the simulation of a physical thermosyphon installed in the ground. The thermosyphon boundary equation in SVHEAT describes the heat flux across the boundary due to the heat extracted by the thermosyphon. Please refer to the information provided by Arctic Foundations Inc. at http://www.arcticfoundations.ca for a description of thermosyphons and their applications.

The heat extraction for a thermosyphon is described by the following equation:

$$Q = \begin{cases} P(T - T_a) & if\ T - T_a >= T_{threshold} \\ 0 & otherwise \end{cases} \qquad [\ 285\ ]$$

where:

Q	= heat extraction rate of the thermosyphon, *w*,
P	= overall performance of the thermosyphon, *w/°C*,
T	= soil temperature, *°C*,
T_a	= air temperature, *°C*, and
$T_{threshold}$	= a threshold of temperature, °C.

The performance of thermosyphon is estimated using Arctic Foundations Method. This method describes the performance as a function of wind speed and thermosyphon radiator surface area. The equation is valid for thermosyphon installed at angles of inclination greater than 5° from the horizontal to the vertical.

$$P = \left(A + B\left(\frac{W_w}{W_{w0}}\right)^C \right) A_{rad} \qquad [\ 286\ ]$$

where:

P	= overall performance characteristic of the thermosyphon, *w/°C*,
W_w	= the wind speed from the climate dataset, *m/s*,
W_{w0}	= reference of wind speed, *1 m/s*,
A_{rad}	= radiator surface area, 6.5 m^2 by default, and
A, B, C	= empirical parameter, *A* = 2.52 w/m^2-*°C*, *B = 4* w/m^2-*°C* by default, and C = 0.62.

The parameters of *A*, *B*, and *C* are related to the working gas and the angle of evaporator for thermosyphon. The following table is the data obtained by Zarling and Haynes (1985):

Working gas	Angle of evaporator	*A* (w/m^2-*°C*)	B (w/m^2-*°C*)	C	A (*Btu/s-ft*^{2}-*°F*)	B (*Btu/s-ft*^{2}-*°F*)	C	Data source
	5	*2.5*	4	0.62			0.62	AFI
CO2	0	*2.59*	3.38	0.23	1.267E-4	1.660E-4	0.23	
	3	*3.02*	4.99	0.3	1.479E-4	2.444E-4	0.3	
	6	*2.92*	4.77	0.4	1.433E-4	2.338E-4	0.4	
	9	*2.91*	7.36	0.15	1.426E-4	3.613E-4	0.15	
	12	*2.74*	6.74	0.28	1.343E-4	3.304E-4	0.28	
NH3	0	*3.94*	1.95	0.38	1.931E-4	9.580E-5	0.38	
	1.5	*4.46*	2.03	0.57	2.188E-4	9.957E-5	0.57	
	3	*4.31*	2.37	0.47	2.112E-4	1.162.E-4	0.47	
	4.5	*4.18*	2.6	0.40	2.052E-4	1.275E-4	0.40	
	6	*4.11*	2.82	0.40	2.014E-4	1.380E-4	0.40	
	9	*4.2*	2.95	0.39	2.059E-4	1.448E-4	0.99	

In SVHEAT two approaches are possible to setup thermosyphon in the model. Approach one regards the thermosyphon as the heat sink, which is implemented as a heat pump-well, or heat tunnel. Another way applies the evaporator of thermosyphon as heat flux boundary condition. In this case the heat extraction rate can be expressed as:

$$q_{thermosyphon} = h_{thermosyphon}(T - T_a) \qquad [\ 287\ ]$$

$$h_{thermosyphon} = \frac{P}{A_{evaporator}} \quad [288]$$

where:

$q_{thermosyphon}$ = heat extraction flux of thermosyphon, w/m^2,

$h_{thermosyphon}$ = heat transfer performance of thermosyphon, w/m^2-^oC, and

$A_{evaporator}$ = area of evaporator of thermosyphon, m^2.

5.2.6 Convection/Radiation

A Convection boundary condition is applied to the boundary where the heat transfers mainly by thermal convection. One example is ventilated pipe used in highway. The heat transfer between air and ventilated pipe is forced convection. The thermal flux on the convection boundary can be expressed as

$$q_c = h_c(T_a - T) \quad [289]$$

where:

q_c = heat flux to thermal convection, w/m^2,

h_c = thermal convection coefficient, $w/(m^2$ -°$C)$,

T_a = environmental temperature, °C, and

T = soil temperature, °C

The default value of the thermal convection coefficient is set to 50 w/m^2-°C, or 4,320,000 J/day-m^2-°C. The thermal convection coefficient is affected by many factors. User can specify a constant value or an expression of the thermal convection coefficient in the text box of *Convection Coefficient Expression.*

It should be noted that the environmental temperature, T_a, can be specified with *Air Temperature* Tab. In this case, SVHEAT regards data specified in *Air Temperature* Tab as more general environmental temperature, rather than atmospheric air temperature.

If the Radiation boundary condition included, thermal flux applied the boundary is expressed as

$$q_r = \varepsilon\sigma(T_a^4 - T^4) \quad [290]$$

where:

q_r = heat flux due to radiation,, w/m^2,

ε = emissivity, a dimensionless factor changing from 0 to 1, for soil material, it is set to 0.94 by default,

σ = 5.67×10^{-8}, Stefan-Boltzmann's constant,

T_a = environmental temperature, K , and

T = soil temperature, K.

The applied thermal boundary condition is,

$$Q|_{surface} = q_c + q_r \quad [291]$$

If the boundary covered with snow, the thermal flux applied to the boundary condition is approximated with the following expression:

$$Q|_{surface} = \begin{cases} Q_G & if\ D_{sn} = 0 \\ \lambda_{sn}\dfrac{T_{sn} - T_g}{D_{sn}} & if\ D_{sn} > 0 \end{cases} \quad [292]$$

The temperature at the snow surface is assumed to equal to the air temperature.

5.3 INSULATION BOUNDARY CONDITION

Thermal insulation is commonly used in the application of heat transfer. The insulation layer can be modeled as a common material. For example, in cold regions to prevent the permafrost from melting, the thermal insulation may be utilized in the basement of embankment. Figure 32 is a simple case for such application scenario. Because a thermal insulator is usually very thin compared to its lateral extents a very dense mesh would have to be generated in the insulation layer. This situation can be improved by using two special boundary conditions termed "Inner Insulation" and "Outer Insulation", as shown in Figure 33.

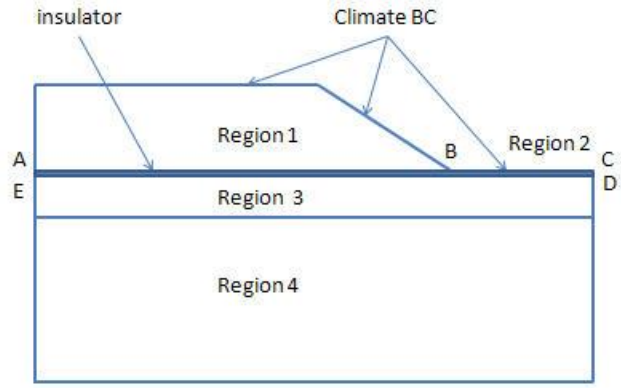

Figure 35 Modeling thermal insulation as a common material

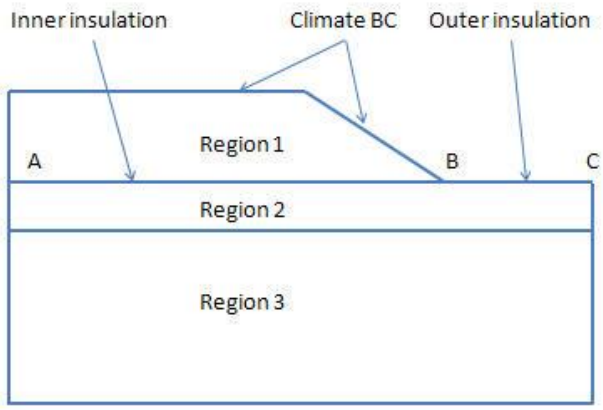

Figure 36 Modeling thermal insulation as Inner Insulation or Outer Insulation

5.3.1 Inner Insulation boundary

Inner insulation boundary is implemented as jump boundary, and can be expressed as

$$contact(T) = \frac{jump(T)}{d_{ins} / \lambda_{ins}} \quad [293]$$

where:

T = temperature of model domain, *°C*,

d_{ins} = thickness of thermal insulator, *m*, and

λ_{ins} = thermal conductivity of thermal insulator, *J/s-m-°C*.

5.3.2 Outer Insulation boundary

The outer insulation is implemented as thermal resistance in SVHEAT. The thermal flux that is applied the boundary can be written as:

$$natural(T) = \frac{\lambda_{ins}(T - T_{ins})}{d_{ins}} \quad [294]$$

where:

T_{ins} = temperature at the surface of insulation. Usually it is equal to the ambient temperature, *°C*,

5.4 CAUCHY BOUNDARY CONDITION

The general form of Cauchy boundary condition is written as:

$$q_n = q_t + R_t (T_0 - T) \quad [295]$$

where:

T_0	= reference temperature °C,), and it can be a function of time *t*
R_t	= heat transfer coefficient (*J/s-m²-°C*), and it can be a function of time *t*
q_t	= prescribed heat flux (W/m²), and it can be a function of time *t*
q_n	= normal heat flux to a boundary (W/m²).

The Cauchy boundary condition (or the 3rd kind BC) is a general boundary condition, which can be converted back to the Dirichlet boundary condition (1st kind BC) or Neumann boundary condition (2nd kind BC). When $R_t = 0$, the 2nd kind BC is obtained from [295]. When $R_t \to \infty$, the 1st kind BC, $T = T_0$, is obtained from [295].

5.5 FLUX SECTIONS

The conductive heat flow, the rate heat flow between two points can be expressed as,

$$Q_H = K \frac{\partial T}{\partial l} A \qquad \textbf{[296]}$$

where:

Q_H	= heat flow, *J/s*,
K	= thermal conductivity, *J/s-m-°C*,
T	= temperature, *°C*, and
A	= cross-sectional area, L^2.

In transient models the total heat flow between two points is the same as shown in the above equation multiplied by the total time. The resulting equation is,

$$Q = K \frac{\partial T}{\partial l} A\, t \qquad \textbf{[297]}$$

where:

Q	= total heat flow, *J*,
K	= thermal conductivity, *J/s-m-°C*,
T	= temperature, *°C*,
A	= cross-sectional area, m^2, and
t	= total time, *s*.

6 WELLS AND TUNNELS

6.1 INTRODUCTION

Heating or cooling by heat pumps is achieved by circulating water through a network of pipes and bore holes in the ground. Subsurface freezing for foundation support can be accomplished by the natural convection of a liquid in a *thermosyphon*. SVHEAT models, these types of features are simulated as heat wells, where heat is injected or extracted along the length of the well.

In a numerical model, tunnels and wells are represented as localized sinks or sources. Numerically, they remove or add heat to cells. For regional scale models, the diameter of a well bore hole or tunnel shaft is too small to model efficiently, as it requires a mesh resolution fine enough to model the physical bore hole.

A traditional method of representing well and tunnel objects is with a line of nodes in a finite element model. Such a representation is efficient in terms of the mesh, but can result in extremely sharp gradients next to the line of the elements. This is especially true if the internal boundary condition applied to the well/tunnel differs greatly from the surrounding domain. Resulting sharp gradients can lead to instabilities in the numerical model.

For these reasons, SVHEAT treats wells differently. SVHEAT models wells as a sink (or source) term in the partial differential equations, rather than as a physical boundary condition. This eliminates the meshing issues with trying to model a bore hole that is very small relative to the extent of the model. This methodology introduces an approximation that affects the distance at which the flux across a closed surface bounding the well screen becomes accurate. The user can set this *influence distance*, and experiment with the level that provides the right mix of accuracy and modeling speed.

In SVHEAT, wells are vertical features, whereas tunnels can be inclined at any angle, and be a sequence of straight line segments. They may be used interchangeably. Both can be included in two- and three-dimensional models.

In this document, tunnels are only referred to where the theory differs from that of wells. Otherwise, the theory holds for tunnels in the same way.

6.2 EQUATIONS

Equation [291] is the heat conduction equation in three-dimensions.

$$\frac{\partial}{\partial x}\left(\lambda_x \frac{\partial T}{\partial x}\right)+\frac{\partial}{\partial y}\left(\lambda_y \frac{\partial T}{\partial y}\right)+\frac{\partial}{\partial z}\left(\lambda_z \frac{\partial T}{\partial z}\right)+\overline{Q}_{well}=\left(C+L_f m_2^i\right)\frac{\partial T}{\partial t} \qquad \textbf{[298]}$$

Where:

T	= Temperature,
λ_x	= thermal conductivity in the *x* direction,
λ_y	= thermal conductivity in the *y* direction,
λ_z	= thermal conductivity in the *z* direction,
C	= volumetric heat capacity
m_2^i	= the derivative of the soil-freezing characteristic curve

The source term, $\overline{Q}_{well}$, equation [299], simulates the wells.

$$\overline{Q}_{well}=\frac{P}{\int_V PdV}Q_{well} \qquad \textbf{[299]}$$

where: Q_{well} is the user-defined pumping/injection rate of the well, and *P*, equation [300], is a function that scales the source term.

$$P=\exp\left(-\frac{|\mathbf{r}|^2}{\alpha^2}\ln 20\right) \qquad \textbf{[300]}$$

where: **r** (described in Section 6.3) is the shortest vector from the well to a point in the model domain, and α is the user-defined *influence distance.* With this definition of *P*, when $|\mathbf{r}|=\alpha$, *P* = 1/20. The integral $\int_V PdV$ in Equation [292] is taken

over the entire volume, *V*, of the model, and normalizes *P* so that $\int_V \overline{Q}_{well} dV = Q_{well}$. Figure 34 shows some examples of *P* for some sample values of α.

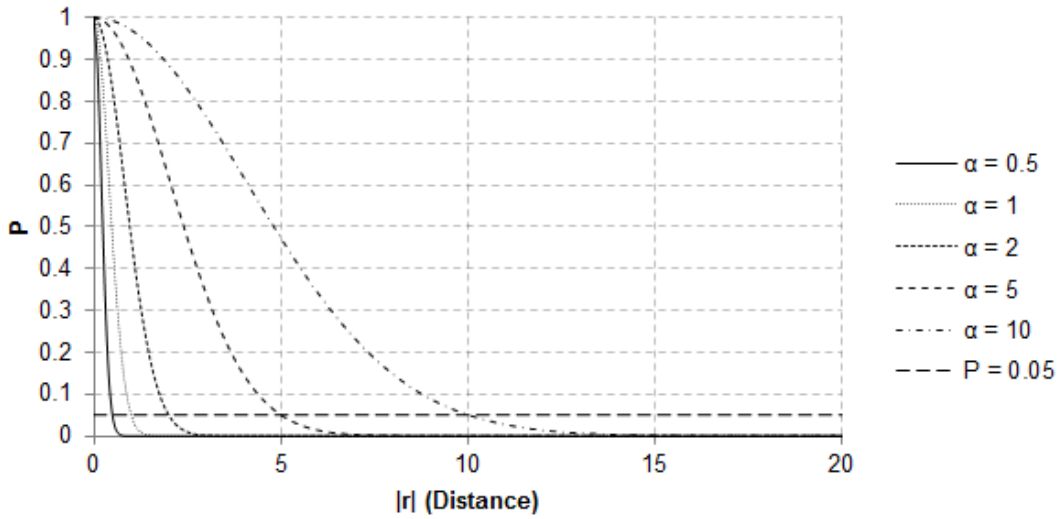

Figure 37: Examples of *P* for values of α.

6.3 GEOMETRY

The vector, **r**, in Equation [293], is either the vector perpendicular to the well screen to the model point, or the vector from the closest end of the screen to the point. Figure 35 shows **r** when the model point is closest to a point in the screened segment, and Figure 36 shows **r** when the model point is the closest to an end of the screen.

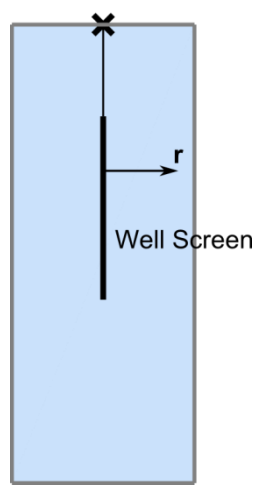

Figure 38: Shortest distance to a model point from the screened segment.

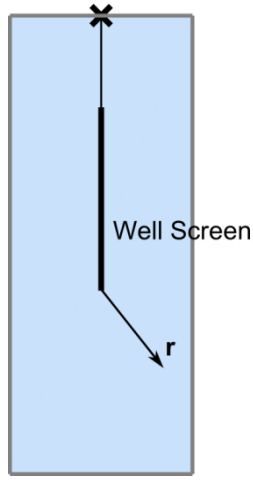

Figure 39: Shortest distance to a model point from an end.

6.4 SETTING THE INFLUENCE DISTANCE

The influence distance affects how far away from the screen Q_{well} becomes realized. Smaller influence distances will cause the well flux to be realized closer to the screen than larger influence distances. The influence distance should be set to a value that represents the scale at which the thermal flux is important. In general, if the model has horizontal extents in the hundreds of meters, the flux in a volume immediately surrounding the screen is less important than the overall affect that the well has on the flow in the region. Therefore, a larger value is appropriate (~10 m). This can produce shallower gradients and prevent the computations in the volume surrounding the well from dominating the system. For simpler models, the influence distance has little effect on the speed of the model. Therefore, the influence distance can be set to a small value (~1 m).

6.5 BOUNDARY CONDITIONS

All well and tunnel boundary conditions are implemented through the sink/source term, $\overline{Q}_{well}$, in Equation [291]. SVHEAT calculates an appropriate value of Q_{well} for each type of boundary condition. The units of Q_{well} are *J/s*, and $\overline{Q}_{well}$ *J/s-m*^{3}.

6.5.1 Rate

The value of Q_{well} in Equation [292] is specified.

6.5.2 Temperature

A specified temperature, T_{well}, is maintained by causing the flow necessary to realize T_{well} along the screen. The flow is given by:

$$Q_{well} = \begin{cases} K(T_{well} - T), & T \le T_{well} \\ -K(T - T_{well}), & T > T_{well} \end{cases} \qquad [301]$$

where T is soil temperature and K is the *Heat Performance* parameter that can be input.

6.5.3 Thermosyphon

A thermosyphon is a well that extracts heat from the soil when the air temperature is less than the soil temperature. The heat extracted is

$$Q_{well} = \begin{cases} P(T - T_a), & T - T_a \ge T_{threshold} \\ 0, & \text{Otherwise} \end{cases} \qquad [302]$$

where: T is soil temperature, T_a is air temperature, $T_{threshold}$ is the temperature difference required before the thermosyphon becomes active, and P is thermosyphon performance (Arctic Foundations Method) given by

$$P = \left(A + B\left(\frac{W_w}{W_{w0}}\right)^C \right) A_{rad} \qquad [303]$$

where*: A, B,* and *C* are fitting parameters, determined from data, W_w is wind speed, W_{w0} is the reference wind speed (1 m/s), and A_{rad} is the surface area of the radiator.
Cauchy-Type ()

6.6 PARAMETERS

Wells and tunnels are controlled by three user definable parameters: *Influence Distance* (α), *Line Mesh Spacing* (ζ), and *Mesh Growth Coefficient* (γ). The influence distance controls the spread of the sink that simulates the well, and line mesh spacing and mesh growth coefficient control the mesh spacing near the well.

The well sink is controlled by the scale factor formula:

$$P = \exp\left(-\frac{|\mathbf{r}|^2}{\alpha^2}\ln 20\right) \qquad \textbf{[304]}$$

This is described in detail in Section 6.3.

The mesh spacing is controlled by:

$$m = \max\left\{\zeta, \gamma|\mathbf{r}|^{1.2}\right\} \qquad \textbf{[305]}$$

Equation [298] ensures that ζ is the smallest element size, and causes the size to grow at a rate proportional to $|\mathbf{r}|^{1.2}$. The exponent of 1.2 was selected to allow the mesh to grow at a rate that is generally appropriate for models.

Figure 34 shows the sink scale factor (*P*) for some values of influence distance, and Figure 37 shows the mesh spacing for some values of the mesh growth coefficient.

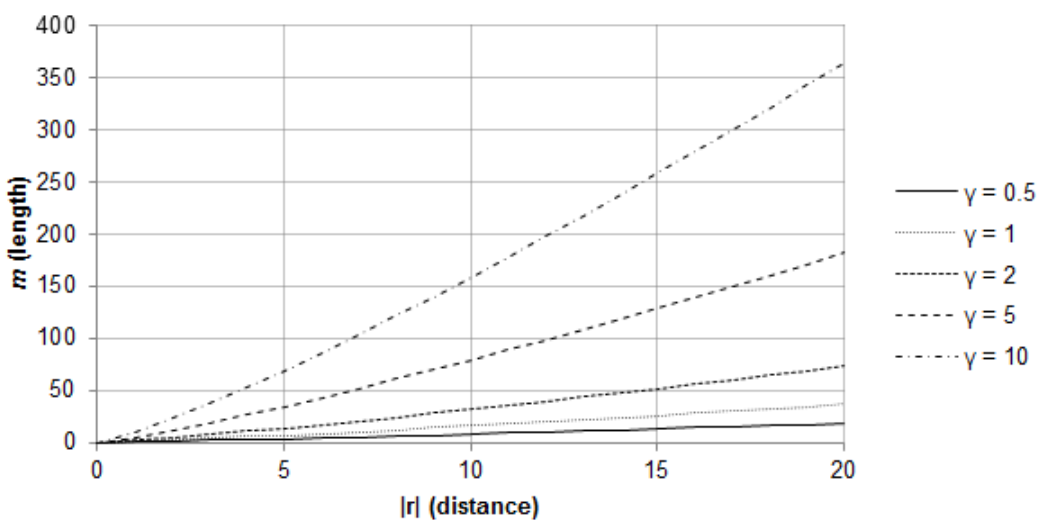

Figure 40: Mesh spacing (*m*) for various values of mesh growth coefficient (γ).

6.7 REMARKS

Changing the default mesh parameters in Equation [298] is only necessary if the automatically generated mesh is not suitable. The mesh may be too coarse or too fine near the well, and adjustment may be necessary to facilitate accurate and efficient modelling.

It is possible that in large models, the mesh generation will not resolve the well. The mesher may fail to resolve the peak of the sink/source, regardless of how the parameters are set. In this case, it is necessary to increase the mesh density of the model by decreasing the mesh size. It is often best to create a region that contains the well, and, if necessary, decrease the mesh size for that region only. Usually, just creating the region is enough for the mesher to resolve the well. The region mesh size will override the mesh size set by Equation [298].

When wells or tunnels are directly represented in a model as a borehole, it causes extremely dense meshing near the borehole, which must be resolved out to the model scale mesh. This can generally be accomplished; however, the resulting mesh is extremely dense close to the well, and the model runs very slow. The advantage of incorporating wells and tunnels as

sinks/sources in the partial differential equation is that the mesh size is determined at the model scale. This generally gives accurate results in much less time. Equations [297] and [298] provide control of the rate of decay of the sink/source and the mesh density so that the model can be fine-tuned.

FlexPDE takes several characteristics of the geometry into consideration when generating the mesh. It is possible that the mesh size set by Equation [298] will be overridden by another size parameter. Since FlexPDE will select the smallest mesh size out of all the possible sizes under consideration, this should not cause any problems with the simulation.

For complex models, especially those for which the well or tunnel is screened across a contact between materials with a large difference in conductivities, the gradients in the immediate vicinity of the well need to be monitored to ensure they are not unrealistically large.

The *Rate* boundary condition in a two-dimensional model is a volume per unit time. When determining the appropriate rate, the user must consider that the well is being applied to a three-dimensional model with the third dimension having unit length. This means that a rate that is suitable for a three-dimensional model may be too large for a corresponding two-dimensional model.

7 NUMERICAL IMPLEMENTATION

The SVHEAT software makes use of a generic finite element solver called FlexPDE. FlexPDE has been designed and maintained by Bob Nelson of PDE Solutions Inc. over the course of the past 31 years and is the result of many years of rigorous testing and peer review. The most detailed source of documentation of the numerical schemes used in the FlexPDE software may be found in the User's Guide and Reference Manual provided with the software. The following sections provide a brief overview of some of the more significant numerical methods used in the software.

Primary advantages of the FlexPDE finite element solver are as follows:

- Fully automatic mesh generation.
- Fully automatic mesh refinement based on any model variable.
- Fully implicit approach in the solver, which provides for a robust solution of difficult models with convergence issues.
- 3, 6, or 9-noded triangles as elements for 2D analysis and 4, 10, or 20-noded tetrahedrons in 3D elements.
- Adaptive time-stepping with automatic generation and control of time steps.
- Newton-Raphson convergence iteration schemes.
- Use matrix preconditioning in conjugate-gradient solutions. The default preconditioner is the diagonal-block inverse matrix.

7.1 EQUATION ANALYZER

A symbolic *equation analyzer* expands defined parameters and relations, performs spatial differentiation, and symbolically applies integration by parts to reduce second order terms to create symbolic Galerkin equations. It then differentiates these equations to form the Jacobian coupling matrix.

7.2 MESH GENERATION

A *mesh generation* module constructs a triangular finite element mesh over an arbitrary two-dimensional model domain. In three-dimensional models, the 2D mesh is extruded into a tetrahedral mesh covering an arbitrary number of non-planar layers in the extrusion dimension. Bilinear interpolation is used in 3D models to approximate a curved surface.

FlexPDE uses an "advancing front" mesh generation method, triangular in 2D and tetrahedral in 3D (the specific algorithm is proprietary, but similar mesh generation methods are widely reported in the literature). The mesh generator allows spatially-varying node density, in order to concentrate cells in regions of structural detail.

Based on the order of the selected analysis the following types of elements can be generated.

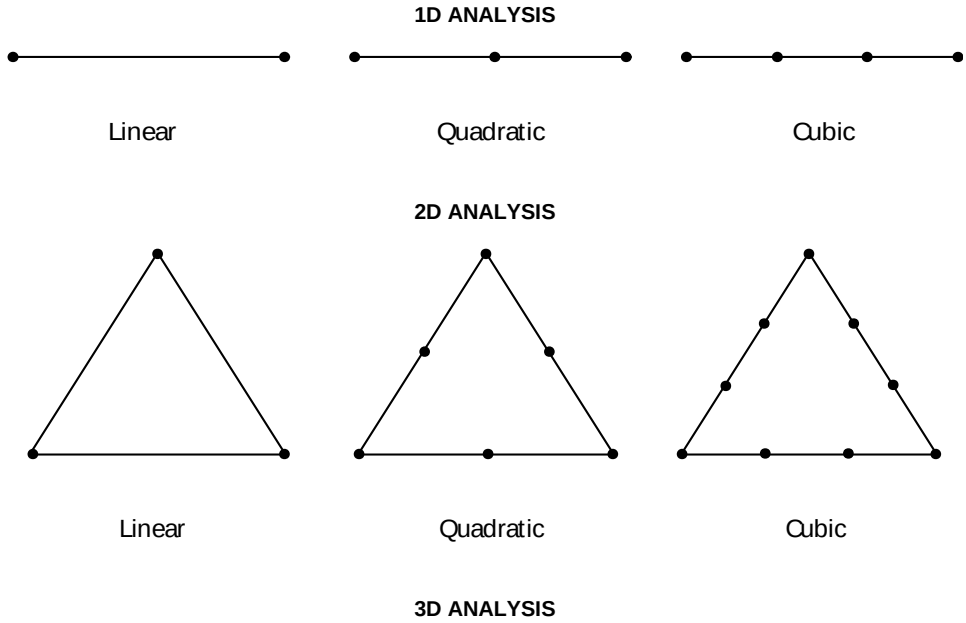

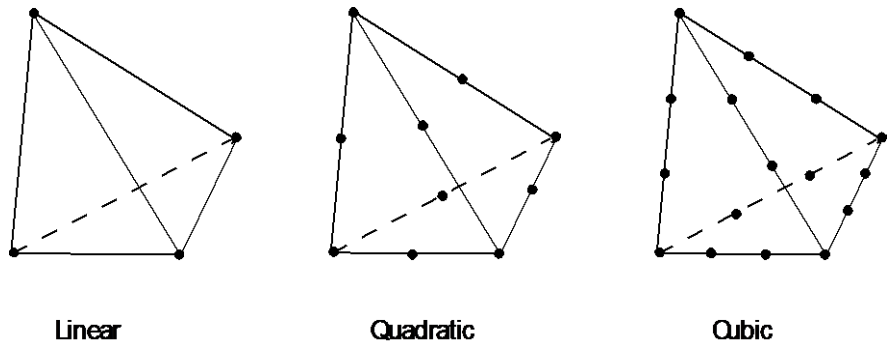

7.3 MESH REFINEMENT

The FlexPDE finite element solver implements fully automatic mesh refinement. The mesh refinement may be triggered based on any model variable through a combination of the RESOLVE statement as well as the XERRLIM variable.

FlexPDE automatically adapts the computation mesh to the needs of the solution. Error estimates are formed in each cell, and cells with high error are split into two new cells, resulting in a new computation mesh and a repeat of the solution process. The reference error is user-selectable (ERRLIM). The exact algorithm is proprietary, but similar techniques are discussed in the open literature.

The error estimation process is based on the following observation. In the finite element method, each nodal value is computed by minimizing the residual of the partial differential equation, PDE, weighted by a node-specific weighting function and integrated over all cells surrounding the node. A centrally-weighted integral of the PDE residual over an individual cell provides an independent measure of the residual, and provides the error estimate.

7.4 INTERPOLATION ORDER

Finite element basis is quadratic.

7.5 TIME STEPPING

Both explicit and implicit methods have been presented in literature as viable methods of solving for nodes while moving forward in time. Explicit methods use known data to "explicitly" define each nodal value at an advanced time. Such explicit methods usually suffer in accuracy and stability unless the timestep is small. Implicit methods solve "implicitly" for self-consistent values at the advanced time (i.e., the simultaneous finite element spatial equations are solved at the advanced time). This improves the stability and accuracy for large timesteps, at the cost of a simultaneous solution for all nodes in the mesh.

Explicit methods can be more economical under the right circumstances.

The implicit generalized Gear (1971) method has been selected in SVHEAT as the most robust method for general application. The research literature supports this decision.

7.5.1 Time Integration

FlexPDE uses a selectable-order Backward Difference Formulation to advance variables in time. The default is second order, but you can select linear or cubic with the TORDER selector. Linear backward difference (torder=1) is equivalent to Backward Euler integration. All the methods are Implicit. The analysis for default quadratic integration is as follows:

Assume that each variable can be approximated as a polynomial in time,

$$U(t) = p0(t)*u0 + p1(t)*u1 + p2(t)*u2$$

where u0 and u1 are known values at times t0 and t1, u2 is the unknown value at time t2, and t0<t1<t2.

The coefficients p0, p1 and p2 are Lagrange Interpolation coefficients,

$$p0(t) = (t-t1)(t-t2) / ((t1-t0)(t2-t0)),$$

$$p1(t) = -(t-t0)(t-t2) / ((t1-t0)(t2-t1)), \text{ and}$$

$$p2(t) = (t-t0)(t-t1) / ((t2-t0)(t2-t1)).$$

With this interpolation, we can find the time derivative of U(t)

U'(t) = p0'*u0 + p1'*u1 + p2'*u2

with,

p0'(t) = ((t-t1)+(t-t2)) / ((t1-t0)*(t2-t0)),

p1'(t) = -((t-t0)+(t-t2)) / ((t1-t0)*(t2-t1)), and

p2'(t) = ((t-t0)+(t-t1))/ ((t2-t0)*(t2-t1)).

The time derivative at t2 is then,

U'(t2) = p0'(t2)*u0 + p1'(t2)*u1 + p2'(t2)*u2

with,

p0'(t2) = (t2-t1)/ ((t1-t0)*(t2-t0)),

p1'(t2) = -(t2-t0) / ((t1-t0)*(t2-t1)), and

p2'(t2) = (2*t2-t1-t0)/ ((t2-t0)*(t2-t1)).

Now, if we are given an equation

dt(U) = F(U)

We can write,

U'(t2) = F(U(t2)) as a fully implicit equation for U2, and

U2 = [F(U2) - p0'(t2)*U0 - p1'(t2)*U1]/p2'(t2).

Solving this system requires either the solution of a linear system or a nonlinear system, depending on the form of F(U). Notice that the core of this solution method is to find a value of U2 such that the interpolated time derivative at the end of the step matches the specified driving term F(U) at the end of the time step. There is no time-centering issue involved with F(U): it is always at the end of the step.

7.5.2 Timestep Control

The approximation described above implies a constant curvature U'' over the interval (t0,t2). When we later advance from t2 to t3, we implicitly assume that U'' is constant over the interval (t1,t3), but with a different U'' than the previous step. There has therefore been an inconsistent assumption about the value of U'' in the overlapped interval (t1,t2).

The FlexPDE timestep control, simply stated, is to measure how much difference the two estimates of U'' imply in U3, and to restrict this difference to the requested ERRLIM.

The curvature over (t0,t2) is:

U''1 = 2*U0/((t1-t0)(t2-t0)) - 2*U1/((t1-t0)(t2-t1)) + 2*U2/((t1-t0)*(t2-t1))

The curvature over (t1,t3) is,

U''2 = 2*U1/((t2-t1)(t3-t1)) - 2*U2/((t2-t1)(t3-t2)) + 2*U3/((t2-t1)*(t3-t2))

The difference is:

E''2 = -2*U0/((t1-t0)(t2-t0)) + 2(t3-t0)U1/((t1-t0)(t2-t1)*(t3-t1)) - 2*U2*(t3-t0)/((t2-t1)(t3-t2)(t2-t0)) + 2*U3/((t3-t2)*(t3-t1))

Integrating over (t2,t3) produces an error,

E3 = -(t3-t2)^2*U0/((t1-t0)*(t2-t0)) + (t3-t2)^2*(t3-t0)U1/((tt-t0)(t2-t1)*(t3-t1)) - (t3-t2)(t3-t0)*U2/((t2-t1)(t2-t0)) + (t3-t2)*U3/(t3-t1)

The Nth power of the nodal values of E is averaged, rooted and divided by the range of the variable U. N is controlled by TNORM in version 5 and ENORM in version 6. N=2^TNORM. The range of U is the larger of the declared Threshold or the observed range of values.

```
Eav      = [SUM((E3/Range(U))^N)]^(1/N), and
deltat4  = deltat3*sqrt(TERRLIM/Eav)
```

This process applies to variables U that are defined by an evolution equation dt(U)=F(U). Steady equations are not assumed to be polynomial in time, and a different rule is applied to generate Eav for these variables.

In this case,

```
E3       = (U3-U2)/Changelim
```

Moving nodes adds another criterion, which is that the cell volume cannot change by more than a prescribed percentage on any cycle. The way this is controlled is different in V6 than in V5.

8 REFERENCES

Anderson, D.M, Tice, A.R, and McKim, H. L. (1973). The unfrozen water and the Apparent Specific Heat Capacity of Frozen Soils. The second International Conference on Permafrost

Côté, J. and Konrad, J.-M. (2005). A generalized thermal conductivity model for soils and construction materials. Can. Geotech. J. 42: 443–458 (2005).

Coutts, R.J. and J.-M. Konrad, (1994). Finite element modeling of transient non-linear heat flow using the node state method. Ground Freezing 94. Balkema, Rotterdam, Netherlands, pp. 39-47

Daanen, R. P., Misra, D., and Epstein, H. (2007). Active-layer hydrology in nonsorted circle ecosystems of the arctic tundra. Vadose Zone Journal, 6(4), 694-704.

Dakshanamurthy, V. and Fredlund, D. W. (1981). A Mathematical Model for Predicting Moisture Flow in an Unsaturated Soil under Hydraulic and Temperature Gradients. Water Resources Res., 17: 714-722

DeVries, D. A. (1963). Thermal properties of soils. In "Physics of plant environment".(Ed. WR van Wijk) pp. 210–235.

Farouki, O. T. (1981). Thermal properties of soils. No. CRREL-MONO-81-1. Cold Regions Research and Engineering Lab, Hanover NH.

Fredlund, D.G. and Rahardjo, H. (1993). Soil Mechanics for Unsaturated Soils. John Wiley & Sons, Inc., New York

Fredlund D.G., and Gitirana, Jr.G. (2005), Unsaturated Soil Mechanics as a Serials of Partial Differential Equations. Proceedings of International Conference on Problematic Soils, 25-27 May 2005, Eastern Mediterranean University, Cyprus

Flerchinger, G. N., and Saxton, K. E. (1989). Simultaneous heat and water model of a freezing snow-residue-soil system I. Theory and development. Trans. ASAE, 32(2), 565-571.

FlexPDE 6 (2007). *Reference Manual*, PDE Solutions Inc., Spokane Valley, WA 99206.

FlexPDE 7 (2017). Reference Manual, PDE Solutions Inc., Spokane Valley, WA 99206.

Goodrich, L. E (1982). The influence of snow cover on the ground thermal regime. Canadian Geotechnical Journal, 1982, 19:421-432.

Harlan, R. L. (1973). Analysis of coupled heat-fluid transport in partially frozen soil. Water Resources Research, 9(5), 1314-1323.

Harlan, R.L. and J.F. Nixon, (1978). Ground Thermal Regime. In Geotechnical Engineering for Cold Regions, eds. Andersland, O.B. and Anderson, D.M. pp. 103-163

Hansson, K., Simunek, J., and Mizoguchi, M. (2004). Water Flow and Heat Transfer in Frozen Soils: Numerical Solution and Freeze-Thaw Applications. Vadose Zone Journal, 3:693-704 (2004)

Heitman, I.L., Horton, R., and Ren, T. (2008). A Test of Coupled Soil Heat and Water Transfer Prediction under Transient Boundary Temperatures. SSSAJ, 72(5): 1197-1207

Hwang, C.T. (1976). Prediction and observations on the behavior of a warm gas pipeline on permafrost. Can. Geotech. J. 13: 452 - 480

Jame, Y.W. (1977). Heat and Mass Transfer in Freezing Soil. Ph.D Thesis. University of Saskatchewan

Johansen, O. (1977). Thermal conductivity of soils (No. CRREL-TL-637). Cold Regions Research and Engineering Lab, Hanover NH.

Lebeau, M., and Konrad, J-M. 2009. Natural Convection of Compressible and Incompressible Gases in Undeformable Porous Media under Cold Climate Conditions. Computer and Geotechnics, 36: 435–445

Kersten, M. S. (1949). Thermal properties of soils. Highway Research Board Special Report, (2).

Kuusisto, E. 1980. On the value and variability of degree-day melting factor in Finland. Nordic Hydrology, 11: 235-242.

Li, Qian., and Sun S. F. (2008). Development of the universal and simplified soil model coupling heat and water transport. Sci China Ser D-Earth Sci, vol 51, No 1, 88-102

Lu, S., Ren, T., Gong, Y., and Horton, R. (2007). An improved model for predicting soil thermal conductivity from water content at room temperature. SSSAJ 71 (1):8-14.

Mackenze, J.M., Voss, C. I., and Siegel, D. I. 2006. Groundwater Flow with Energy Transport and Water-ice Phase Change: Numerical Simulations, Benchmarks, and Application to Freezing in Peat Bogs. Advances in Water Resources. Doi:10.1016/j.advances.2006.08.008

Milly, P. C. D. (1984). A simulation analysis of thermal effects on evaporation from soil. Water Resources Research, 20(8), 1087-1098.

Newman, G. P. (1995). Heat and Mass Transfer in Unsaturated Soils During Freezing. M.Sc Thesis, University of Saskatchewan

Nield, D.A., and Bejan A. (2006). Convection in Porous Media (3rd Edit). Springer Inc., New York

Pentland, J.S. (2000). Use of a General Partial Differential Equation Solver for Solution of Heat and Mass Transfer Problems in Soils, University of Saskatchewan, Saskatchewan, DC

Sakai, M., Toride, N., and Šimůnek, J. (2009). Water and vapor movement with condensation and evaporation in a sandy column. Soil Science Society of America Journal, 73(3), 707-717.

Schrefler, B.A., Zhan, X., and Simoni, L. (1995). A Coupled Model for Water Flow, Air Flow and Heat Flow in Deformable Porous Media. Int. Num. Meth. Heat Fluid Flow, 5: 531-547

Tarnawski, V.R., Momose, T., and Leong, W.H. (2009). Assessing the impact of quartz content on the prediction of soil thermal conductivity. Geotechnique 59(4): 331-338.

Tang, A. Cui, Y., and Lee, T. (2008). A study on the thermal conductivity of compacted bentonites. Applied clay science, 41: 181-189.

TEMP/W User's Guide, (1991-2001). GEO-SLOPE International Ltd., Calgary, Alberta, Canada

Thomas, H.R. and He, Y. (1997). A Coupled Heat-Moisture Transfer Theory for Deformable Unsaturated Soil and Its Algorithmic Implementation. Internal Journal for Numerical Methods in Engineering, 40:3421-3441

Tice, A.R., Anderson, D.M., and Banin, A. (1976). The prediction of dozen water contents in born soils from liquid limit determinations. CRREL Report 76-8, 9 p.

Yang, D.Q., Rahardjo, H, and Leong, E.C, et al. (1997). A Coupled Heat, Moisture and Air Flow Model for Unsaturated Soils. Proceedings of 3rd Asian Young Geotechnical Engineers Conference, May 14-16, 1997, Singapore, pp 337-346.

Yen, Y. C, (1969). Recent studies on snow properties. Advances in Hydroscience, 5: 173-214.

Zarling, J.P. and Haynes, F.D. (1985). Thermosyphon devices and Slab-on-grade foundation design. Report No AK-RD-86-16